Supporting Information

CO_2-Catalyzed Efficient Dehydrogenation of Amines with Detailed Mechanistic and Kinetic Studies

Daniel Riemer[a], Waldemar Schilling[a], Anne Goetz[a], Yu Zhang[a], Sascha Gehrke[b], Igor Tkach[c], Oldamur Hollóczki[b], Shoubhik Das[a]*

Institut für Organische und Biomolekulare Chemie
Georg-August-Universität Göttingen
Tammannstraße 2, Göttingen, Germany

[a]Institut für Organische und Biomolekulare Chemie, Georg-August-Universität Göttingen, Tammannstraße 2, 37077 Göttingen, Germany.
[b]Mulliken Center for Theoretical Chemistry, Institut für Physikalische und Theoretische Chemie, Universität Bonn, Beringstraße 4+6, 53115 Bonn, Germany.
[c]Electron-Spin Resonance Spectroscopy, Max Planck Institute for Biophysical Chemistry, Am Faßberg 11, 37077 Göttingen, Germany.

Corresponding Author

*E-mail: shoubhik.das@chemie.uni-goettingen.de

Contents:

1. Materials and methods

Commercial reagents were used without purification and reactions were run under CO_2 atmosphere with exclusion of moisture from reagents using standard techniques for manipulating air-sensitive compounds. In case of dry DBN used for reactions, commercial DBN was dried over activated molecular sieves (3 Å) in a flame-dried Schlenk tube and degassed (several vacuum/argon cycles) prior to use. ^{1}H NMR spectra (300, 400 and 500 MHz) and ^{13}C NMR spectra (75.58, 100.62 and 125.71 MHz) were recorded using Bruker spectrometers AVANCE III 300, AVANCE III HD 400, AVANCE III 400, AVANCE III HD 500 and Varian spectrometers Mercury VX 300, VNMRS 300 and Inova 500 with $CDCl_3$ and DMSO-d_6 as solvent. NMR spectra were calibrated using the solvent residual signals ($CDCl_3$: δ ^{1}H = 7.26, δ ^{13}C = 77.16; DMSO-d_6: δ ^{1}H = 2.50, δ ^{13}C = 39.52; D_2O: δ ^{1}H = 4.79). ESI mass spectra were recorded on Bruker Daltonic spectrometers maXis (ESI-QTOF-MS) and micrOTOF (ESI-TOF-MS). GC-MS mass spectra were recorded on Thermo Finnigan spectrometers TRACE (Varian GC Capillary Column; wcot fused silica coated CP-SIL 8CB for amines; 30 m x 0.25 mm x 0.25 µm) and DSQ (Varian FactorFour Capillary Column; VF-5ms 30 m x 0.25 mm x 0.25 µm). Gas chromatography was performed on an Agilent Technologies chromatograph 7890A GC System (Supelcowax 10 Fused Silica Capillary Column; 30 m x 0.32 mm x 0.25 µm). GC calibrations were carried out with authentic samples and *n*-dodecane as an internal standard. Gas-phase GC measurements were conducted by a Shimadzu GC-2014 equipped with a TCD detector and a ShinCarbon ST 80/100 Silco column. Absorption-emission spectra were recorded on a Jasco FP-8500 Spectrofluorometer and UV/Vis spectra were recorded on a Jasco V-770 Spectrophotometer.

2. General procedure for the dehydrogenation of amines to imines

A 10 mL two-necked flask containing a stirring bar was charged with 0.134 mmol substrate. After purging the flask three times with vacuum and two times with nitrogen the CO_2 atmosphere was incorporated through a CO_2-filled balloon. Afterwards dry DMSO (2.5 mL) and DBN (1.2 eq.; 0.16 mL of a 1 M solution in dry DMSO) were added. The resulting mixture was stirred for 48 h at irradiation of visible blue light (the progress can be monitored *via* GC-MS or TLC). Then, the resulting mixture underwent an aqueous workup (using distilled water; or brine in case of slurry phase separation) and was extracted three times with ethyl acetate. The combined organic layers were dried over anhydrous Na_2SO_4, filtered and concentrated *in vacuo*. Products were purified *via* silica gel chromatography with ethyl acetate and *n*-hexane and 1 V% triethylamine as solvents (typically 20:80 ethyl acetate:*n*-hexane).

3. Setup for photocatalytic reactions

The reaction setup is depicted in **Chart S1**. The reaction setup consists of a self-constructed light source configuration, made up of a crystallizing dish with a diameter of 140 mm. Inside of the crystallizing dish, commercially available 5 m LED-Strip is glued with separable LED elements. In total, 3 m LED strip is used in a crystallizing dish, with a total power of 24 W. Light intensity of the light source can be adjusted by a self-constructed dimmer. Construction of the reaction setup and the dimmer was performed by the electronic services of the faculty for chemistry of the Georg-August-Universität Göttingen. Cooling of the setup is performed by a commercially available 120 mm computer fan. To ensure constant room temperature the dimmer setting was used at 50% (12 W). During the first experiment the temperature was monitored inside the crystallizing dish and did not exceed the room temperature (25–30 °C). Magnetic stirring was performed with 250 rpm.

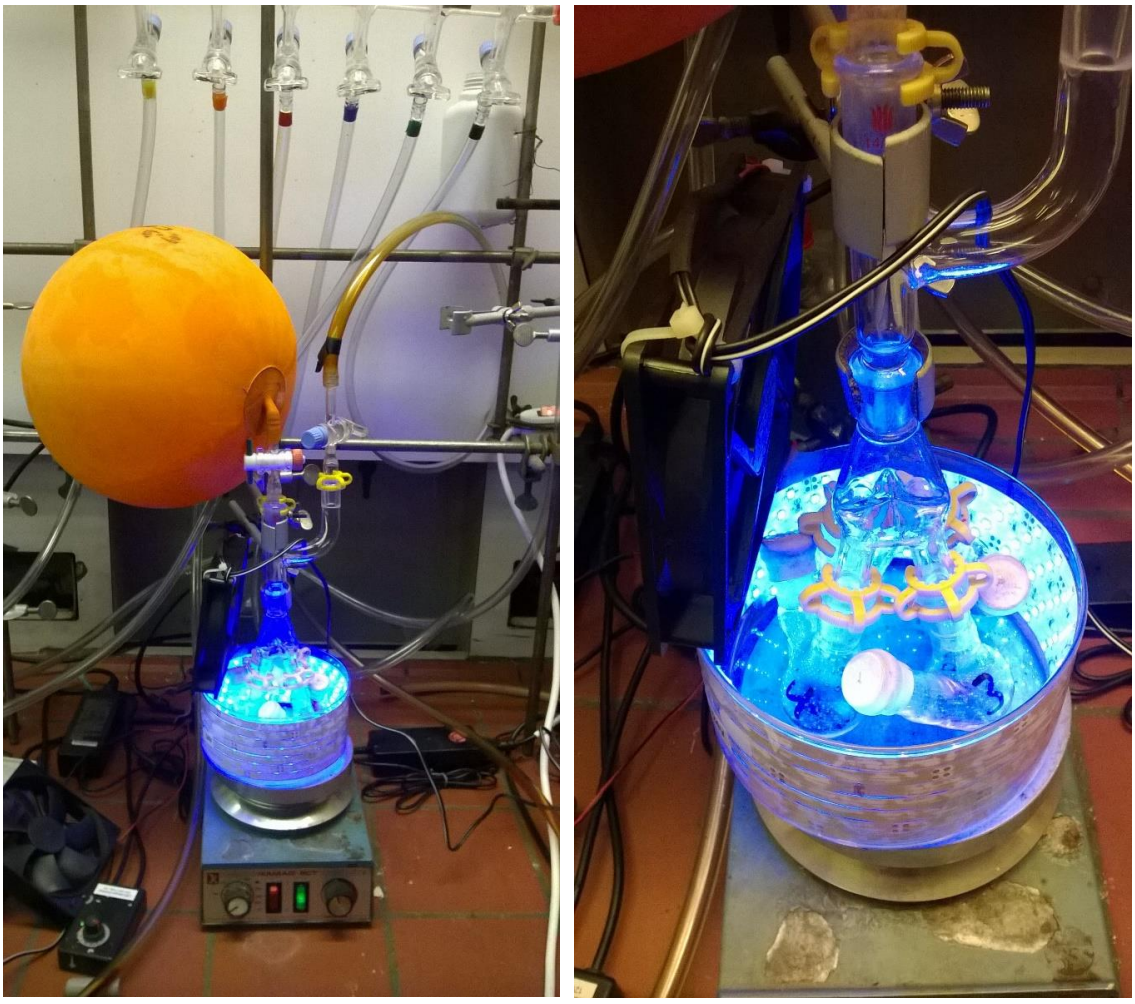

Chart S1: LED reaction setup.

4. Optimization

Table S1: Optimization table using benzyl aniline as starting material.

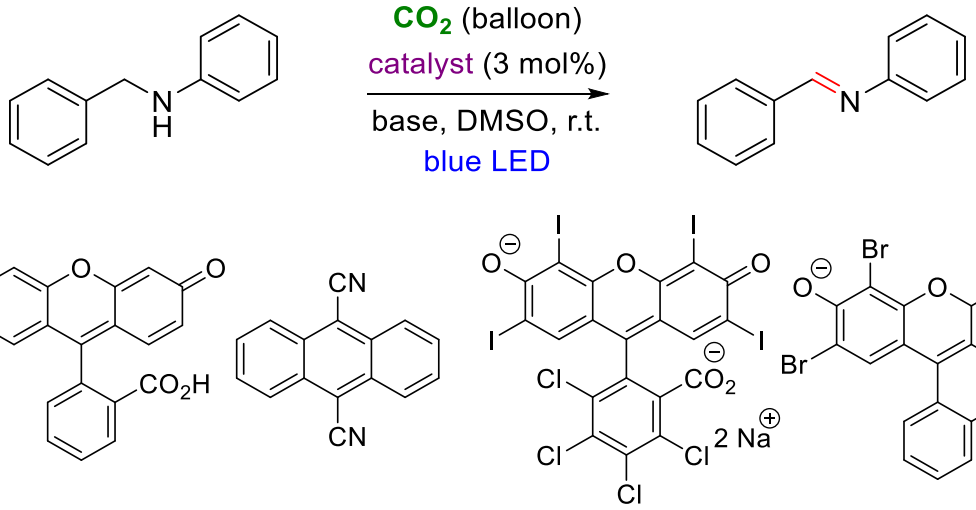

Fluorescein, **A** 9,10-Dicyano anthracene, **B** Rose Bengal, **C** Eosin Y, **D**

Catalyst	Catalyst amount [mol%]	Base	Base amount [eq.]	Reaction time [h]	Yield [%]
A	3	DBU	1	16	**16**
B	3	DBU	1	16	**8**
C	3	DBU	1	16	**38**
D	3	DBU	1	16	**45**
D	3	TBD	1	16	**25**
D	3	Pyridine	1	16	**25**
D	3	DBN	0.5	16	**56**
D	3	DBN	1	16	**70**
D	3	DBN	1.2	16	**81**
D	3	DBN	1.5	16	**83**
D	1	DBN	1.2	16	**23**
D	2	DBN	1.2	16	**43**
D	4	DBN	1.2	16	**82**
D	5	DBN	1.2	16	**84**
D	3	DBN	1.2	24	**86**
D	3	DBN	1.2	48	**96**
D	3	dry DBN	0.5	24	**88**
D	3	dry DBN	1.2	24	**95**

Reaction conditions: Benzyl aniline (0.134 mmol), photocatalyst (3 mol%), base (0.5–1.2 eq.), DMSO (2.5 mL), CO_2 (balloon), 12 W blue LED, rt, 16–48 h. Yields were determined by GC using *n*-dodecane as internal standard.

5. Mechanistic experiments

In situ gas GC:

An *in situ* gas GC measurement of the gas phase of a reaction from cinnamyl alcohol to cinnamaldehyde was carried out after 48 h reaction time. The curve is indicating that there is no other gas than CO_2. The source of N_2 gas is the front part of the needle of the used gas-tight syringe; **7.5 min: N_2, 29.5 min: CO_2.**

Chart S2: *in situ* gas GC measurement.

Different amounts of CO_2

The reaction flask (see **2. General Procedure**) containing a nitrogen atmosphere after three vacuum/N_2 cycles was charged with the volumetric amount of 1.0 and 0.2 equivalents of CO_2, respectively, through a septum *via* syringe. The syringe was purged with CO_2 gas thrice prior to use. The necessary amount was calculated according to the ideal gas law:

$$pV = nRT$$

The temperature in the laboratory was measured to be 20 °C, the pressure was estimated to be 1 atm = 101325 Pa. This is an example calculation for the case of 1.0 equivalent of CO_2 with the scale of the reaction being 0.134 mmol:

$$V = \frac{nRT}{p} = \frac{0.134 * 10^{-3}\ mol * 8.314\ kg\ m^2 * 293.15\ K\ m\ s^2}{101325\ s^2\ mol\ K\ kg} = 3.2 * 10^{-6}\ m^3 = 3.2\ ml$$

KIE experiments

Mono- and di-deuterated starting materials **1a-*d*$_1$** and **1a-*d*$_2$** were synthesized according to literature procedure[1]:

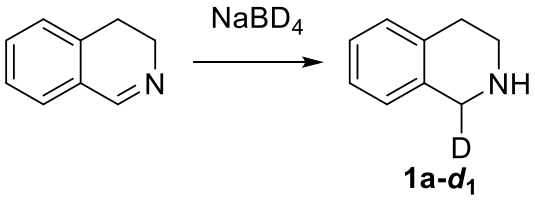

Scheme S1: Deuteration of 3,4-dihydroisoquinoline to **1a-*d*$_1$**.

1a-*d*$_1$: 6.5 ml ethanol were added to 3.1 mmol $NaBD_4$ (127.9 mg) followed by slow addition of 0.35 ml 3,4-dihydroisoquinoline (2.962 mmol). The mixture was stirred at room temperature for 1 h, cooled to 0 °C and quenched with 1 M HCl. Afterwards, solid NaOH was added until the solution became basic (controlled by pH indicator paper). The solution was dried with Na_2SO_4 and concentrated in vacuo to give **1a-*d*$_1$** which was used without further purification (quantitative conversion; > 95% deuteration).

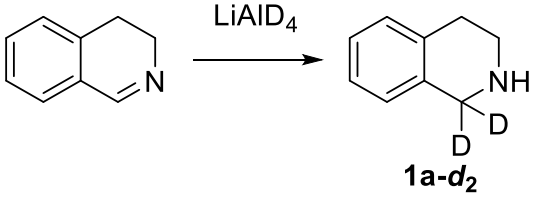

Scheme S2: Deuteration of 3,4-dihydroisoquinoline to **1a-*d*$_2$**.

1a-*d*$_1$: 15 ml dry THF were added to 6.6 mmol $LiAlD_4$ (277.1 mg) followed by addition of 0.35 ml 3,4-dihydroisoquinoline (2.962 mmol) under nitrogen atmosphere. The mixture was refluxed for 40 h, cooled to 0 °C and quenched with 1 M HCl. After extraction with ethyl acetate the solution was dried with Na_2SO_4 and concentrated in vacuo to give **1a-*d*$_1$** which was used without further purification (quantitative conversion; > 95% deuteration).

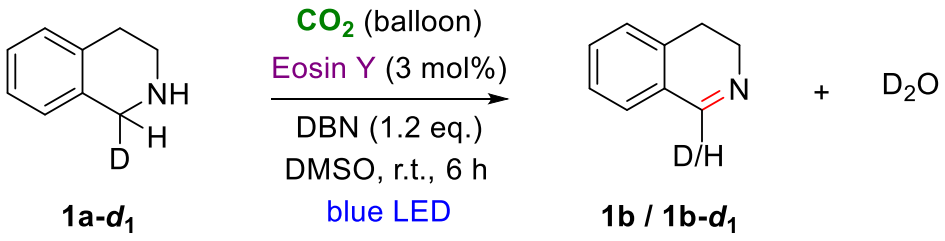

1a-*d*$_1$ **1b / 1b-*d*$_1$**

Scheme S3: Reaction of **1a-*d*$_1$** to **1b** and **1b-*d*$_1$**, respectively.

Starting materials **1a-*d*$_1$** and **1a-*d*$_2$**, respectively, were dehydrogenated according to the general reaction procedure described in **2. General procedure**. After 7 h the resulting products were analyzed by GC using *n*-dodecane as internal standard and in case of **1a-*d*$_2$** compared with a non-deuterated sample under the same reaction conditions. The calculated KIE is a result of the average of three independent runs for each starting material:

$$\frac{k_H}{k_D} \sim \frac{n(P_H)}{n(P_D)} = 0.13$$

Both starting materials give the same KIE so that we can assume that there is no effect of the orientation of the deuterium atom in **1a-*d*$_1$** neither an effect of the double deuteration of **1a-*d*$_1$.**

Carbamate as possible intermediate/by-product from benzyl aniline

1a

Scheme S4: Reaction of **1a** to the respective methyl carbamate.

A 10 mL two-necked flask containing a stirring bar was charged with 0.134 mmol benzyl aniline (24.3 mg). After purging the flask three times with vacuum and two times with argon the CO_2 atmosphere was incorporated through a CO_2-filled balloon. Afterwards dry DMSO (2.5 mL), DBN (1.2 eq.; 0.16 mL of a 1 M solution in dry DMSO) and degassed methyl iodide (0.03 mL; 0.48 mmol; 3.6 eq.) were added. The resulting mixture was stirred for 24 h at room temperature.

ESI-HRMS: *m/z* calcd. for $C_{15}H_{15}NO_2$ [M+H$^+$]: 242.1176, found: 242.1174; *m/z* calcd. for $C_{15}H_{15}NO_2$ [M+Na$^+$]: 264.0995, found: 264.0996.

Bicarbonate salt as possible intermediate/by-product from non-dried DBN

CO_2 was bubbled through commercial DBN for about 3 minutes. The formed white precipitate was collected and submitted to ^{1}H and ^{13}C NMR in D_2O as solvent, thus confirming the formation of a $DBNH^+$ bicarbonate salt:

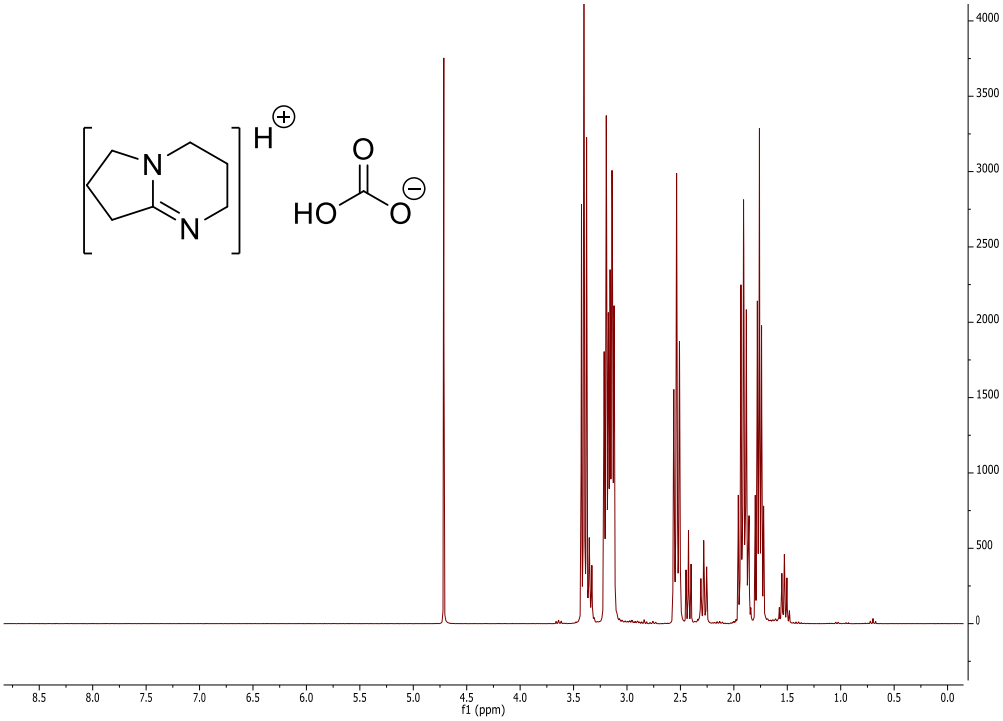

Chart S3: ^{1}H NMR in D_2O.

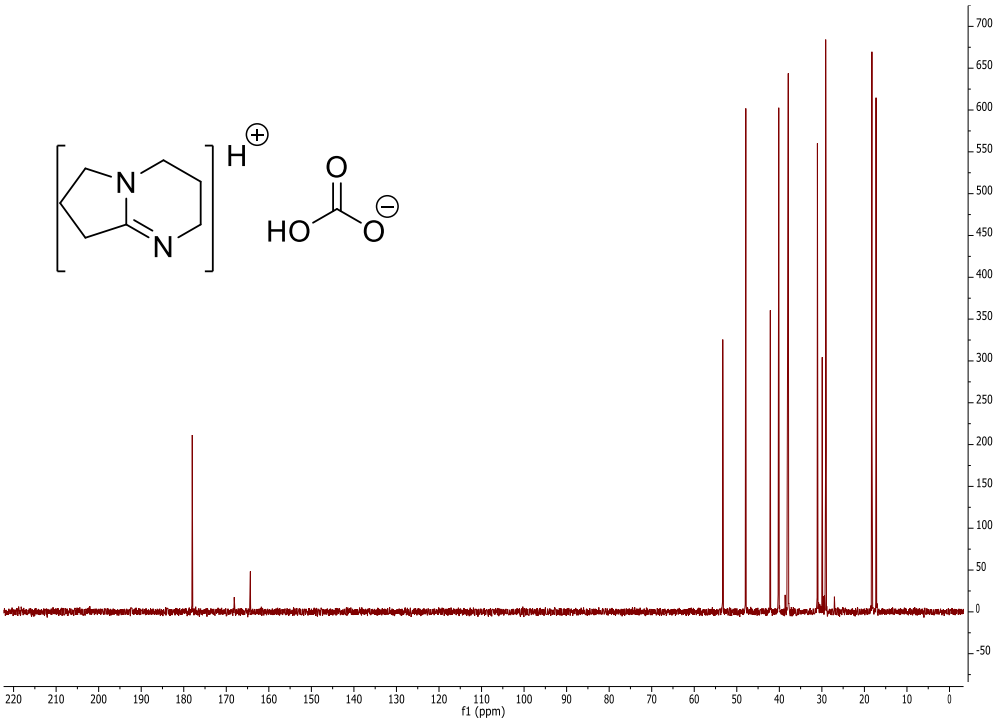

Chart S4: ^{13}C NMR in D_2O.

Deuterium NMR

A ^{2}H NMR spectrum was recorded in order to detect possible deuterated byproducts from the reaction of deuterated starting material **1a-*d*$_2$** in non-deuterated DMSO. We found a hint for D_2O as byproduct at 3.30 ppm in ^{2}H NMR. The signal at 8.88 ppm could be assigned to **1b-*d*$_1$** and at 4.97 to **1a-*d*$_2$**.

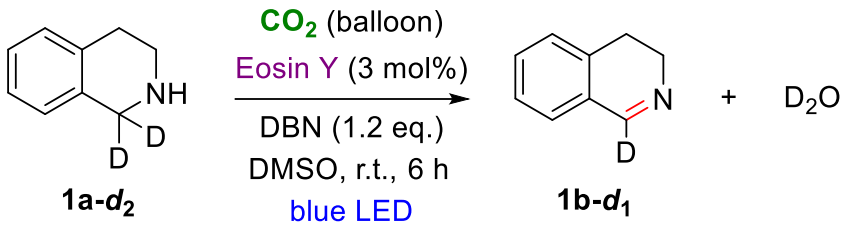

Scheme S5: Reaction of **1a-*d*$_2$** to **1b-*d*$_1$** with D_2O as byproduct.

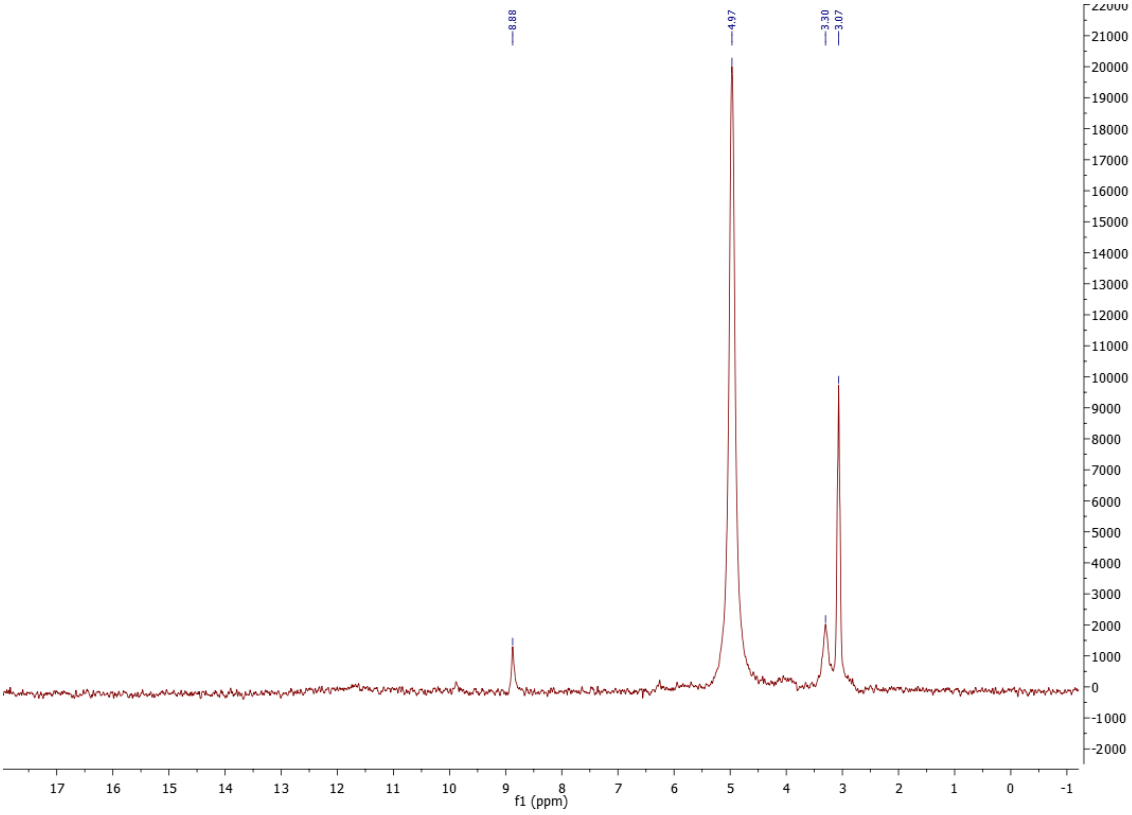

Chart S5: ^{2}H NMR in DMSO-d_0.

Stern-Volmer Plot

To determine the reactive species in the beginning of the photocatalytic reaction absorption-emission spectra for a Stern-Volmer plot were acquired. Firstly, a 3D spectrum for excitation and emission of Eosin Y was recorded in order to detect the maxima of absorption and emission. The resulting spectrum is depicted in **Chart S6** with 3 absorption bands.

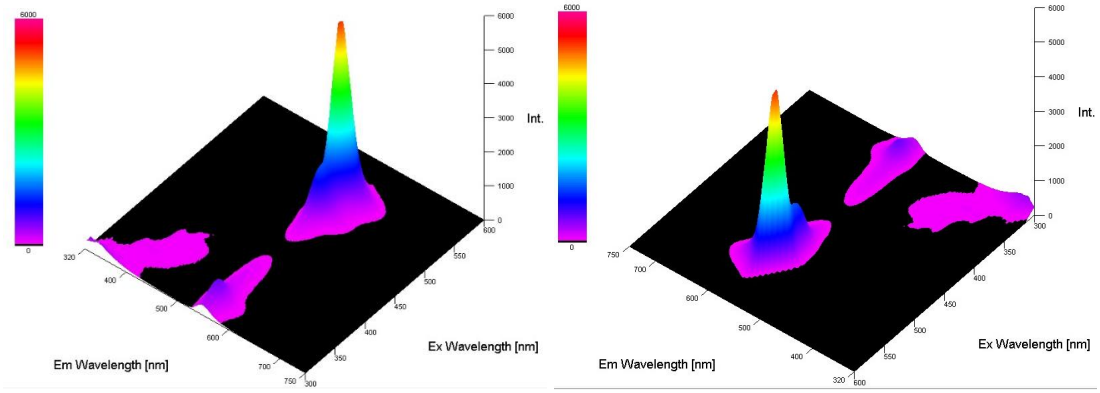

Chart S6: 3D absorption-emission spectrum of Eosin Y in DMSO.

Chart S7 shows a comparison spectrum of DBN. The excitation maximum was measured at 533 nm and the emission maximum at 550 nm. These wavelengths were used for further measurements.

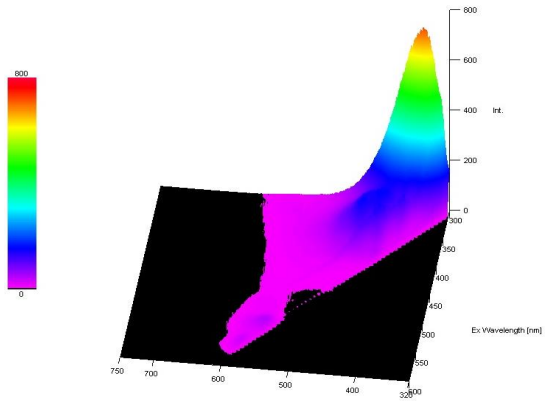

Chart S7: 3D absorption-emission spectrum of DBN in DMSO.

Kinetic studies

In general, the kinetic experiments were carried out according to the general reaction procedure described in **2. General procedure** but with varying concentrations of *N*-benzyl aniline, DBN or Eosin Y as depicted in **Table S2, S3** and **S4**. Samples (as whole reaction mixtures, no aliquots) were taken after the indicated timespan and analyzed *via* GC with *n*-dodecane as internal standard. The obtained values were plotted as product concentration against the time at different concentrations of starting material, base or catalyst, respectively (**Chart S8**, **S9** and **S10**).

Table S2: Different concentrations of benzyl aniline

c(SM) [M]	c(P) [M]	t [h]
0,018	0,001587	2
0,018	0,002433	4
0,018	0,003736	6
0,018	0,003928	8
0,036	0,003046	2
0,036	0,008246	4
0,036	0,012415	6
0,036	0,013664	8
0,0536	0,002441	2
0,0536	0,009151	4
0,0536	0,013523	6
0,0536	0,017532	8
0,108	0,002128	2
0,108	0,005401	4
0,108	0,013822	6
0,108	0,024697	8
0,2144	0,002121	2
0,2144	0,015682	4
0,2144	0,028238	6
0,2144	0,040826	8

Table S3: Different concentrations of DBN

c(base) [M]	c(P) [M]	t [h]
0,01608	0,006332	2
0,01608	0,008924	4
0,01608	0,008748	6
0,01608	0,010432	8
0,03216	0,014200	2
0,03216	0,018053	4
0,03216	0,019290	6
0,03216	0,024817	8
0,06432	0,012441	2
0,06432	0,018151	4
0,06432	0,021523	6
0,06432	0,025532	8
0,09648	0,014121	2
0,09648	0,019443	4
0,09648	0,025681	6
0,09648	0,030455	8
0,12864	0,021188	2
0,12864	0,031779	4
0,12864	0,038768	6
0,12864	0,046392	8

Table S4: Different concentrations of Eosin Y

c(cat) [mM]	c(P) [M]	t [h]
0,536	0,00219	2
0,536	0,02417	4
0,536	0,02921	6
0,536	0,03671	8
1,072	0,00712	2
1,072	0,01706	4
1,072	0,03433	6
1,072	0,04596	8
1,608	0,00244	2
1,608	0,00915	4
1,608	0,01352	6
1,608	0,03753	8
2,68	0,00615	2
2,68	0,01169	4
2,68	0,02434	6
2,68	0,05623	8
5,36	0,00400	2
5,36	0,02402	4
5,36	0,04037	6
5,36	0,04647	8

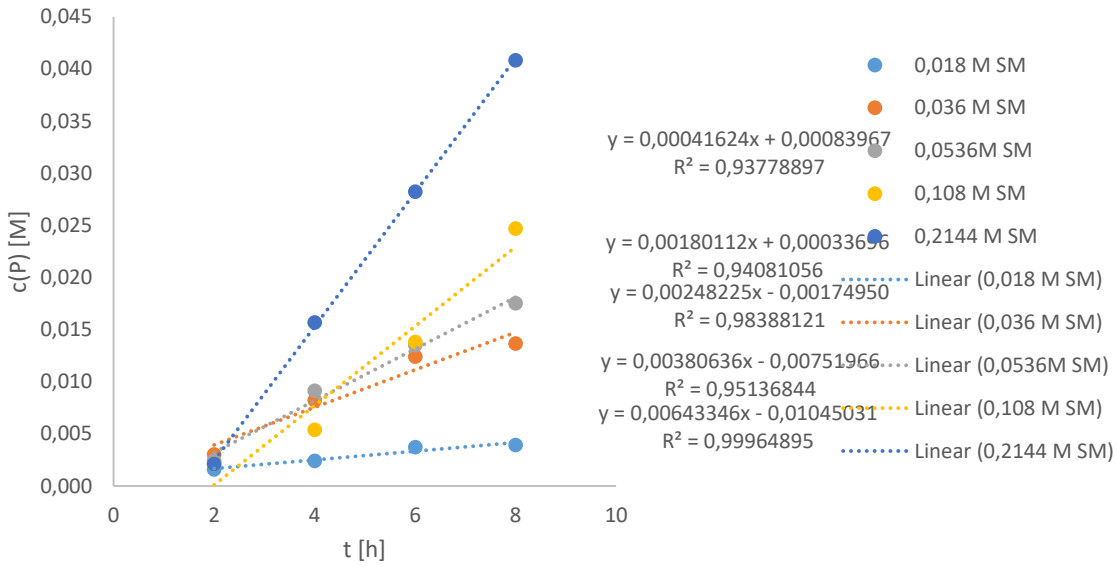

Chart S8: Product concentration plotted against reaction time at different benzyl aniline concentrations; for each data point a separate reaction was conducted using different concentrations of benzyl aniline (18 mmol l^{-1}, 36 mmol l^{-1}, 53.6 mmol l^{-1}, 108 mmol l^{-1}, 214.4 mmol l^{-1}) with constant concentration of DBN (64.3 mmol l^{-1}) and Eosin Y (1.61 mmol l^{-1}) in 2.5 ml DMSO at room temperature under a CO_2 atmosphere (balloon) and blue LED light irradiation and submitted to GC analysis with *n*-dodecane as internal standard after the indicated timespan.

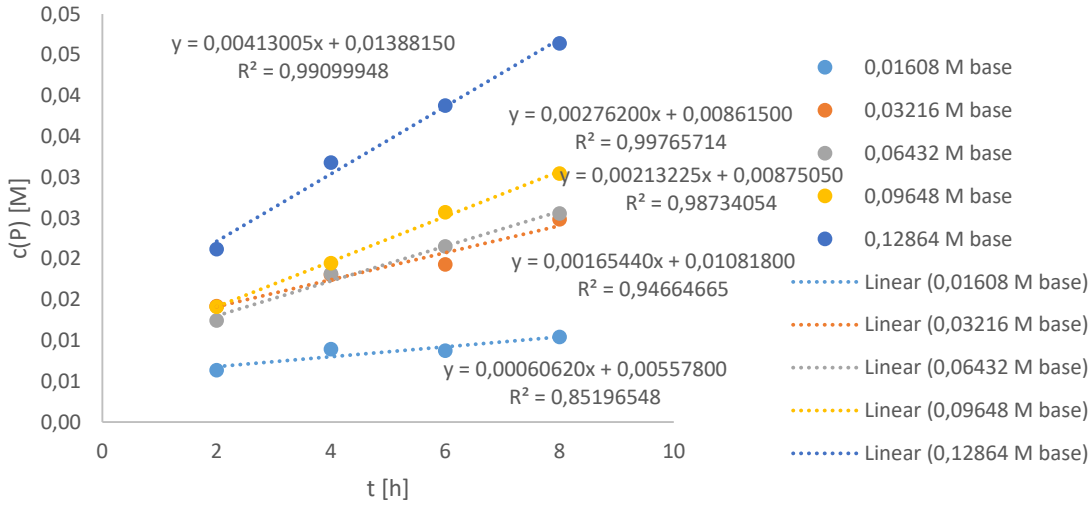

Chart S9: Product concentration plotted against reaction time at different DBN concentrations; for each data point a separate reaction was conducted using different concentrations of DBN (16.1 mmol l^{-1}, 32.2 mmol l^{-1}, 64.3 mmol l^{-1}, 96.5 mmol l^{-1}, 128.6 mmol l^{-1}) with constant concentration of benzyl aniline (0.0536 mol l^{-1}) and Eosin Y (1.61 mmol l^{-1}) in 2.5 ml DMSO at room temperature under a CO_2 atmosphere (balloon) and blue LED light irradiation and submitted to GC analysis with *n*-dodecane as internal standard after the indicated timespan.

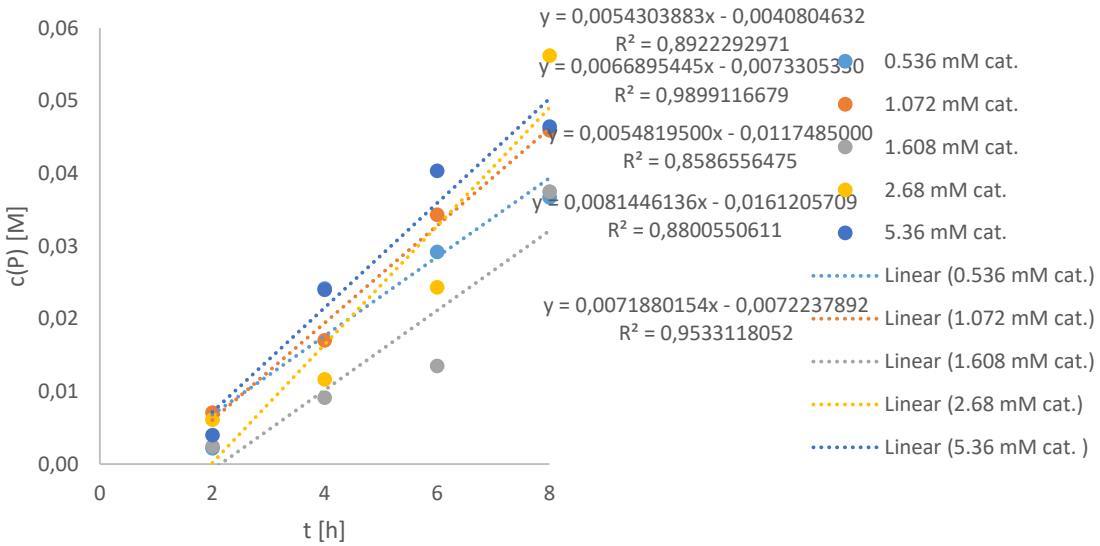

Chart S10: Product concentration plotted against reaction time at different Eosin Y concentrations; for each data point a separate reaction was conducted using different concentrations of Eosin Y (0.536 mmol l^{-1}, 1.072 mmol l^{-1}, 1.608 mmol l^{-1}, 2.68 mmol l^{-1}, 5.46 mmol l^{-1}) with constant concentration of benzyl aniline (0.0536 mol l^{-1}) and DBN (64.3 mmol l^{-1}) in 2.5 ml DMSO at room temperature under a CO_2 atmosphere (balloon) and blue LED light irradiation and submitted to GC analysis with *n*-dodecane as internal standard after the indicated timespan.

With the slopes of these curves we were now able to plot the logarithmic concentration of starting material, base and catalyst, respectively, against the logarithmic observed rate constant k_{obs} (**Chart S11**, **S12** and **S13**).

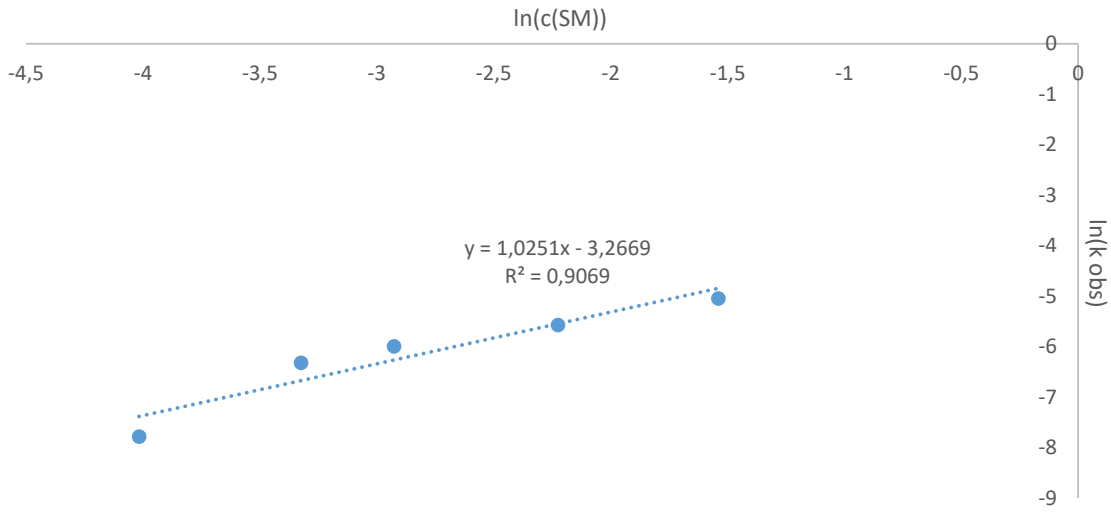

Chart S11: ln(k_{obs}) against ln(c_{SM}); standard error: 0.36529.

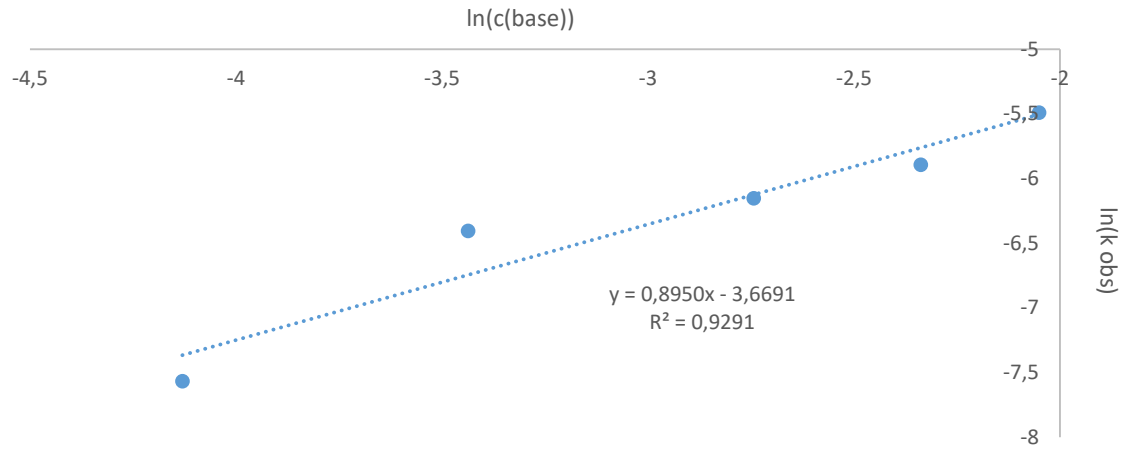

Chart S12: ln(k_{obs}) against ln(c_{base}); standard error: 0.24111.

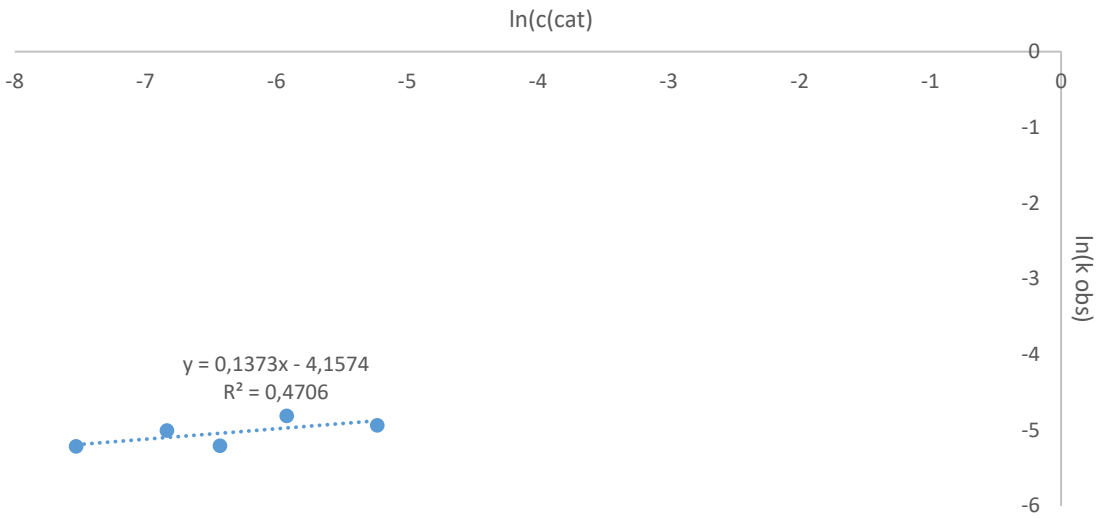

Chart S13: ln(k_{obs}) against ln(c_{cat}); standard error: 0.14743.

6. Theoretical calculations

All structures were optimized by the ORCA 4.0.1 software package[2] with the M06 functional[3] with a D3 dispersion correction with zero dumping[4] and a def2-TZVPP basis set.[5] Influences of the solvent on the structures were introduced by a conductor-like polarizable continuum model (CPCM) for DMSO.[6] The Hessian was calculated to verify the nature of the obtained stationary points.

DLPNO-CCSD(T) single point energies were calculated with a def2-TZVPP and a def2-QZVPP basis set as well as with a def2-TZVPP basis set and tight settings for the local pairs. The obtained energies were used in the extrapolation scheme developed by Neese and Liakos to the corresponding DLPNO-CCSD(T)/CBS complete basis set energies.[7]

The Gibbs free energies of solvation were estimated by the COSMO-RS method[8] as implemented in the COSMOthermX14 program package.[9] With the aim to achieve the best available accuracy the BP-TZVPD-FINE method was applied, which calculates the correction based on single point calculations performed by Turbomole[10] with the BP86 functional[11] and a def2-TZVPD basis set.[5,12]

The redox potential was calculated from the sum of all energy contributions above, based on a scheme originally developed for metal cations.[13] Due to the fact, that redox potentials are generally listed as relative values compared to the standard hydrogen electrode (SHE) the obtained potentials were transformed to analogous representatives by calculating the difference to the total potential of the SHE of 4.44 eV.[14]

7. Characterization of products

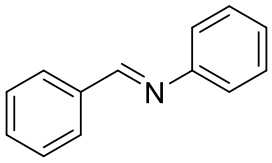

1b, *N*-Benzylidene aniline: ^{1}H NMR (400 MHz, $CDCl_3$): δ 8.50 (s, 1H), 8.01 – 7.89 (m, 2H), 7.56 – 7.50 (m, 3H), 7.49 – 7.41 (m, 2H), 7.32 – 7.21 (m, 3H); **^{13}C NMR** (101 MHz, $CDCl_3$): δ 160.46, 152.20, 136.34, 131.47, 129.25, 128.92, 128.87, 126.04, 120.98; **MS (GC-MS):** *m/z* 181 (M^+)[15]; 96% yield.

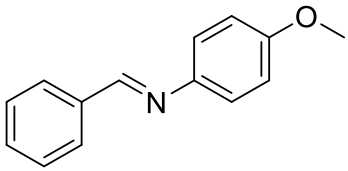

2b, 1-(4-Methoxyphenyl)-*N*-phenylmethanimine: **^{1}H NMR** (300 MHz, $CDCl_3$): δ 8.49 (s, 1H), 7.93 – 7.86 (m, 2H), 7.50 – 7.42 (m, 3H), 7.26 – 7.20 (m, 2H), 6.98 – 6.91 (m, 2H), 3.84 (s, 3H); **^{13}C NMR** (75 MHz, $CDCl_3$): δ 158.56, 158.44, 145.10, 136.62, 131.17, 128.87, 128.73, 122.33, 114.55, 55.66; **MS (GC-MS):** *m/z* 211 (M^+)[16]; 99% yield.

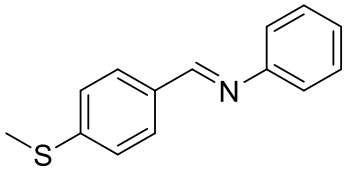

3b, 1-(4-(methylthio)phenyl)-N-phenylmethanimine: **^{1}H NMR** (300 MHz, $CDCl_3$): δ 8.40 (s, 1H), 7.88 – 7.76 (m, 2H), 7.48 – 7.28 (m, 4H), 7.27 – 7.18 (m, 3H), 2.54 (s, 3H); **^{13}C NMR** (75 MHz, $CDCl_3$): δ 159.71, 152.26, 143.35, 133.08, 130.12, 129.27, 125.90, 125.38, 121.00, 15.29; **MS (GC-MS):** *m/z* 227 (M^+)[17]; 99% yield.

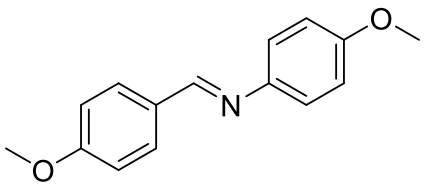

4b, *N*-1-bis(4-methoxyphenyl)methanimine: **^{1}H NMR** (300 MHz, $CDCl_3$): δ 9.89 (s, 1H), 7.91 – 7.78 (m, 4H), 7.08 – 6.93 (m, 4H), 3.90 (s, 6H); **^{13}C NMR** (75 MHz, $CDCl_3$): δ 190.94, 164.76, 132.14, 130.14, 114.47, 55.74; **MS (GC-MS):** *m/z* 241 (M^+)[18]; 92% yield.

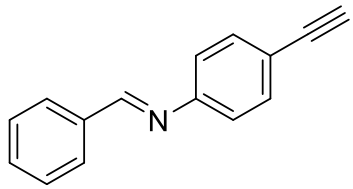

5b, N-(4-ethynylphenyl)-1-phenylmethanimine: **^{1}H NMR** (300 MHz, $CDCl_3$): δ 7.42 – 7.26 (m, 5H), 7.26 (s, 1H), 6.66 – 6.52 (m, 4H), 2.96 (s, 1H); **^{13}C NMR** (75 MHz, $CDCl_3$): δ 160.51, 154.19, 133.62, 131.46, 130.38, 127.33, 127.07, 119.67, 117.13, 112.58, 107.19; **MS (GC-MS):** *m/z* 205 (M^+)[17]; 99% yield.

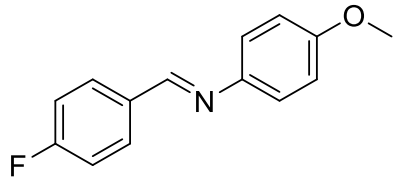

6b, 1-(4-fluorophenyl)-*N*-(4-methoxyphenyl)methanimine: **^{1}H NMR** (300 MHz, $CDCl_3$): δ 8.46 (s, 1H), 7.96 – 7.86 (m, 2H), 7.31 – 7.21 (m, 2H), 7.17 (dd, J = 8.9, 8.4 Hz, 2H), 7.01 – 6.78 (m, 2H), 3.85 (s, 3H); **^{13}C NMR** (75 MHz, $CDCl_3$): δ 166.32, 158.50, 156.89, 144.86, 130.57, 122.29, 116.14, 115.85, 114.58, 55.64; **MS (GC-MS):** *m/z* 229 (M^+)[19]; 92% yield.

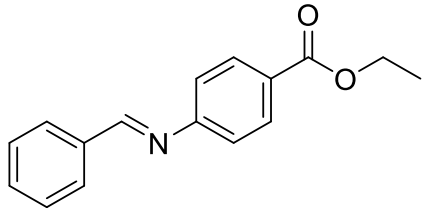

7b, Ethyl 4-(benzyldeneamino)benzoate: **^{1}H NMR** (300 MHz, $CDCl_3$): δ 8.43 (s, 1H), 8.19 – 8.02 (m, 2H), 7.99 – 7.87 (m, 2H), 7.61 – 7.41 (m, 3H), 7.21 (d, J = 8.7 Hz, 2H), 4.39 (q, J = 7.1 Hz, 2H), 1.41 (t, J = 7.1 Hz, 3H); **^{13}C NMR** (75 MHz, $CDCl_3$): δ 166.45, 161.70, 156.26, 135.93, 131.97, 130.92, 129.15, 128.96, 127.85, 120.74, 61.00, 14.49; **MS (GC-MS):** *m/z* 253 (M^+)[20]; 73% yield.

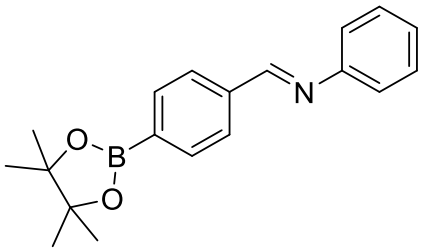

8b, *N*-Phenyl-1-(4(4,4,5,5-tetramethyl-1,3,2-dioxaborolan-2-yl)phenyl)methan-imine: **^{1}H NMR** (300 MHz, $CDCl_3$): δ 8.48 (s, 1H), 7.91 – 7.86 (m, 2H), 7.49 – 7.44 (m, 3H), 7.21 – 7.16 (m, 2H), 6.90 – 6.85 (m, 2H), 2.17 (s, 12H); **^{13}C NMR** (126 MHz, $CDCl_3$): δ 207.20, 158.46, 154.87, 144.86, 136.56, 131.16, 128.87, 128.71, 122.50, 116.07, 58.86, 31.10; **MS (ESI-HRMS):** *m/z* calcd. for $C_{19}H_{22}BNO_2$ [M+H$^+$]: 308.1816, found: 308.1818; 64% yield.

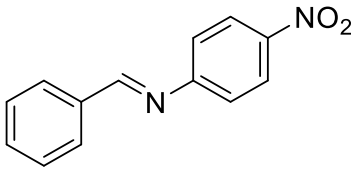

9b, N-(4-Nitrophenyl)-1-phenylmethanimine: ^{1}H NMR (300 MHz, $CDCl_3$): δ 8.36 (s, 1H), 8.24 – 8.17 (m, 2H), 7.85 (dt, J = 7.7, 1.2 Hz, 2H), 7.52 – 7.40 (m, 3H), 7.23 – 7.12 (m, 2H); **^{13}C NMR** (75 MHz, $CDCl_3$): δ 162.79, 132.56, 129.44, 129.13, 125.20, 121.39; **MS (GC-MS):** *m/z* 226 (M$^+$)[21]; 72% yield.

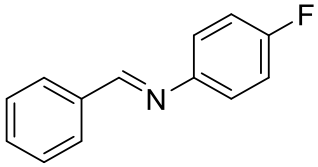

10b, *N*-(4-fluorophenyl)-1-phenylmethanimine: **^{1}H NMR** (300 MHz, $CDCl_3$): δ 8.45 (s, 1H), 7.94 – 7.86 (m, 2H), 7.53 – 7.45 (m, 3H), 7.24 – 7.17 (m, 2H), 7.13 – 7.02 (m, 2H); **^{13}C NMR** (75 MHz, $CDCl_3$): δ 160.28, 136.28, 131.58, 128.95, 128.93, 122.49, 122.39, 116.16, 115.86; **MS (GC-MS):** *m/z* 199 (M$^+$)[22]; 99% yield.

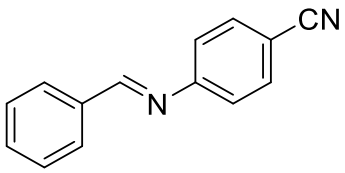

11b, 4-(Benzylideneamino)benzonitrile: **^{1}H NMR** (300 MHz, $CDCl_3$): δ 8.40 (s, 1H), 7.95 – 7.88 (m, 2H), 7.71 – 7.65 (m, 2H), 7.58 – 7.46 (m, 3H), 7.30 – 7.18 (m, 2H); **^{13}C NMR** (75

MHz, $CDCl_3$): δ 162.51, 156.19, 135.62, 133.46, 132.38, 129.33, 129.07, 121.67, 119.13, 109.19; **MS (GC-MS):** *m/z* 206 (M^+)[23]; 62% yield.

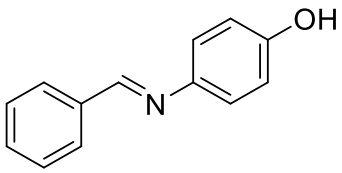

12b, 4-(Benzylideneamino)phenol: **^{1}H NMR** (300 MHz, $CDCl_3$): δ 8.48 (s, 1H), 7.94 – 7.82 (m, 2H), 7.47 (ddd, J = 3.4, 2.7, 1.5 Hz, 3H), 7.23 – 7.12 (m, 2H), 6.93 – 6.83 (m, 2H), 4.90 (s, 1H); **^{13}C NMR** (75 MHz, $CDCl_3$): δ 158.74, 131.24, 128.90, 128.77, 122.52, 116.06; **MS (GC-MS):** *m/z* 197 (M^+)[24]; 99% yield.

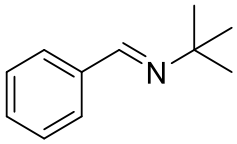

13b, *N-tert*-butyl-1-phenylmethanimine: **^{1}H NMR** (300 MHz, $CDCl_3$): δ 8.29 (s, 1H), 7.83 – 7.71 (m, 2H), 7.45 – 7.35 (m, 3H), 1.32 (s, 9H); **^{13}C NMR** (75 MHz, $CDCl_3$): δ 155.23, 137.31, 130.25, 128.61, 128.01, 57.34, 29.86; **MS (GC-MS):** *m/z* 161 (M^+)[25]; 99% yield.

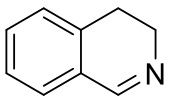

14b, 3,4-dihydroisoquinoline: **^{1}H NMR** (300 MHz, $CDCl_3$): δ 8.32 (t, J = 2.0 Hz, 1H), 7.39 – 7.10 (m, 4H), 3.80 – 3.72 (m, 2H), 2.79 – 2.67 (m, 2H); **^{13}C NMR** (75 MHz, $CDCl_3$): δ 160.33, 136.37, 131.06, 128.57, 127.45, 127.21, 127.11, 47.45, 25.08; **MS (GC-MS):** *m/z* 131 (M^+)[26]; 87% yield.

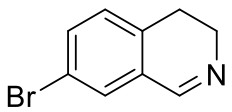

15b, 7-Bromo-3,4-dihydroisoquinoline: **^{1}H NMR** (300 MHz, $CDCl_3$): δ 8.33 – 8.19 (s, 1H), 7.47 (dd, J = 8.0, 2.1 Hz, 1H), 7.41 (d, J = 2.1 Hz, 1H), 7.05 (d, J = 8.0 Hz, 1H), 3.83 – 3.74 (m, 2H), 2.76 – 2.64 (m, 2H); **^{13}C NMR** (75 MHz, $CDCl_3$): δ 159.01, 135.21, 133.97, 130.17, 129.26, 120.58, 120.14, 47.43, 24.62; **MS (GC-MS):** *m/z* 209 (M^+)[27]; 99% yield.

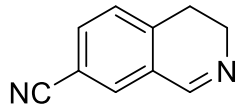

16b, 3,4-Dihydroisoquinoline-7-carbonitrile: **^{1}H NMR** (300 MHz, $CDCl_3$): δ 8.35 (s, 1H), 7.64 (dd, J = 7.8, 1.7 Hz, 1H), 7.59 – 7.53 (m, 1H), 7.31 – 7.27 (m, 1H), 3.89 – 3.78 (m, 2H), 2.88 – 2.76 (m, 2H); **^{13}C NMR** (75 MHz, $CDCl_3$): δ 158.11, 141.53, 134.31, 130.36, 128.51, 118.15, 111.32, 46.78, 42.68, 25.03; **MS (ESI-HRMS):** *m/z* calcd. for $C_{10}H_8N_2$ [M+H$^+$]: 157.0760, found: 157.0762; 94% yield.

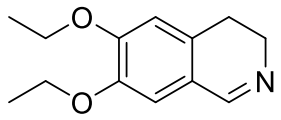

17b, 6,7-Diethoxy-3,4-dihydrotetraisoquinoline: **^{1}H NMR** (300 MHz, $CDCl_3$): δ 8.20 (s, 1H), 6.81 (s, 1H), 6.66 (s, 1H), 4.11 (dq, J = 8.4, 7.0 Hz, 4H), 3.72 (ddd, J = 8.1, 7.0, 2.2 Hz, 2H), 2.69 – 2.62 (m, 2H), 1.46 (td, J = 7.0, 4.7 Hz, 6H); **^{13}C NMR** (75 MHz, $CDCl_3$): δ 159.91, 151.40, 147.51, 130.13, 121.66, 113.05, 112.19, 65.13, 64.73, 47.44, 42.83, 24.94, 14.98; **MS (ESI-HRMS):** *m/z* calcd. for $C_{13}H_{17}NO_2$ [M+H$^+$]: 220.1332, found: 220.1335; 91% yield.

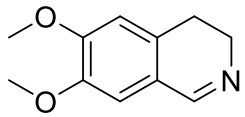

18b, 6,7-Dimethoxy-3,4-dihydroisoquinoline: **^{1}H NMR** (300 MHz, $CDCl_3$): δ 9.05 (s, 1H), 8.39 (d, J = 5.8 Hz, 1H), 7.51 (d, J = 5.6 Hz, 1H), 7.26 (s, 2H), 7.20 (s, 1H), 7.07 (s, 1H), 4.04 (s, 6H); **^{13}C NMR** (75 MHz, $CDCl_3$): δ 150.12, 142.18, 132.70, 119.37, 105.49, 104.73, 56.25, 56.21; **MS (GC-MS):** *m/z* 191 (M$^+$)[27]; 97% yield.

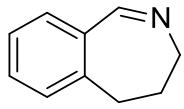

19b, 4,5-Dihydro-3H-benzo[c]azepine: **^{1}H NMR** (300 MHz, $CDCl_3$): δ 8.50 (s, 1H), 7.60 – 7.28 (m, 4H), 3.63 (td, J = 6.2, 1.7 Hz, 2H), 2.78 (t, J = 6.8 Hz, 2H), 2.35 – 2.17 (m, 2H); **^{13}C NMR** (75 MHz, $CDCl_3$): δ 163.90, 130.15, 129.91, 129.11, 126.29, 51.60, 32.71, 32.20; **MS (GC-MS):** *m/z* 145 (M$^+$)[28]; 72% yield.

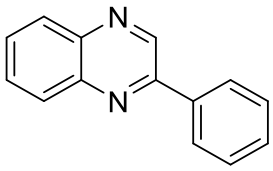

20b, 2-Phenylquinoxaline: **^{1}H NMR** (300 MHz, $CDCl_3$): δ 9.33 (s, 1H), 8.25 – 8.09 (m, 4H), 7.84 – 7.71 (m, 2H), 7.63 – 7.52 (m, 3H); **^{13}C NMR** (75 MHz, $CDCl_3$): δ 152.01, 143.50, 142.46, 141.73, 136.94, 130.42, 130.33, 129.77, 129.29, 129.26, 127.70; **MS (GC-MS):** *m/z* 206 (M^+)[29]; 99% yield.

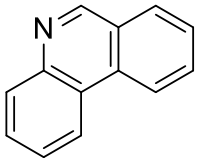

21b, Phenanthridine: **^{1}H NMR** (300 MHz, $CDCl_3$): δ 7.73 – 7.69 (m, 1H), 7.72 – 7.63 (m, 1H), 7.34 – 7.27 (m, 2H), 7.21 (td, J = 7.4, 1.3 Hz, 1H), 7.17 – 7.06 (m, 2H), 6.84 (ddd, J = 7.8, 7.3, 1.2 Hz, 1H), 6.67 (ddd, J = 7.9, 1.2, 0.5 Hz, 1H); **^{13}C NMR** (75 MHz, $CDCl_3$): δ 145.86, 132.89, 128.95, 127.80, 127.27, 126.15, 123.74, 122.57, 120.16, 119.43, 115.26, 46.56; **MS (GC-MS):** *m/z* 179 (M^+)[30]; 98% yield.

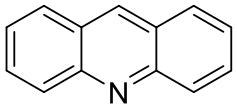

22b, Acridine: **^{1}H NMR** (300 MHz, $CDCl_3$): δ 8.73 (s, 1H), 8.24 (dd, J = 8.9, 1.0 Hz, 2H), 8.02 – 7.92 (m, 2H), 7.77 (ddd, J = 8.8, 6.6, 1.4 Hz, 2H), 7.52 (ddd, J = 8.5, 6.6, 1.1 Hz, 2H); **^{13}C NMR** (75 MHz, $CDCl_3$): δ 149.21, 136.11, 130.38, 129.55, 128.31, 126.70, 125.77; **MS (GC-MS):** *m/z* 179 (M^+)[31]; 97% yield.

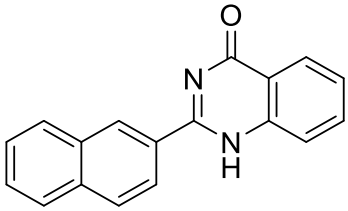

23b, 2-(Naphthalen-2-yl)quinazolin-4-one: **^{1}H NMR** (300 MHz, DMSO-d_6): δ 8.38 (s, 1H), 8.10 – 7.89 (m, 4H), 7.68 (ddd, J = 15.3, 8.1, 1.7 Hz, 2H), 7.54 (dd, J = 6.2, 3.3 Hz, 2H), 7.31 – 7.22 (m, 1H), 6.81 – 6.75 (m, 1H), 6.69 (td, J = 7.5, 1.2 Hz, 1H); **^{13}C NMR** (75 MHz, DMSO-d_6): δ 163.59, 147.86, 138.86, 133.33, 132.99, 132.46, 128.10, 127.95, 127.56, 127.37, 126.40,

125.84, 124.82, 117.17, 114.94, 114.41; **MS (ESI-HRMS):** *m/z* calcd. for $C_{18}H_{12}N_2O$ [M+H$^+$]: 273.1022, found: 273.1020; 61% yield.

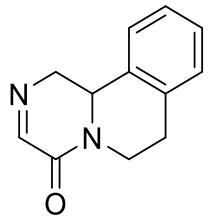

24b, 3,6,7,11b-Tetrahydro-4*H*-pyrazino[2,1-*a*]isoquinolin-4-one: **^{1}H NMR** (300 MHz, $CDCl_3$): δ 7.91 – 7.84 (m, 1H), 7.24 – 7.15 (m, 4H), 4.74 – 4.04 (m, 2H), 3.50 – 3.00 (m, 2H), 3.00 – 2.80 (m, 2H); **^{13}C NMR** (75 MHz, $CDCl_3$): δ 157.32, 134.50, 132.19, 129.54, 127.57, 127.23, 125.79, 122.49, 56.00, 52.41, 37.38, 29.25; **MS (GC-MS):** *m/z* 200 (M$^+$)[32]; 77% yield.

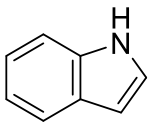

25b, Indole: **^{1}H NMR** (300 MHz, $CDCl_3$): δ 8.10 – 8.04 (m, 1H), 7.81 (ddt, *J* = 7.7, 1.5, 0.8 Hz, 1H), 7.48 (dq, *J* = 8.1, 1.0 Hz, 1H), 7.39 – 7.24 (m, 3H), 6.70 (ddd, *J* = 3.1, 2.0, 1.0 Hz, 1H); **^{13}C NMR** (75 MHz, $CDCl_3$): δ 135.89, 127.97, 124.27, 122.08, 120.84, 119.93, 111.16, 102.67; **MS (GC-MS):** *m/z* 117 (M$^+$)[33]; 79% yield.

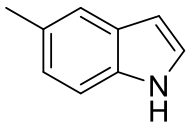

26b, 5-Methylindole: **^{1}H NMR** (300 MHz, $CDCl_3$): δ 7.96 (s, 1H), 7.49 (dd, *J* = 1.7, 0.8 Hz, 1H), 7.30 (d, *J* = 8.3 Hz, 1H), 7.20 – 7.12 (m, 1H), 7.08 (dd, *J* = 8.3, 1.6 Hz, 1H), 6.52 (ddd, *J* = 3.1, 2.1, 1.0 Hz, 1H), 2.51 (s, 3H); **^{13}C NMR** (75 MHz, $CDCl_3$): δ 134.22, 129.11, 128.25, 124.35, 123.72, 120.45, 110.78, 102.19, 21.55; **MS (GC-MS):** *m/z* 131 (M$^+$)[33]; 96% yield.

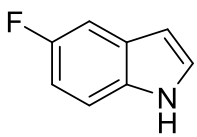

27b, 5-Fluoroindole: **^{1}H NMR** (300 MHz, $CDCl_3$): δ 8.12 (s, 1H), 7.36 – 7.23 (m, 3H), 7.01 – 6.93 (m, 1H), 6.54 (ddd, *J* = 3.1, 2.1, 0.9 Hz, 1H); **^{13}C NMR** (75 MHz, $CDCl_3$): δ 159.65, 156.55, 132.45, 128.40, 128.27, 126.02, 111.76, 111.63, 110.71, 110.36, 105.71, 105.40, 102.96, 102.90, **MS (GC-MS):** *m/z* 135 (M$^+$)[27]; 93% yield.

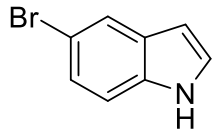

28b, 5-Bromoindole: **^{1}H NMR** (300 MHz, $CDCl_3$): δ 8.14 (s, 1H), 7.81 – 7.76 (m, 1H), 7.34 – 7.18 (m, 3H), 6.51 (ddd, J = 3.1, 2.1, 0.8 Hz, 1H); **^{13}C NMR** (75 MHz, $CDCl_3$): δ 134.52, 129.76, 125.48, 124.98, 123.34, 113.16, 112.56, 102.45; **MS (GC-MS):** *m/z* 195 (M^+)[34]; 91% yield.

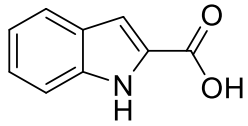

29b, Indole-2-carboxylic acid: **^{1}H NMR** (300 MHz, $CDCl_3$): δ 8.91 (s, 1H), 7.78 – 7.68 (m, 1H), 7.48 – 7.43 (m, 1H), 7.41 – 7.33 (m, 2H), 7.25 – 7.13 (m, 1H); **^{13}C NMR** (75 MHz, $CDCl_3$): δ 166.05, 137.30, 127.48, 126.12, 126.07, 122.90, 121.10, 111.96, 110.87; **MS (GC-MS):** *m/z* 161 (M^+)[35]; 91% yield.

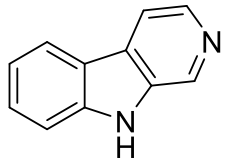

30b, Pyrido[3,4-*b*]indole: **^{1}H NMR** (300 MHz, $CDCl_3$): δ 8.97 (s, 1H), 8.56 (s, 1H), 8.47 (d, J = 5.3 Hz, 1H), 8.15 (d, J = 7.9 Hz, 1H), 7.99 (dd, J = 5.3, 1.1 Hz, 1H), 7.63 – 7.51 (m, 2H), 7.32 (ddd, J = 8.0, 6.3, 1.8 Hz, 1H); **^{13}C NMR** (126 MHz, $CDCl_3$): δ 140.85, 138.31, 135.92, 133.21, 129.58, 129.05, 122.03, 121.46, 120.51, 115.02, 111.88; **MS (GC-MS):** *m/z* 168 (M^+)[36]; 78% yield.

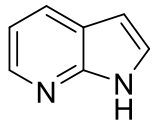

31b, Pyrrolo[2,3-*b*]pyridine: **^{1}H NMR** (300 MHz, $CDCl_3$): δ 11.86 (s, 1H), 8.38 (dd, J = 4.8, 1.6 Hz, 1H), 7.99 (dd, J = 7.8, 1.6 Hz, 1H), 7.42 (d, J = 3.5 Hz, 1H), 7.11 (dd, J = 7.8, 4.8 Hz, 1H), 6.53 (d, J = 3.5 Hz, 1H); **^{13}C NMR** (75 MHz, $CDCl_3$): δ 149.04, 142.36, 129.16, 125.50, 120.72, 115.81, 100.64; **MS (GC-MS):** *m/z* 118 (M^+)[37]; 97% yield.

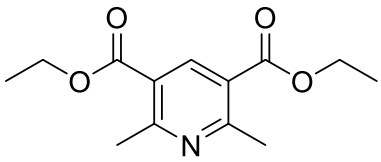

32b, Diethyl 2,6-dimethylpyridine-3,5-dicarboxylate: **^{1}H NMR** (300 MHz, $CDCl_3$): δ 8.66 (s, 1H), 4.38 (q, J = 7.1 Hz, 4H), 2.83 (s, 6H), 1.40 (t, J = 7.1 Hz, 6H); **^{13}C NMR** (75 MHz, $CDCl_3$): δ 166.09, 162.34, 141.02, 123.20, 61.53, 25.09, 14.41; **MS (GC-MS):** *m/z* 251 (M^+)[38]; 99% yield.

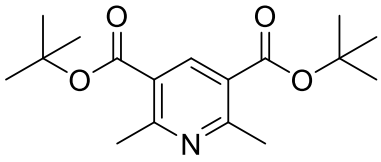

33b, Di-*tert*-butyl-2,6-dimethylpyridine-3,5-dicarboxylate: **^{1}H NMR** (300 MHz, $CDCl_3$): δ 8.52 (s, 1H), 2.80 (s, 6H), 1.61 (s, 18H); **^{13}C NMR** (75 MHz, $CDCl_3$): δ 175.17, 161.28, 140.90, 124.79, 82.25, 28.37, 25.13; **MS (GC-MS):** *m/z* 307 (M^+)[39]; 95% yield.

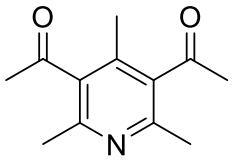

34b, 1,1‘-(2,4,6-Trimethylpyridine-3,5-diyl)bis(ethan-1-one): **^{1}H NMR** (300 MHz, $CDCl_3$): δ 2.49 (s, 6H), 2.43 (s, 6H), 2.11 (s, 3H); **^{13}C NMR** (75 MHz, $CDCl_3$): δ 205.91, 152.01, 137.60, 135.69, 32.38, 22.61, 16.10; **MS (GC-MS):** *m/z* 205 (M^+)[40]; 98% yield.

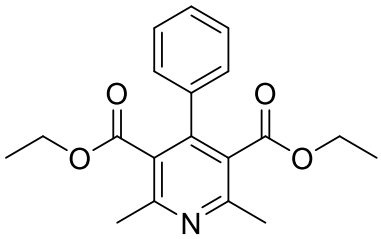

35b, Diethyl-2,6-dimethyl-4-phenylpyridine-3,5-dicarboxylate: **^{1}H NMR** (300 MHz, $CDCl_3$): δ 7.41 – 7.30 (m, 3H), 7.30 – 7.20 (m, 2H), 3.99 (q, J = 7.1 Hz, 4H), 2.60 (s, 6H), 0.89 (t, J = 7.1 Hz, 6H); **^{13}C NMR** (75 MHz, $CDCl_3$): δ 167.99, 155.54, 146.23, 136.72, 128.52, 128.23, 128.18, 127.05, 61.44, 23.04, 13.67; **MS (GC-MS):** *m/z* 327 (M^+)[41]; 99% yield.

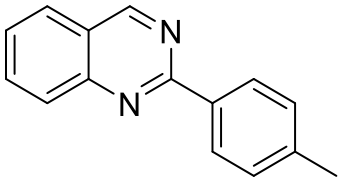

36b, 2-*p*-Tolylquinazoline: ^{1}H NMR (300 MHz, $CDCl_3$): δ 9.47 (s, 1H), 8.55 – 8.52 (m, 2H), 8.11 – 8.07 (m, 1H), 7.95 – 7.89 (m, 2H), 7.64 – 7.59 (m, 1H), 7.38 – 7.34 (m, 2H), 2.47 (s, 3H); **^{13}C NMR** (75 MHz, $CDCl_3$): δ 161.29, 160.55, 150.95, 140.99, 135.47, 134.15, 129.54, 128.70, 128.67, 128.67, 127.24, 127.15, 123.66, 21.65; **MS (GC-MS)**: *m/z* 220 $(M^+)^{[42]}$; 88% yield.

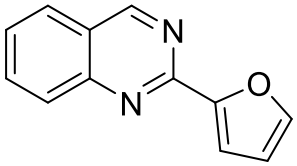

37b, 2-(Furan-2-yl)quinazoline: **^{1}H NMR** (300 MHz, $CDCl_3$): δ 9.41(s, 1H), 8.14 – 8.10 (m, 1H), 7.95 – 7.90 (m, 2H), 7.72 – 7.71 (m, 1H), 7.65 – 7.60 (m, 1H), 7.47 – 7.49 (m, 1H), 6.65 – 6.63 (m, 1H); **^{13}C NMR** (75 MHz, $CDCl_3$): δ 160.7, 150.5, 145.3, 134.5, 128.4, 127.3, 123.4, 114.1, 112.3; **MS (GC-MS)**: *m/z* 196 $(M^+)^{[42]}$; 86% yield.

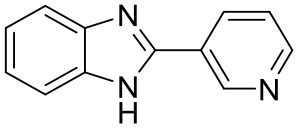

38b, 2-(Pyridin-3-yl)benzimidazole: ^{1}H NMR (300 MHz, $CDCl_3$): δ 9.07 – 9.06 (m, 1H), 8.72 – 8.69 (m, 1H), 8.31 – 8.28 (m, 1H), 7.45 – 7.40 (m, 1H), 7.15 – 7.10 (m, 2H), 6.83 – 6.76 (m, 2H); **^{13}C NMR** (75 MHz, $CDCl_3$): δ 153.99, 151.72, 150.72, 142.73, 136.34, 134.84, 132.18, 128.51, 123.79, 118.47, 117.03, 115.69; **MS (GC-MS)**: *m/z* 195 $(M^+)^{[43]}$; 91% yield.

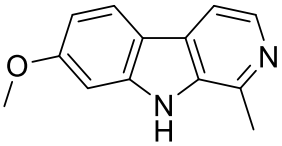

39b, Harmine: ^{1}H NMR (300 MHz, $CDCl_3$): δ 8.15 (s, 1H), 7.47 (dd, J = 8.6, 0.7 Hz, 2H), 7.01 – 6.72 (m, 3H), 3.86 (s, 3H), 2.35 (s, 3H); **^{13}C NMR** (126 MHz, DMSO-d_6): δ 157.12, 156.72, 137.48, 128.51, 120.35, 119.39, 114.53, 110.20, 94.55, 55.14, 47.61, 22.01; **MS (ESI-HRMS):** *m/z* calcd. for $C_{13}H_{12}N_2O$ $[M+H^+]$: 213.1022, found: 213.1024; yield: 71% (CO_2 balloon), 45% (0.2 eq. CO_2, 16 h), 54% (0.2 eq. CO_2, 24 h), 58% (0.2 eq. CO_2, 40 h).

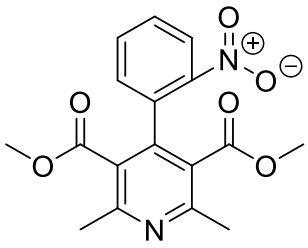

40b, Dehydronifedipine: ^{1}H NMR (300 MHz, $CDCl_3$): δ 7.49 – 7.28 (m, 4H), 2.49 (s, 6H), 2.43 (s, 6H); **^{13}C NMR (75 MHz, $CDCl_3$):** δ 164.49, 130.74, 130.50, 129.70, 126.88, 52.19, 33.31; **MS (ESI-HRMS):** *m/z* calcd. for $C_{17}H_{16}N_2O_6$ [M+H$^+$]: 345.1081, found: 345.1078; yield: 84% (CO_2 balloon), 72% (0.2 eq. CO_2, 16 h), 74% (0.2 eq. CO_2, 24 h).

8. References

[1] Chen, L.; Zhang, L.; Lv, J.; Cheng, J.-P.; Luo, S. Catalytic Enantioselective *tert*-Aminocyclization by Asymmetric Binary Acid Catalysis (ABC): Stereospecific 1,5-Hydrogen Transfer. *Chem. Eur. J.* **2012**, *18*, 8891–8895.

[2] (a) Neese, F. The ORCA program system. *WIREs: Comp. Mol. Sci.* **2012**, *2*, 73–78. (b) Neese, F. The ORCA program system. *WIREs: Comp. Mol. Sci.* **2018**, *8*, e1327.

[3] Zhao, Y.; Truhlar, D. G. The M06 suite of density functionals for main group thermochemistry, thermochemical kinetics, noncovalent interactions, excited states, and transition elements: two new functionals and systematic testing of four M06-class functionals and 12 other functionals. *Theor. Chem. Acc.* **2008**, *120*, 215–241.

[4] Grimme, S.; Antony J.; Ehrlich S.; Krieg J. A consistent and accurate *ab initio* parametrization of density functional dispersion correction (DFT-D) for the 94 elements H–Pu. *J. Chem. Phys.* **2010**, *132*, 154104.

[5] Weigend, F.; Ahlrichs, R. Balanced basis sets of split valence, triple zeta valence and quadruple zeta valence quality for H to Rn: Design and assessment of accuracy. *Phys. Chem. Chem. Phys.* **2005**, *7*, 3297–3305.

[6] Barone, V.; Cossi, M. Quantum Calculation of Molecular Energies and Energy Gradients in Solution by a Conductor Solvent Model. *J. Phys. Chem. A* **1998**, *102*, 1995–2001.

[7] (a) Riplinger, C.; Sandhoefer, B.; Hansen, A.; Neese F. Nature triple excitations in local coupled cluster calculations with pair natural orbitals. *J. Chem. Phys.* **2013**, *139*, 134101. (b) Liakos, D. G.; Sparta, M.; Kesharwani, M. K.; Martin, J. M.; Neese, F. Exploring the Accuracy Limits of Local Pair Natural Orbital Coupled-Cluster Theory. *J. Chem. Theory Comput.* **2015**, *11*, 1525–1539. (c) Liakos, D.G.; Neese, F. Is It Possible To Obtain Coupled Cluster Quality Energies at near Density Functional Theory Cost? Domain-Based Local Pair Natural Orbital Coupled Cluster vs Modern Density Functional Theory. *J. Chem. Theory Comput.* **2015**, *11*, 4054–4063. (d) Liakos, D. G.; Neese, F. Improved Correlation Energy Extrapolation Schemes Based on Local Pair Natural Orbital Methods. *J. Phys. Chem. A* **2012**, *116*, 4801–4816.

[8] (a) Klamt, A. Conductor-like Screening Model for Real Solvents: A New Approach to the Quantitative Calculation of Solvation Phenomena. *J. Phys. Chem.* **1995**, *99*, 2224–2235. (b) Klamt, A. Refinement and Parametrization of COSMO-RS. *J. Phys. Chem. A* **1998**, *102*, 5074–5085.

[9] (a) Eckert, F.; Klamt, A. Fast solvent screening *via* quantum chemistry: COSMO-RS approach. *AIChE Journal* **2002**, *48*, 369–385. (b) Klamt, A.; *WIRes: Comp. Mol. Sci.* **2018**, *8*, e1338.

[10] Ahlrichs, R.; Bär, M.; Häser, M.; Horn, H.; Kölmel, C. Electronic structure calculations on workstation computers: The program system turbomole. *Chem. Phys. Lett.* **1989**, *162*, 165–169.

[11] Treutler, O.; Ahlrichs, R. Efficient molecular numerical integration schemes. *J. Chem. Phys.* **1995**, *102*, 346–354.

[12] Schäfer, A.; Horn, H.; Ahlrichs, R. Fully optimized contracted Gaussian basis sets for atoms Li to Kr. *J. Chem. Phys.* **1992**, *97*, 2571–2577.

[13] Li, J.; Fisher, C.; Chen, J.; Bashford, D.; Noodleman, L. Calculation of Redox Potentials and pK_a Values of Hydrated Transition Metal Cations by a Combined Density Functional and Continuum Dielectric Theory. *Inorg. Chem.* **1996**, *35*, 4694–4702.

[14] *IUPAC. Compendium of Chemical Terminology, 2nd ed.* (the "Gold Book") **1997.**

[15] Ziarati, A.; Badiei, A.; Ziarani, G. M.; Eskandarloo, H. Simultaneous photocatalytic and catalytic activity of p–n junction NiO@anatase/rutile-TiO_2 as a noble-metal free reusable nanoparticle for synthesis of organic compounds. *Catal. Commun.* **2017**, *95*, 77–82.

[16] Liu, M.; Wang, J.; Yuan, X.; Jiang, R.; Fu, N. One-pot synthesis of *trans-β*-lactams from ferrocenylketene generated by thermal Wolff rearrangement. *Synth. Commun.* **2017**, *47*, 2369–2377.

[17] Stemmler, T.; Surkus, A. E.; Pohl, M. M.; Junge, K.; Beller, M. Iron-Catalyzed Synthesis of Secondary Amines: On the Way to Green Reductive Aminations. *ChemSusChem* **2014**, *7*, 3012–3016.

[18] Saranya, S.; Ramesh, R.; Malecki, J. G. One-Pot Catalytic Approach for the Selective Aerobic Synthesis of Imines from Alcohols and Amines Using Efficient Arene Diruthenium(II) Catalysts under Mild Conditions. *Eur. J. Org. Chem.* **2017**, 6726–6733.

[19] López, F. I.; de la Cruz, F. N.; López, J.; Martínez, J. M.; Alcaraz, Y.; Delgado, F.; Sánches-Recillas, A.; Estrada-Soto, S.; Vázquez, M. A. A simple method for the synthesis of 1,3-diaminopropan-2-ols derivatives and their *ex vivo* relaxant activity on isolated rat tracheal rings. *Med. Chem. Res.* **2017**, *26*, 1325–1345.

[20] Kuppuswamy, U.; Krishnakumar, K.; Bhat, A. A Mechanism-Based Kinetic Analysis of Succinimide-Mediated Deamidation, Racemization, and Covalent Adduct Formation in a Model Peptide in Amorphous Lyophiles. *J. Pharm. Res.* **2012**, *5*, 3096–3109.

[21] Solic, I.; Reich, D.; Lim, J.; Bates, R. W. Bimetallic Catalysis: Palladium/Lanthanide co-Catalyzed Allylation of Anilines. *Asian J. Org. Chem.* **2017**, *6*, 658–661.

[22] Bananezhad, B.; Islami, M. R. Stereoselective Synthesis of 3-(5-Benzoyl-1-methyl-1*H*-pyrrol-2-yl)-2-azetidinone Derivatives via an in Situ Generated Ketene. *Synlett* **2017**, *28*, 1453–1456.

[23] García Ruano, J. L.; Alemán, J.; Alonso, I.; Parra, A.; Marcos, V.; Aguirre, J. π-π Stacking versus Steric Effects in Stereoselectivity Control: Highly Diastereoselective Synthesis of *syn*-1,2-Diarylpropylamines. *Chem. Eur. J.* **2007**, *13*, 6179–6195.

[24] Chen, G.; Gao, W.; Wang, X.; Huo, H.; Li, W.; Zhang, L.; Li, R.; Li, Z. Magnetic NiO nanoparticles confined within open ends MWCNTs: a novel and highly active catalyst for hydrogenation and synthesis of imines. *RSC Adv.* **2016**, *63*, 58805–58812.

[25] Ji, F.; Li, J.; Li, X.; Guo, W.; Wu, W.; Jiang, H. Carbonylation Access to Phthalimides Using Self-Sufficient Directing Group and Nucleophile. *J. Org. Chem.* **2018**, *83*, 104–112.

[26] Deb, M. L.; Pegu, C. D.; Borpatra, P. J.; Saikia, P. J.; Baruah, P. K. Catalyst-free multi-component cascade C–H-functionalization in water using molecular oxygen: an approach to 1,3-oxizanes. *Green Chem.* **2017**, *19*, 4036–4042.

[27] Zhang, J.; Chen, S.; Chen, F.; Xu, W.; Deng, G.-J.; Gong, H. Dehydrogenation of Nitrogen Heterocycles Using Graphene Oxide as a Versatile Metal-Free Catalyst under Air. *Adv. Synth. Catal.* **2017**, *359*, 2358–2363.

[28] Barta, P.; Szatmári, I.; Fülöp, F.; Hexdenreich, M.; Koch, A.; Kleinpeter, E. Synthesis and stereochemistry of new naphth[1,3]oxazino[3,2-*a*]benzazepine and naphth[1,3]oxazino[3,2-*e*]thienopyridine derivatives. *Tetrahedron* **2016**, *72*, 2402–2410.

[29] Pardeshi, S. D.; Sathe, P. A.; Vadagaonkar, K. S.; Chaskar, A. C. One-Pot Protocol for the Synthesis of Imidazoles and Quinoxalines using *N*-Bromosuccinimide. *Adv. Synth. Catal.* **2017**, *359*, 4217–4226.

[30] Evoniuk, C. J.; dos Passos Gomes, G.; Hill, S. P.; Fujita, S.; Hanson, K.; Alabugin, I. V. Coupling N–H Deprotonation, C–H Activation, and Oxidation: Metal-Free C(sp^3)–H Aminations with Unprotected Anilines. *J. Am. Chem. Soc.* **2017**, *139*, 16210–16221.

[31] Wang, M.; Fan, Q.; Jiang, X. Nitrogen–Iodine Exchange of Diaryliodonium Salts: Access to Acridine and Carbazole. *Org. Lett.* **2018**, *20*, 216–219.

[32] Yang, Z.; Guo, X.; Xu, S.; Jiao, H.; Tan, Z.; Zhang, F. One-Pot Palladium-Catalyzed Racemization of *(S)*-Praziquanamine: A Key Intermediate for the Anthelmintic Agent *(R)*-Praziquantel. *Heterocycles* **2017**, *94*, 122–130.

[33] Llabres-Campaner, P. J.; Ballesteros-Garrido, R.; Ballesteros, R.; Abarca, B. Straight Access to Indoles from Anilines and Ethylene Glycol by Heterogneous Acceptorless Dehydrogenative Condensation. *J. Org. Chem.* **2018**, *83*, 521–526.

[34] Sahoo, M. K.; Jaiswal, G.; Rana, J.; Balaraman, E. Organo-Photoredox Catalyzed Oxidative Dehydrogenation of *N*-Heterocycles. *Chem. Eur. J.* **2017**, *23*, 14167–14172.

[35] Jiang, T.; Liu, N.; Jiang, Y.-W.; Ye, P.-P.; Xu, W.-M. A Practical Synthesis of Indole-2-carboxylic Acid. *Org. Prep. Proced. Int.* **2017**, *49*, 476–478.

[36] Durham, S. D.; Sierra, B.; Gomez, M. J.; Tran, J. K.; Anderson, M. O.; Whittington-Davis, N. A.; Eagon, S. Synthesis of *β*-carbolines *via* a silver-mediated oxidation of tetrahydro-*β*-carbolines. *Tetrahedron Lett.* **2017**, *58*, 2747–2750.

[37] Pires, M. J. D.; Poeira, D. L.; Purificacao, S. I.; Marques, M. M. B. Synthesis of Substituted 4-, 5-, 6-, and 7-Azaindoles from Aminopyridines *via* a Cascade C–N Cross-Coupling/Heck Reaction. *Org. Lett* **2016**, *18*, 3250–3253.

[38] Buzzetti, L.; Prieto, A.; Roy, S. R.; Melchiorre, P. Radical-Based C–C Bond-Forming Processes Enabled by the Photoexcitation of 4-Alkyl-1,4-dihydropyridines. *Angew. Chem. Int. Ed.* **2017**, *56*, 15039–15043.

[39] Yan, Y.; Li, H.; Li, Z.; Niu, B.; Shi, M.; Liu, M. Copper-Catalyzed Oxidative Coupling of *β*-Keto Esters with *N*-Methylamides for the Synthesis of Symmetrical 2,3,5,6-Tetraysubstituted Pyridines. *J. Org. Chem.* **2017**, *82*, 8628–8633.

[40] Lu, Z.; Yang, Y.-Q.; Li, H.-X. Photoinduced Aromatization of Dihydropyridines. *Synthesis* **2016**, *48*, 4221–4227.

[41] Wang, C.; Lu, Z. Intermolecular [2+2] Cycloaddition of 1,4-Dihydropyridines with Olefins *via* Energy Transfer. *Org. Lett.* **2017**, *19*, 5888–5891.

[42] Ma, J.; Wan, Y.; Hong, C.; Li, M.; Hu., X.; Mo, W.; Hu, B.; Sun, N.; Jin, L.; Shen, Z. ABNO-Catalyzed Aerobic Oxidative Synthesis of 2-Substituted 4*H*-3,1-Benzoxazines and Quinazolines. *Eur. J. Org. Chem.* **2017**, 3335–3342.

[43] Nguyen, T. B.; Ermolenko, L.; Al-Mourabit; A. Selective autoxidation of benzylamines: application to the synthesis of some nitrogen heterocycles. *Green Chem.* **2013**, *15*, 2713–2717.

9. NMR spectra

1b

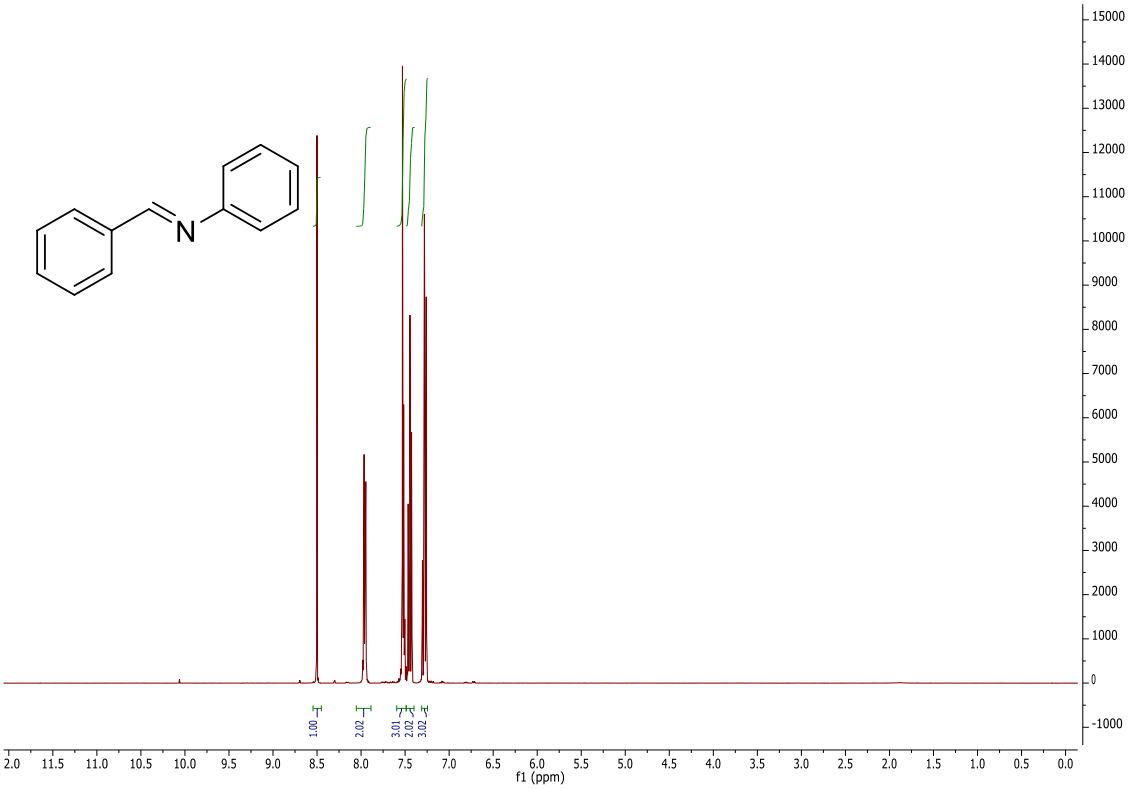

^{1}H NMR spectrum in $CDCl_3$.

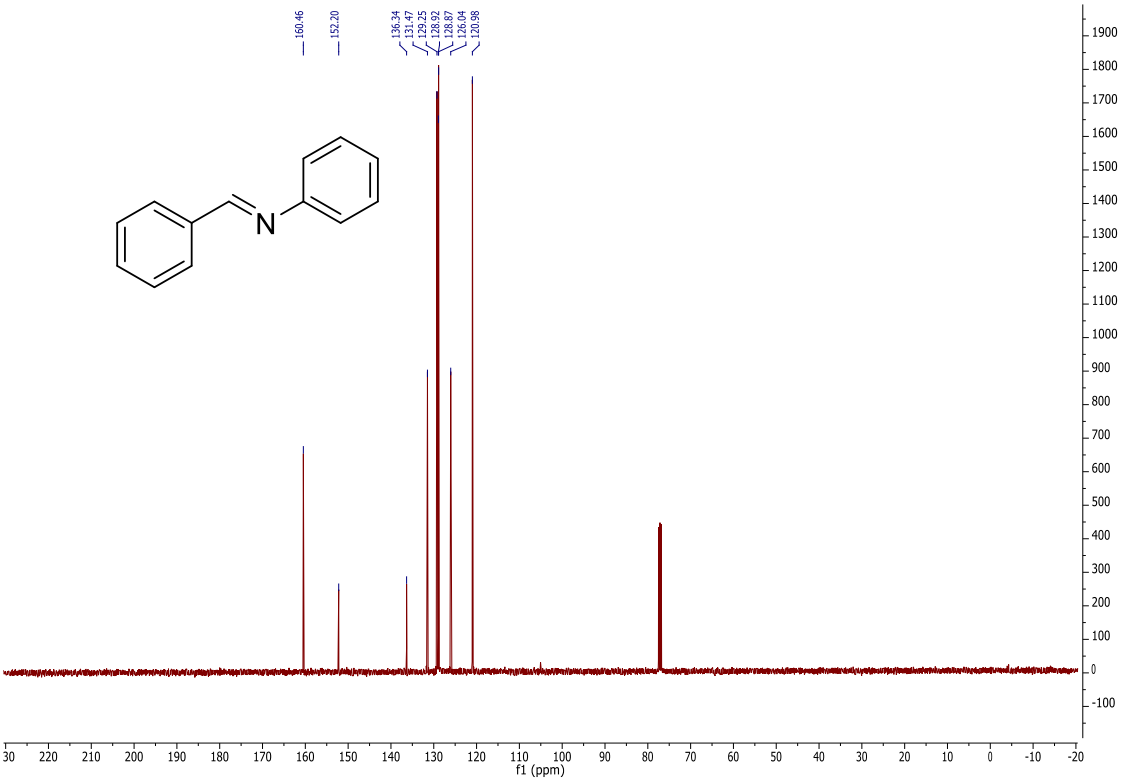

^{13}C NMR spectrum in $CDCl_3$.

2b

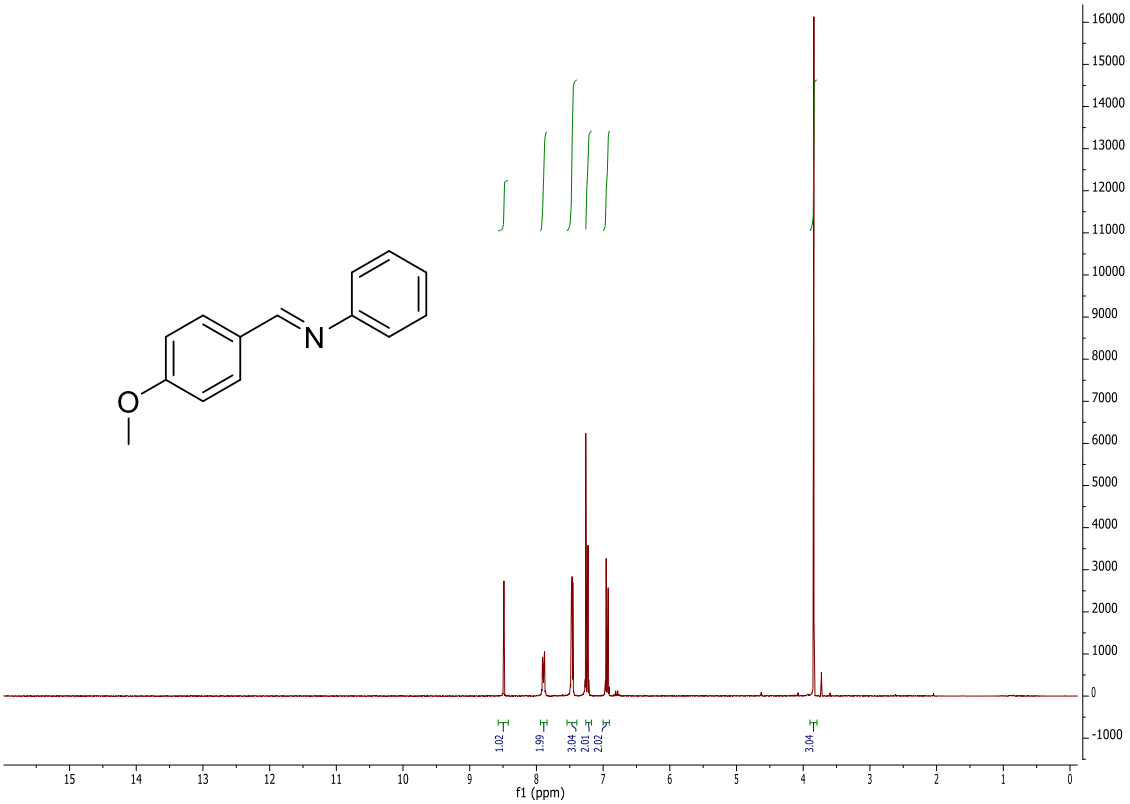

^{1}H NMR spectrum in $CDCl_3$.

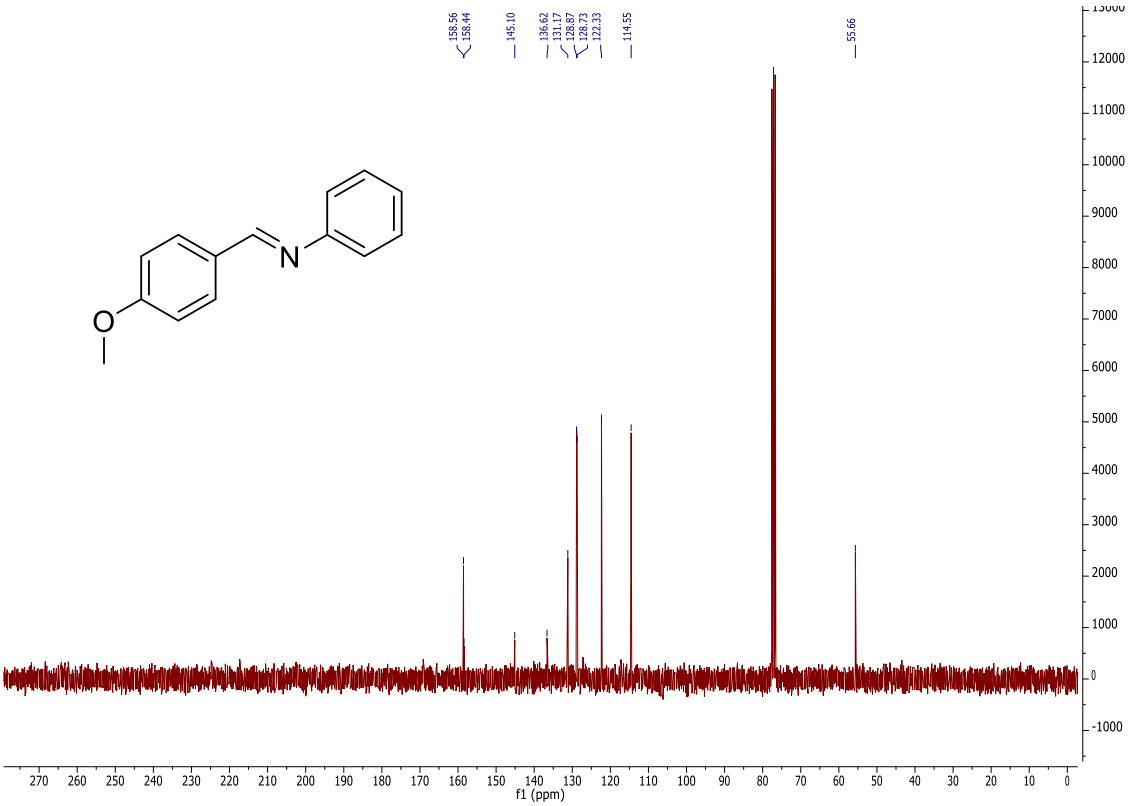

^{13}C NMR spectrum in $CDCl_3$.

3b

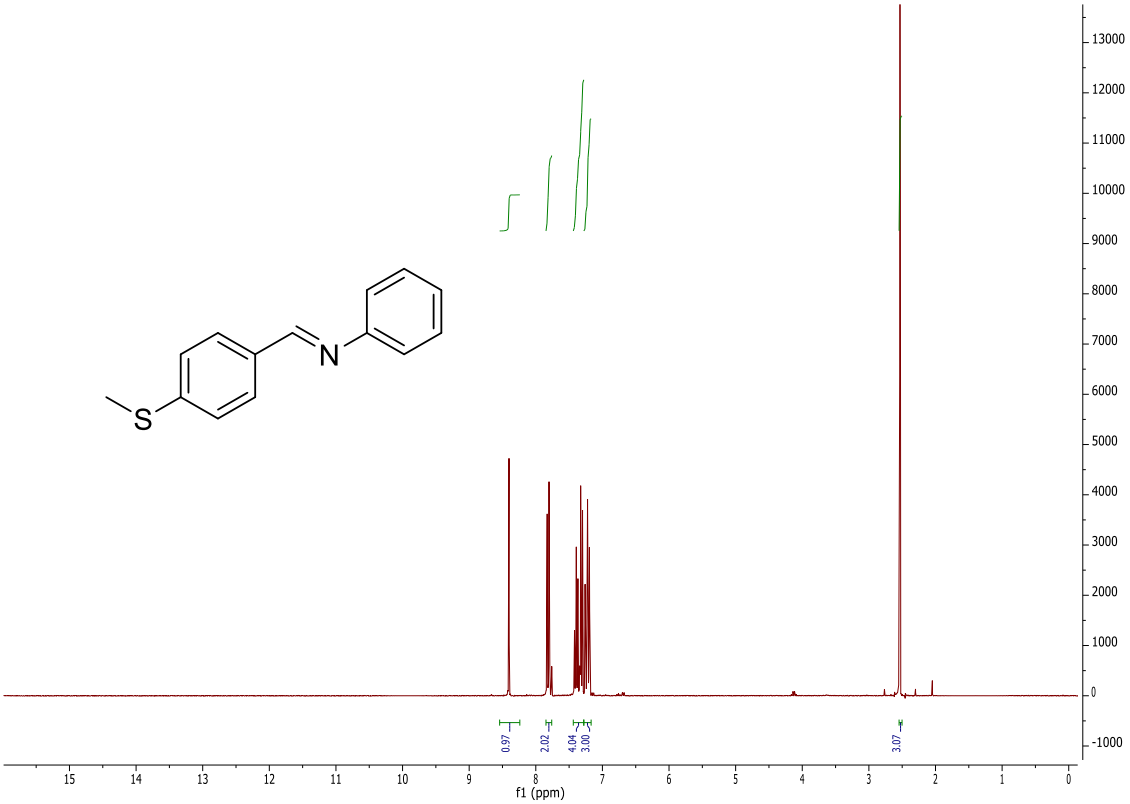

^{1}H NMR spectrum in $CDCl_3$.

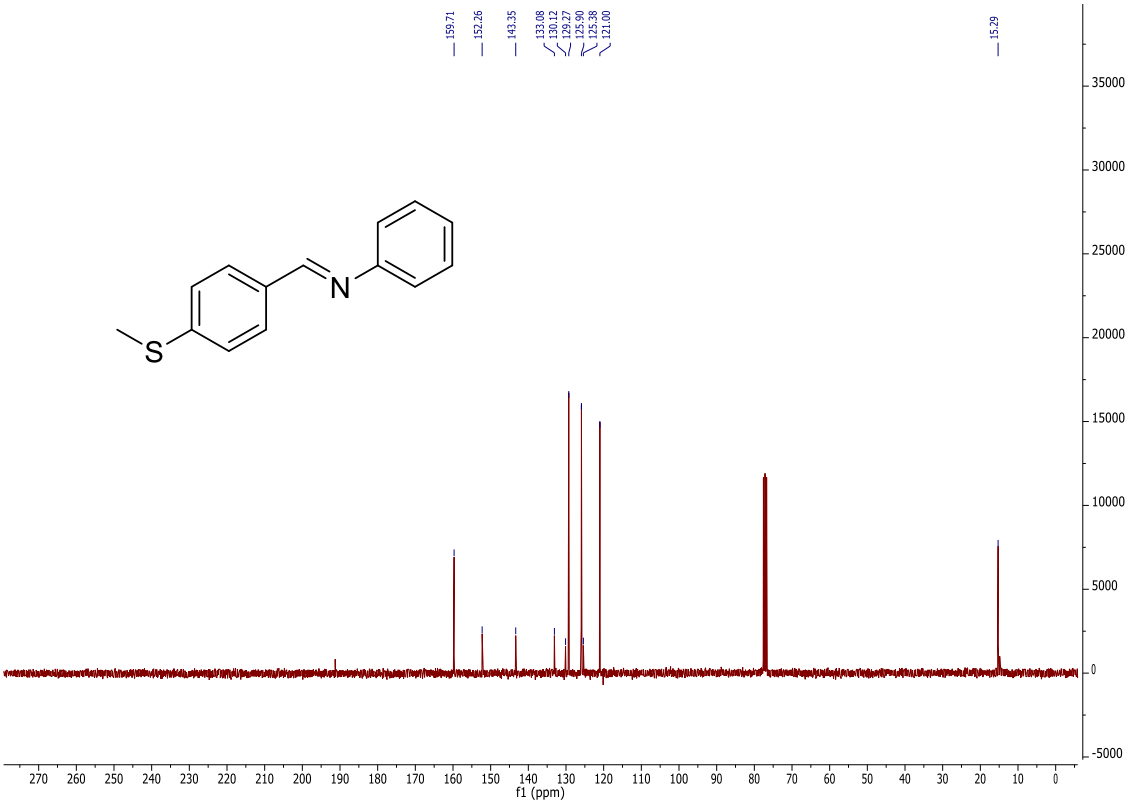

^{13}C NMR spectrum in $CDCl_3$.

4b

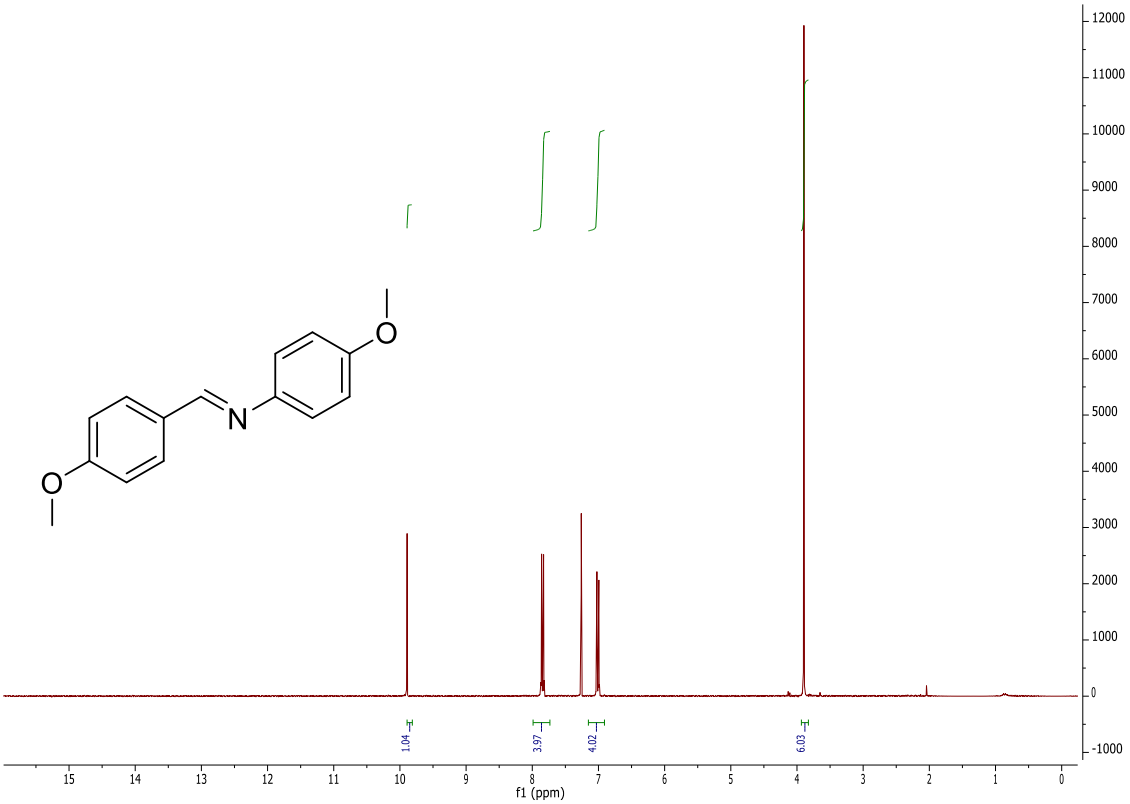

^{1}H NMR spectrum in $CDCl_3$.

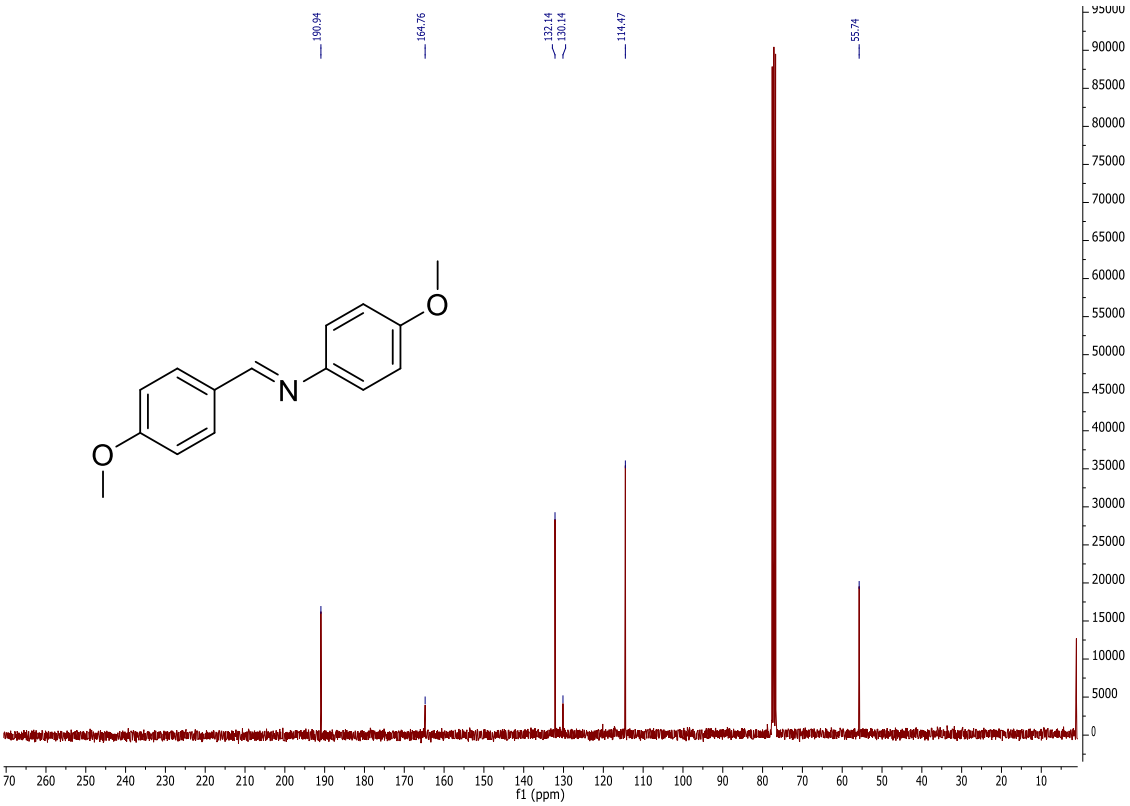

^{13}C NMR spectrum in $CDCl_3$.

5b

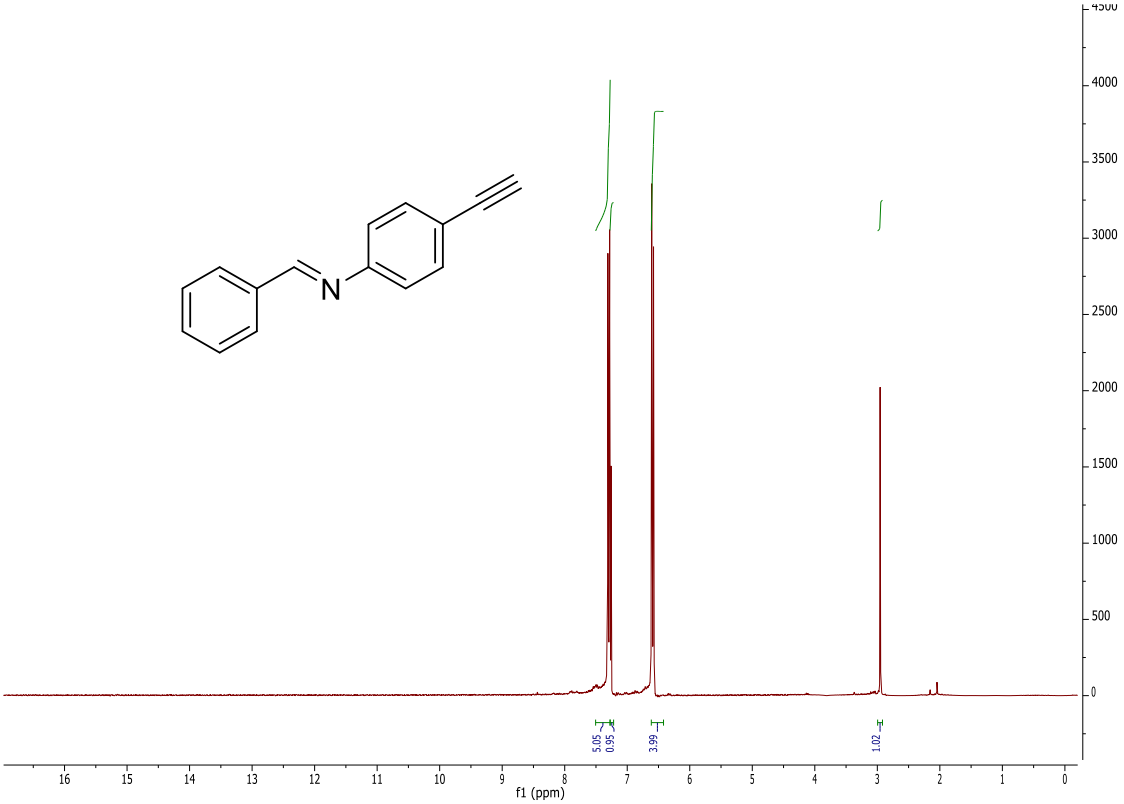

^{1}H NMR spectrum in $CDCl_3$.

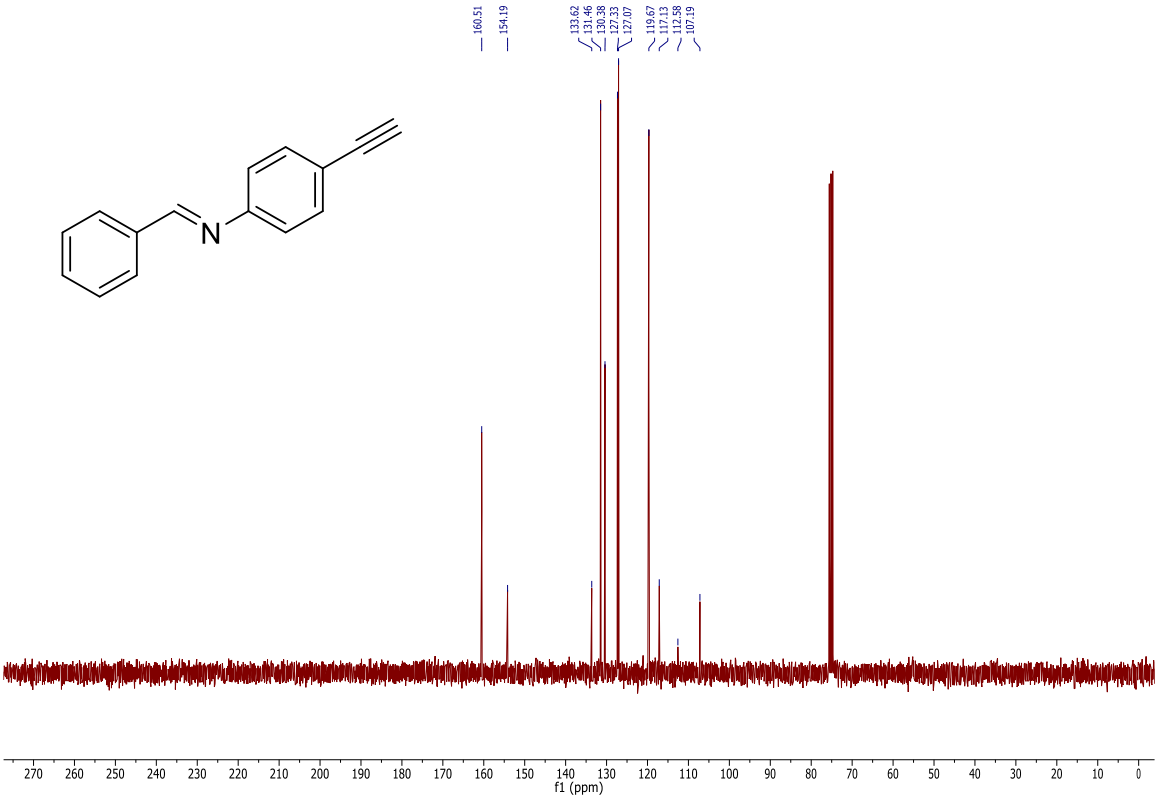

^{13}C NMR spectrum in $CDCl_3$.

6b

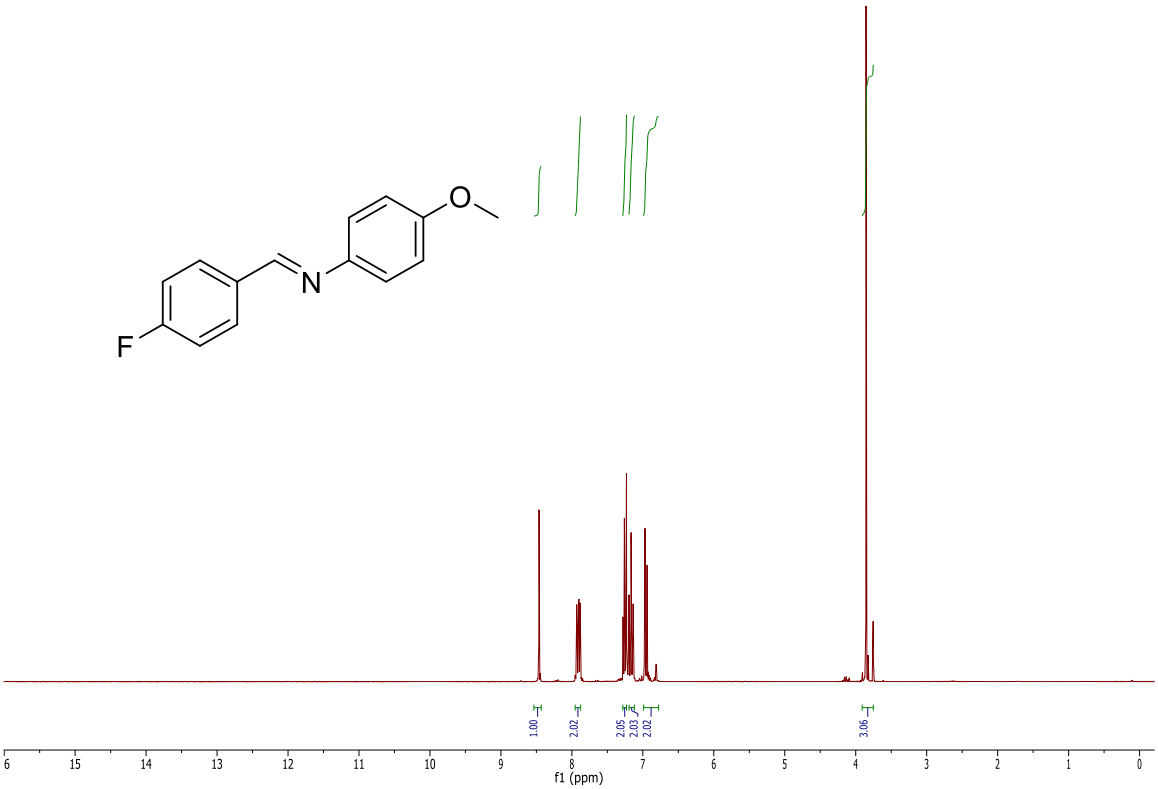

^{1}H NMR spectrum in $CDCl_3$.

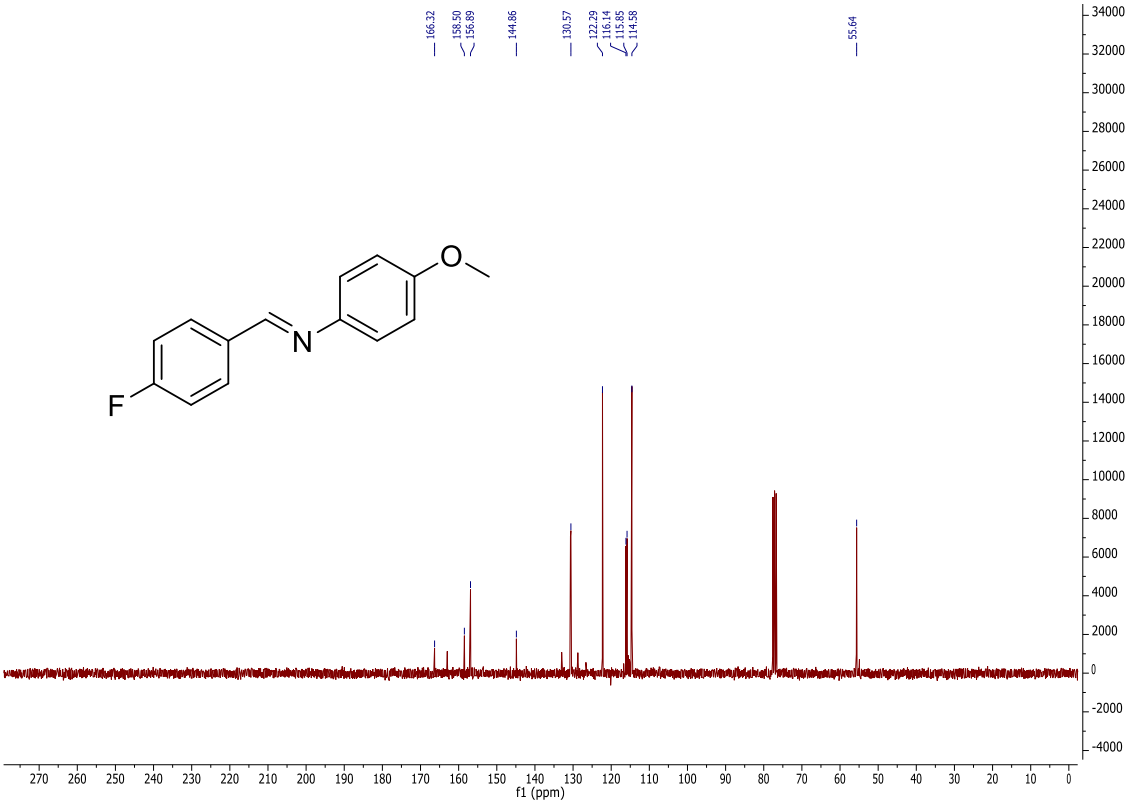

^{13}C NMR spectrum in $CDCl_3$.

7b

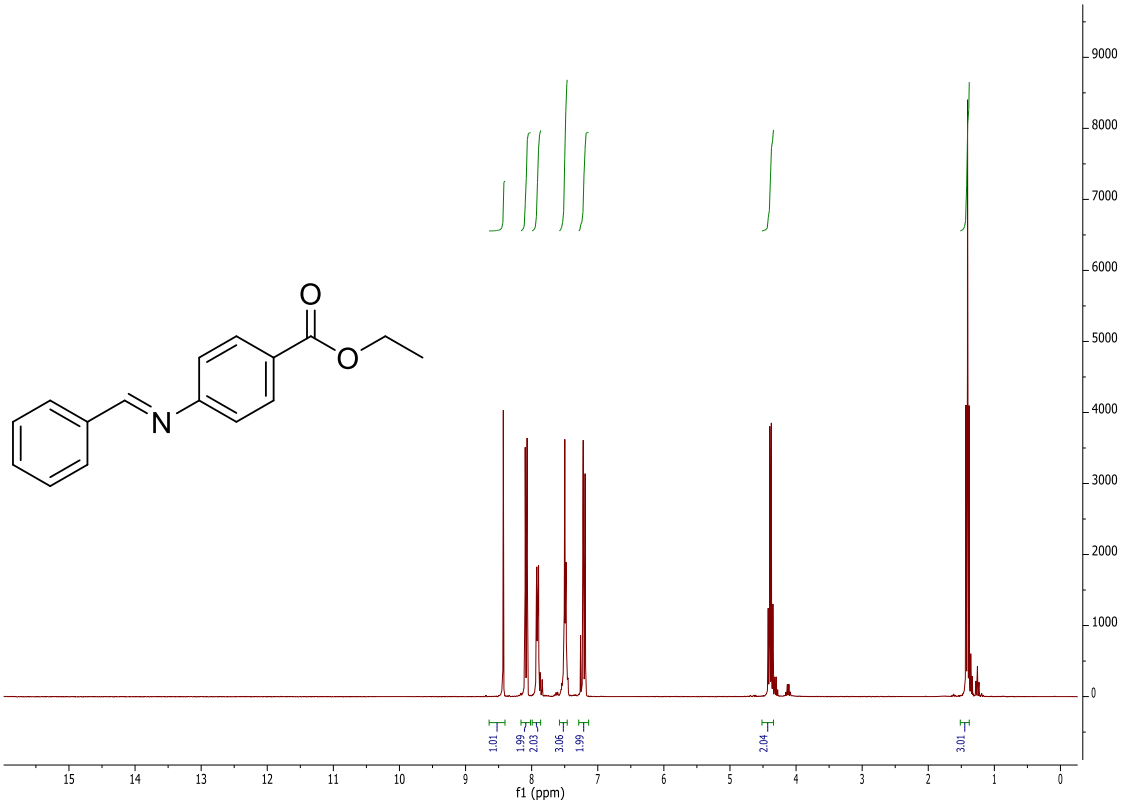

^{1}H NMR spectrum in $CDCl_3$.

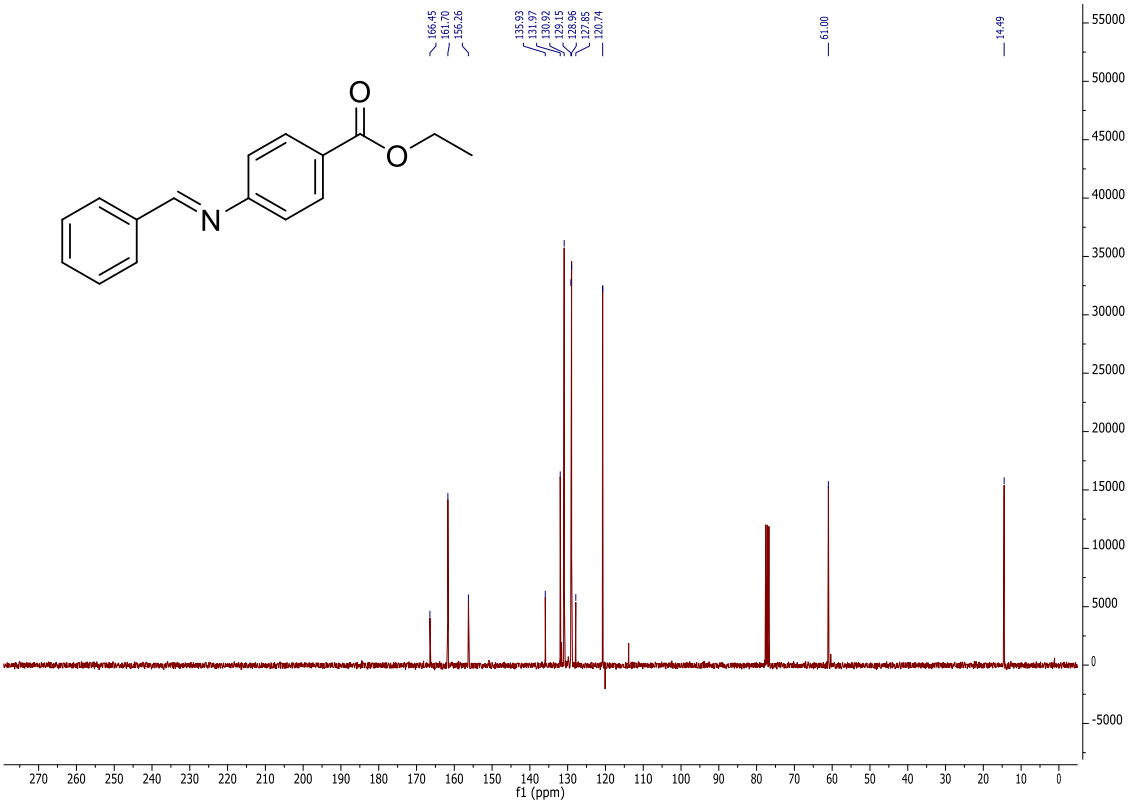

^{13}C NMR spectrum in $CDCl_3$.

8b

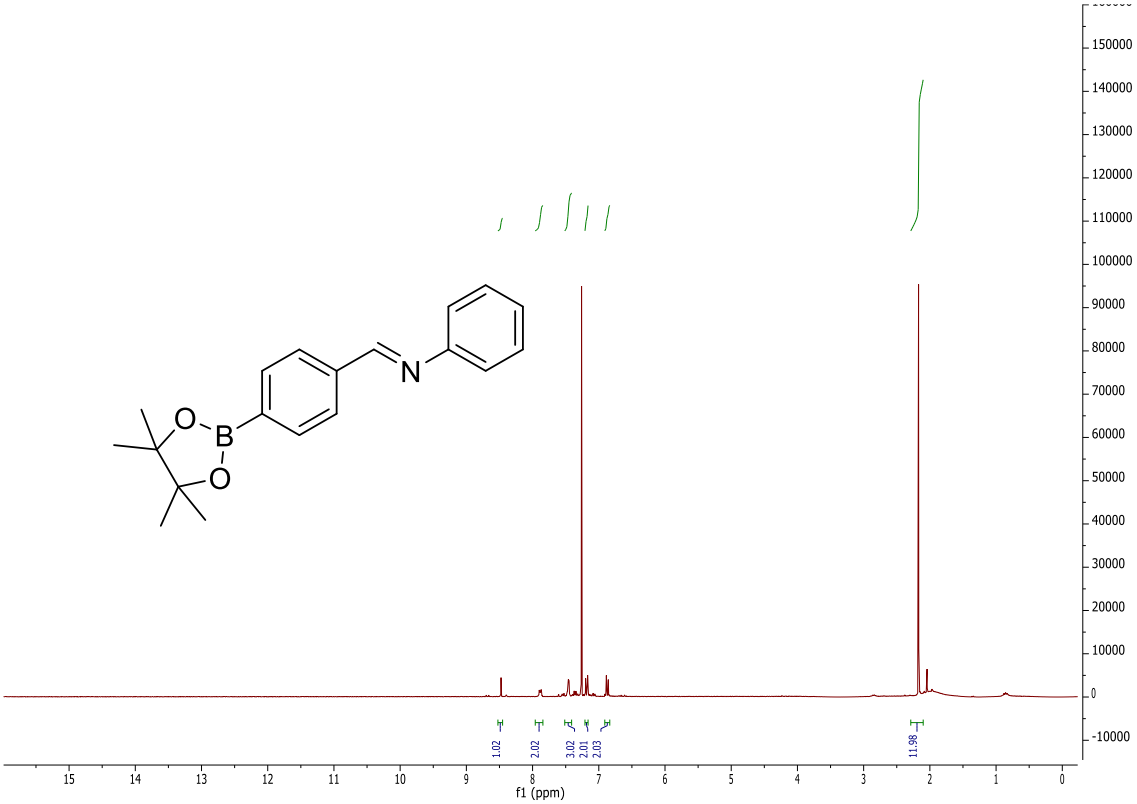

^{1}H NMR spectrum in $CDCl_3$.

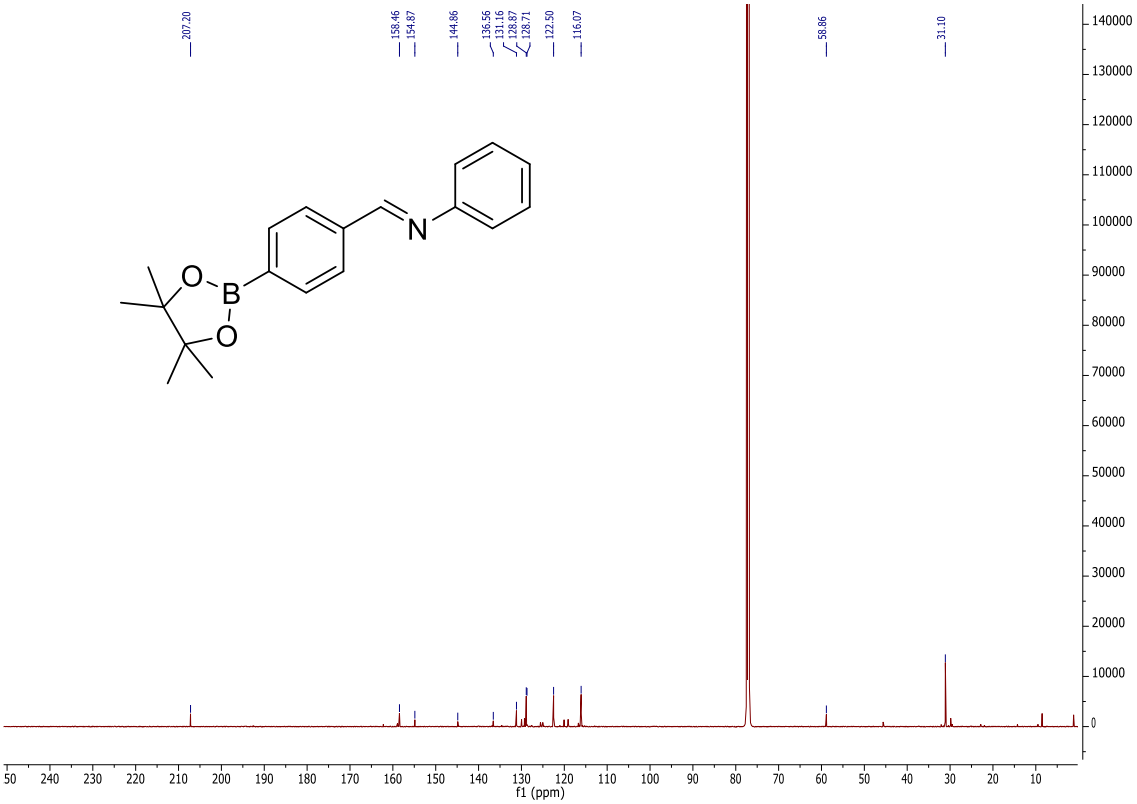

^{13}C NMR spectrum in $CDCl_3$.

9b

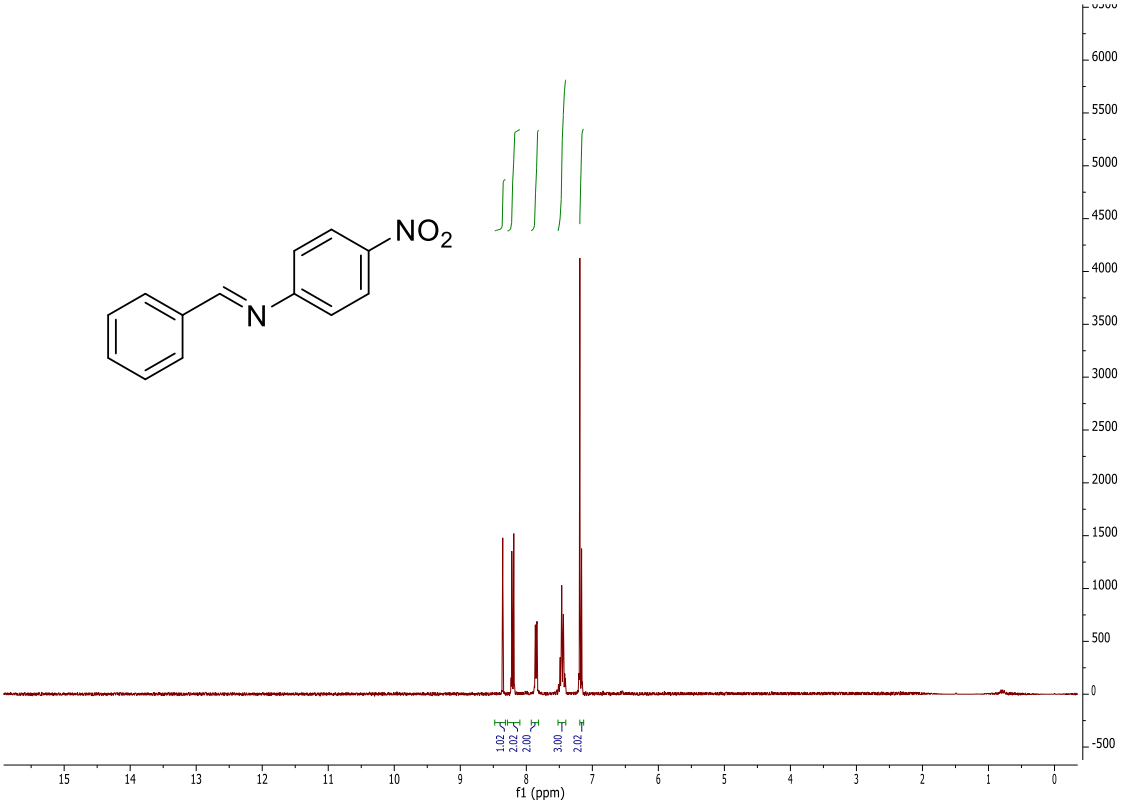

^{1}H NMR spectrum in $CDCl_3$.

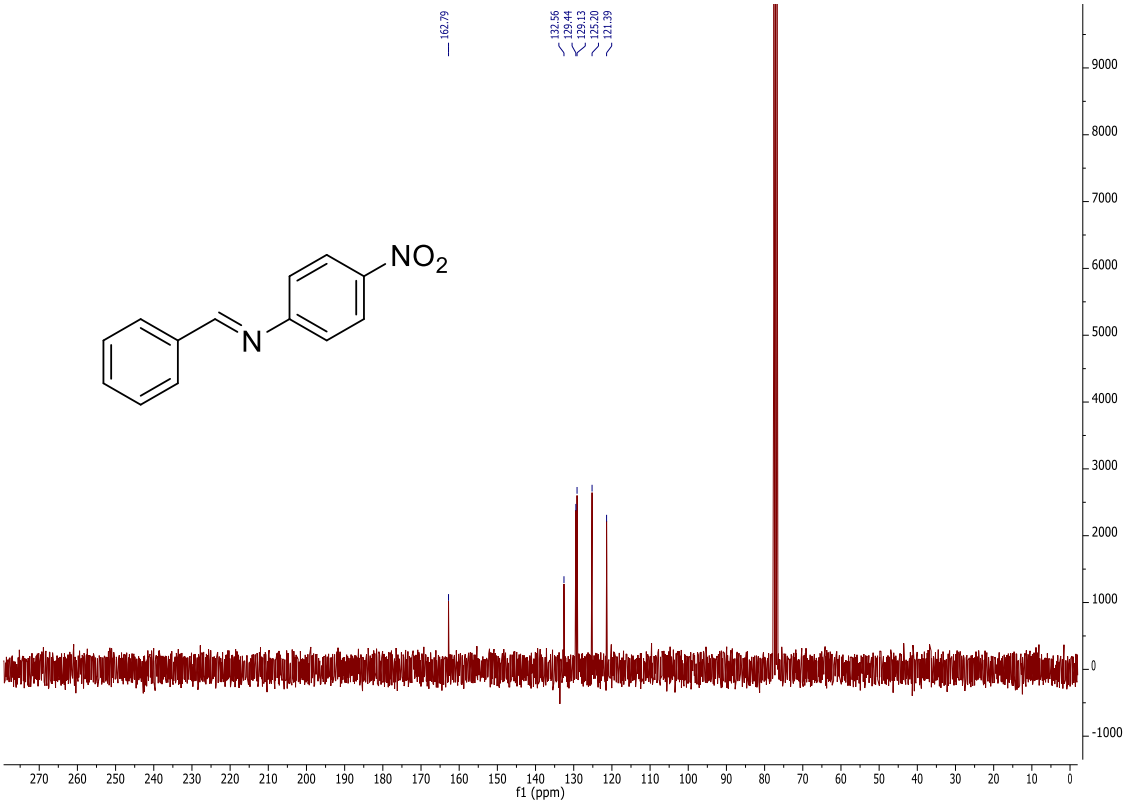

^{13}C NMR spectrum in $CDCl_3$.

10b

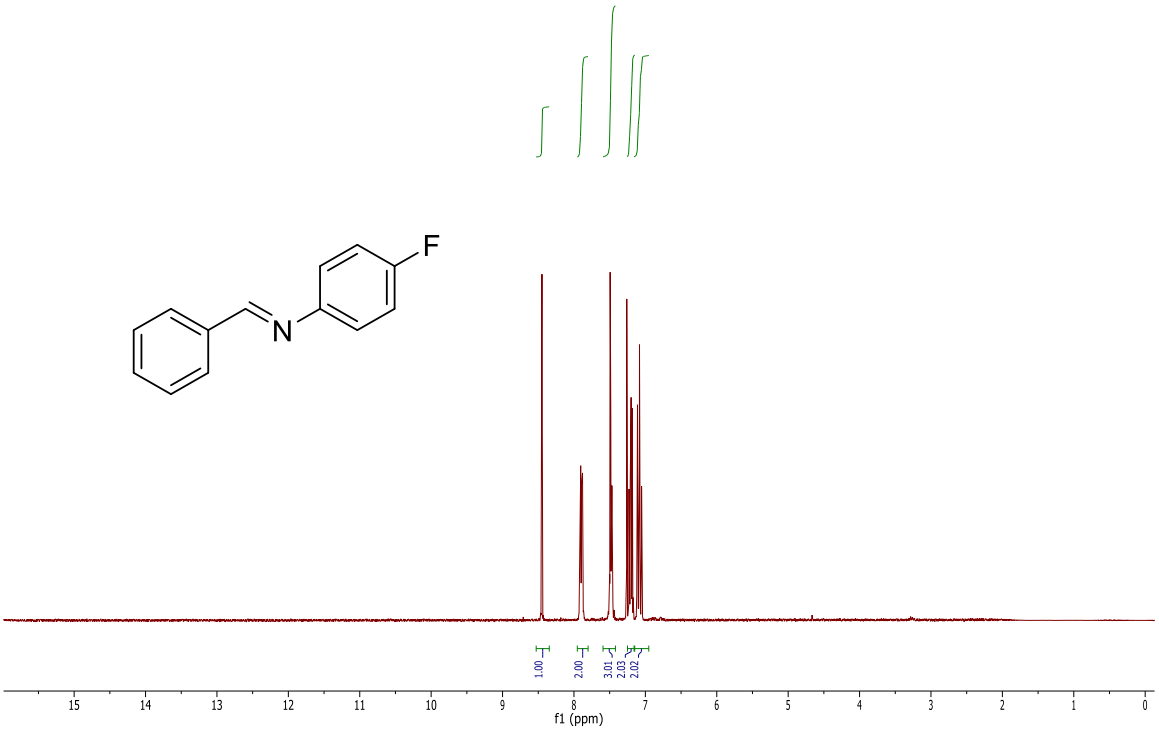

^{1}H NMR spectrum in $CDCl_3$.

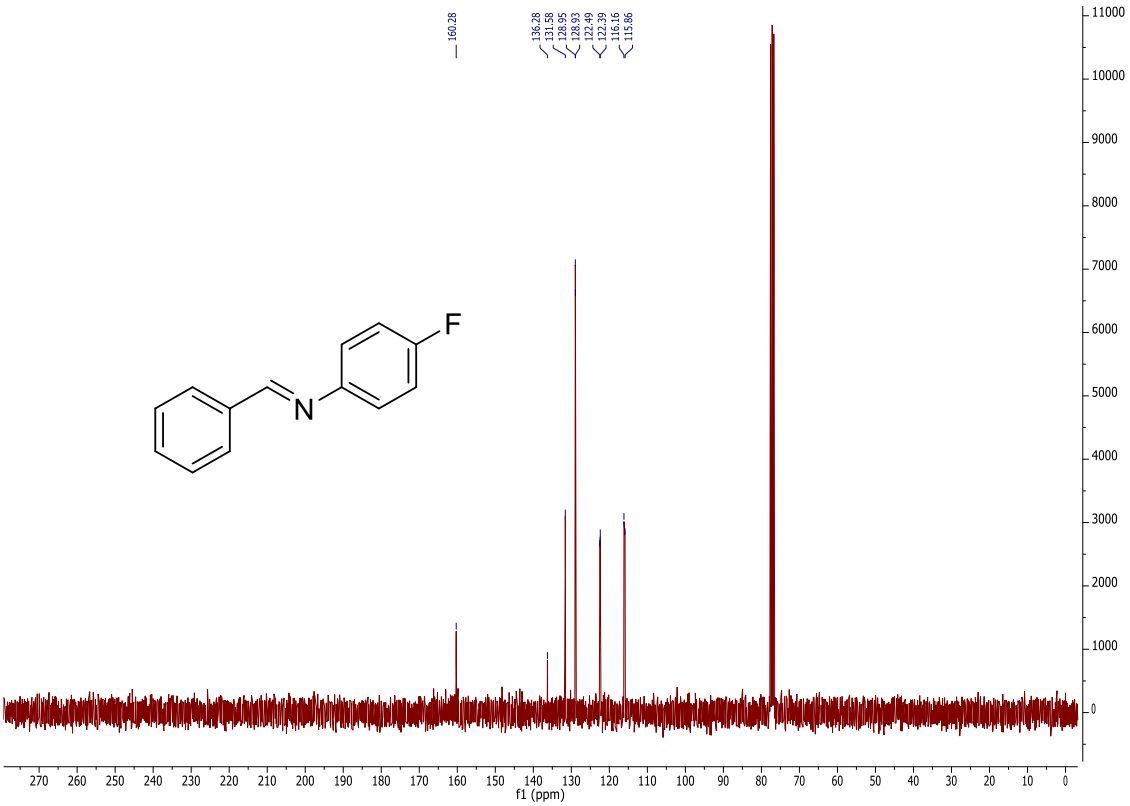

^{13}C NMR spectrum in $CDCl_3$.

11b

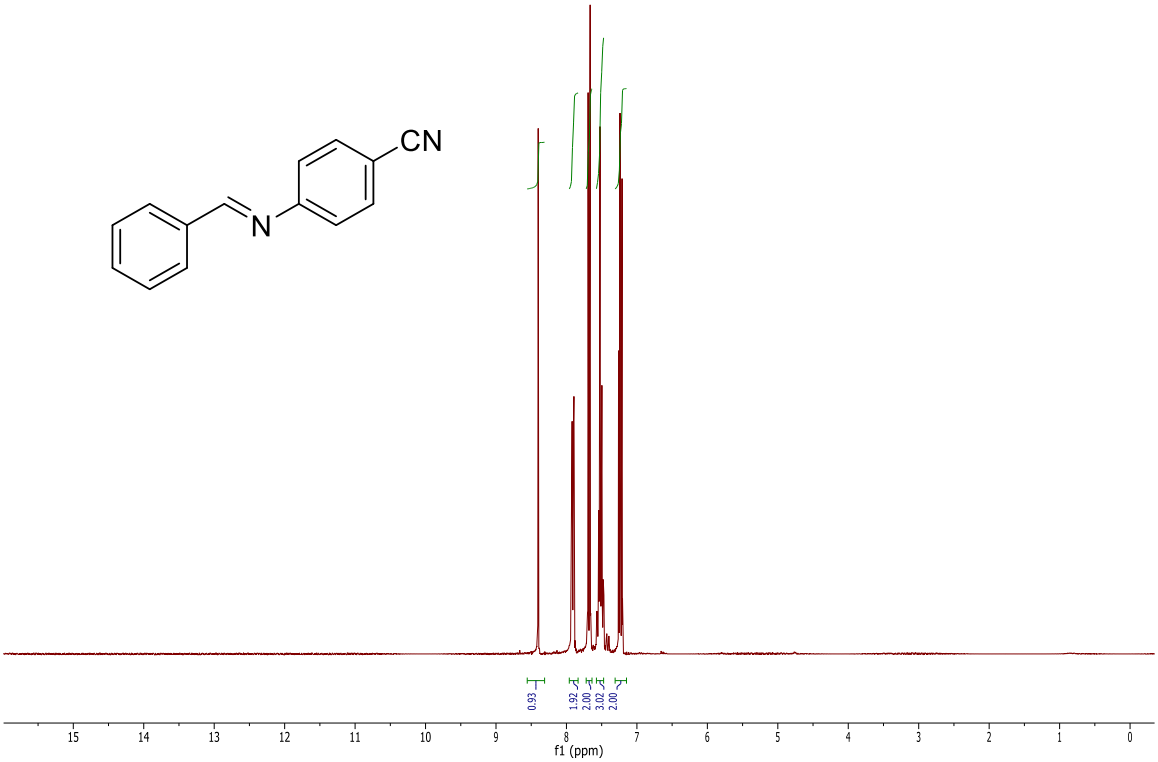

^{1}H NMR spectrum in $CDCl_3$.

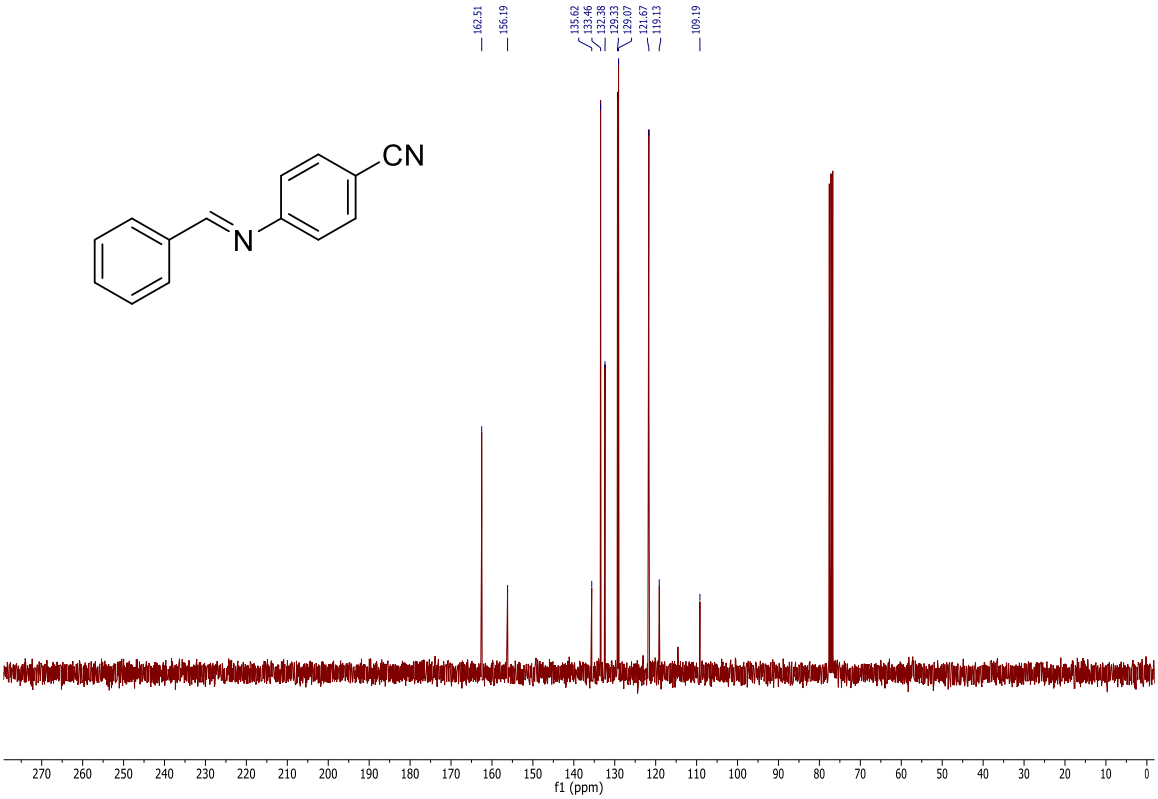

^{13}C NMR spectrum in $CDCl_3$.

12b

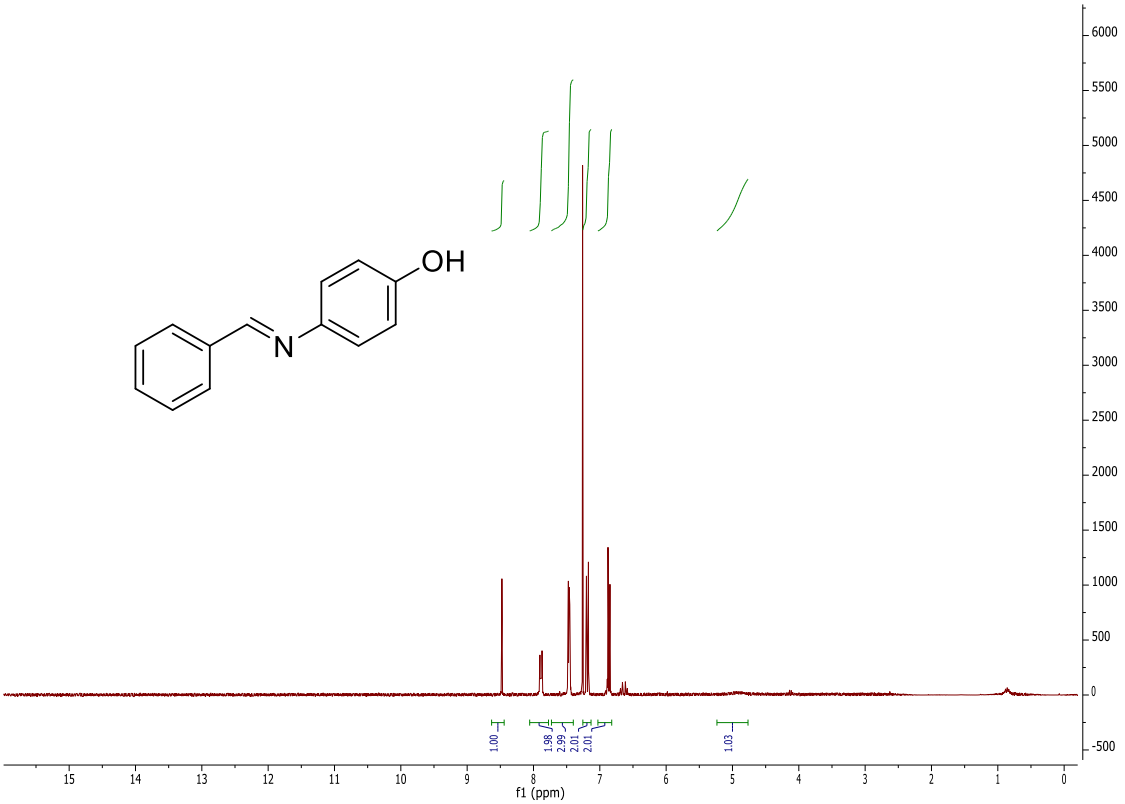

^{1}H NMR spectrum in $CDCl_3$.

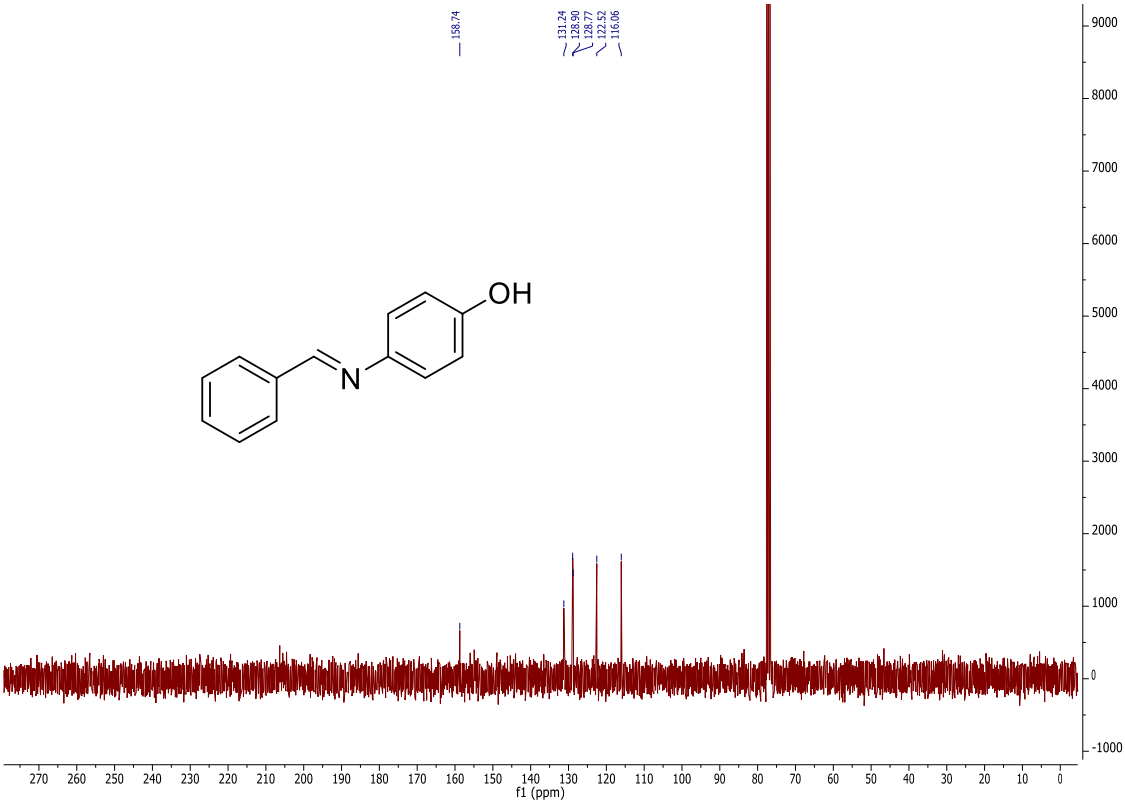

^{13}C NMR spectrum in $CDCl_3$.

13b

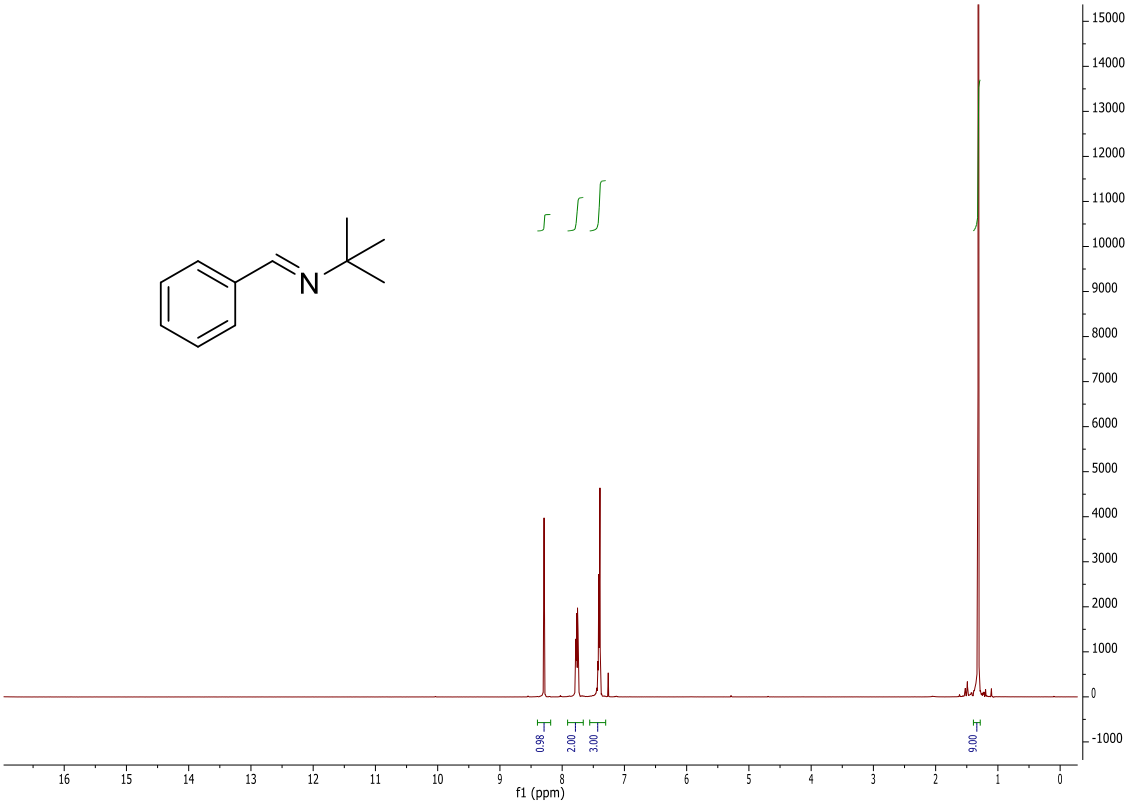

^{1}H NMR spectrum in $CDCl_3$.

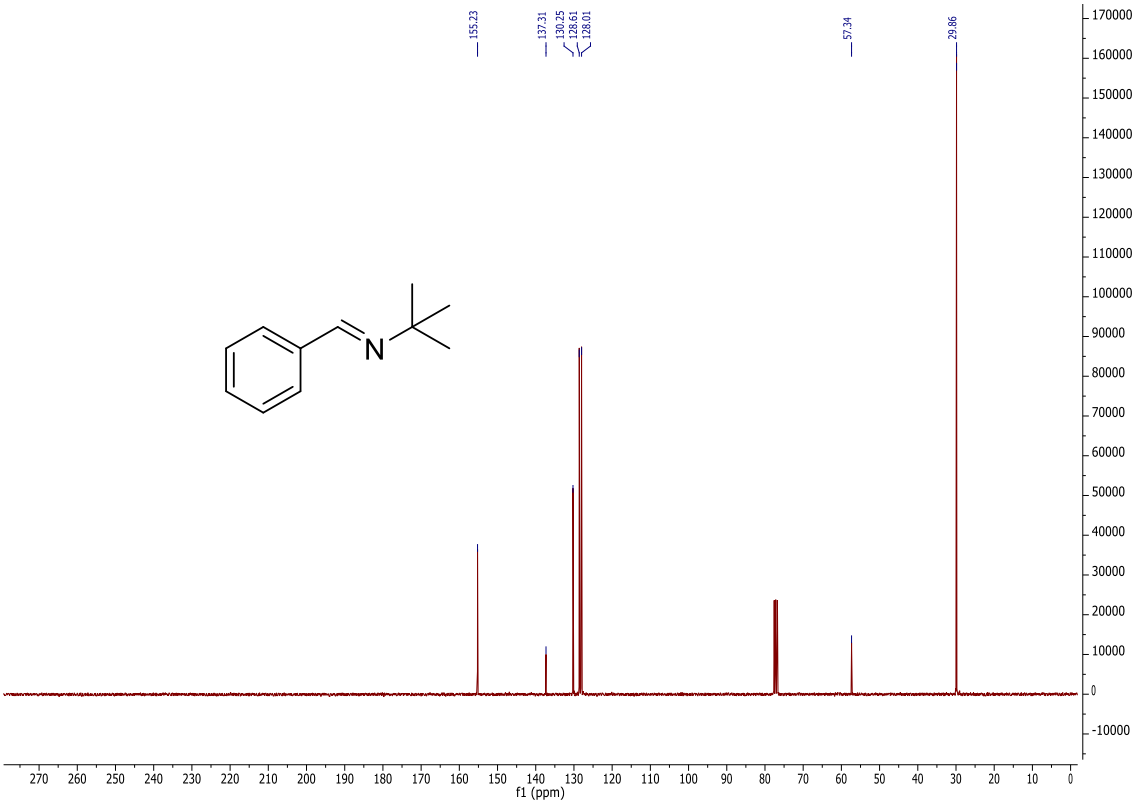

^{13}C NMR spectrum in $CDCl_3$.

14b

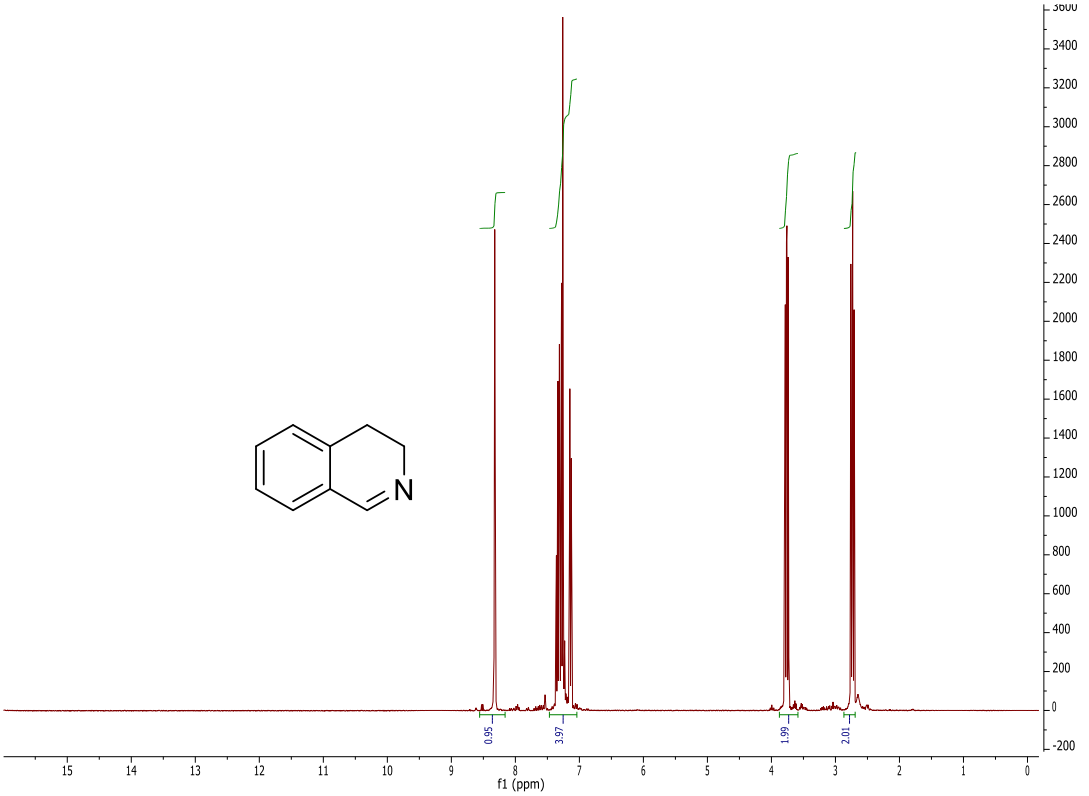

^{1}H NMR spectrum in $CDCl_3$.

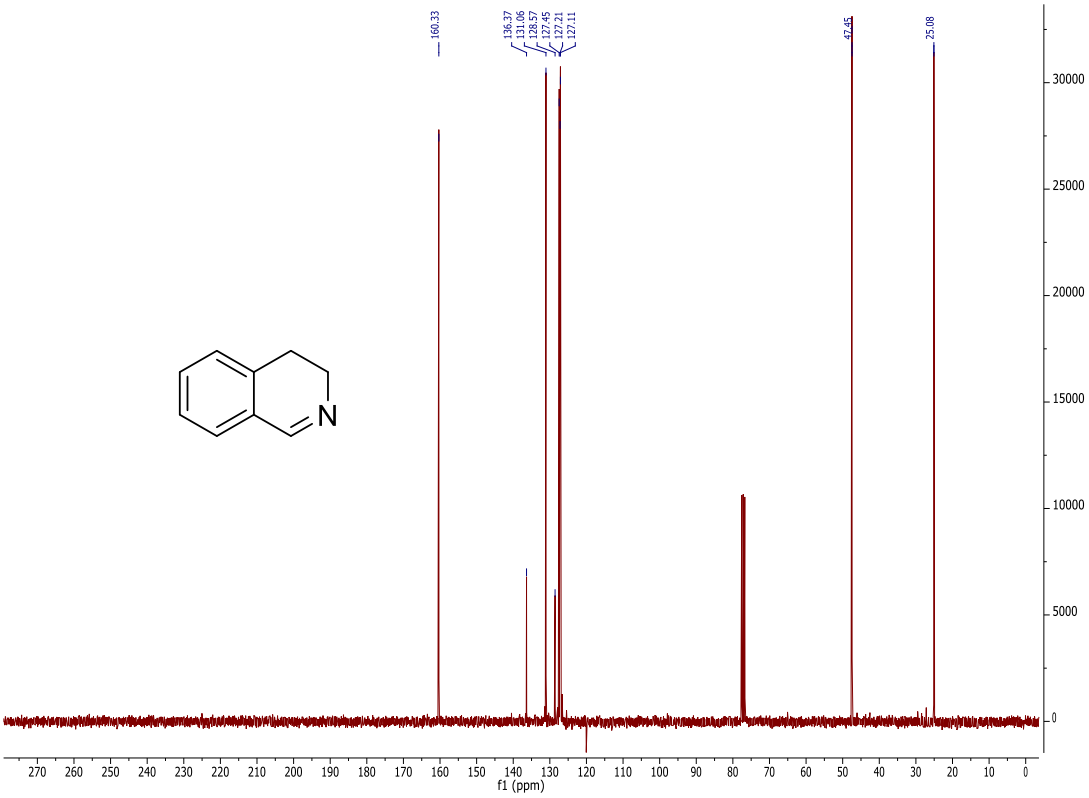

^{13}C NMR spectrum in $CDCl_3$.

15b

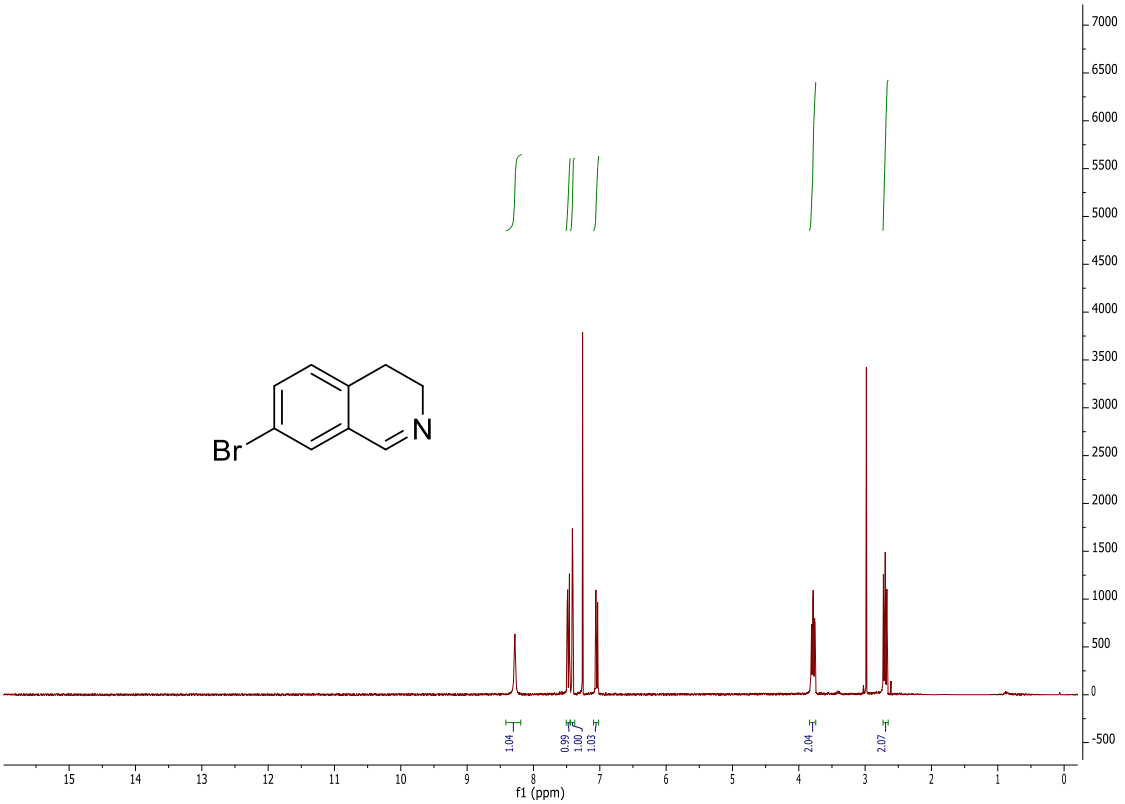

^{1}H NMR spectrum in $CDCl_3$.

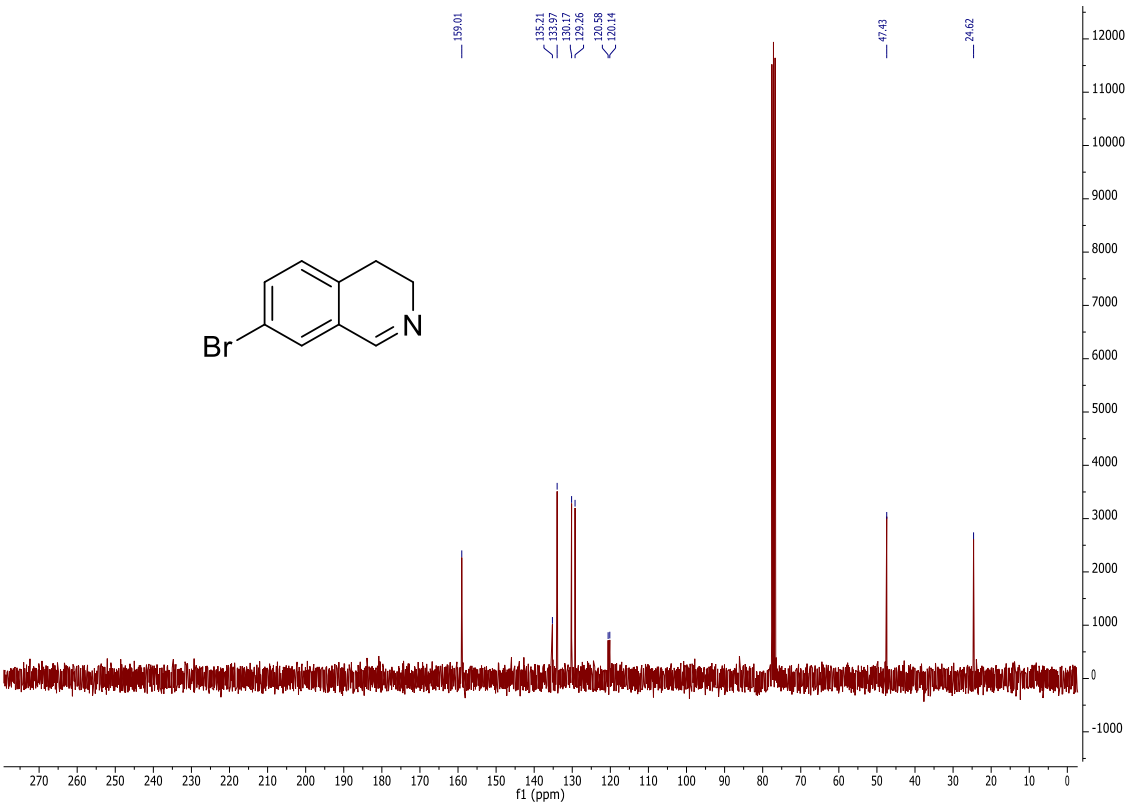

^{13}C NMR spectrum in $CDCl_3$.

16b

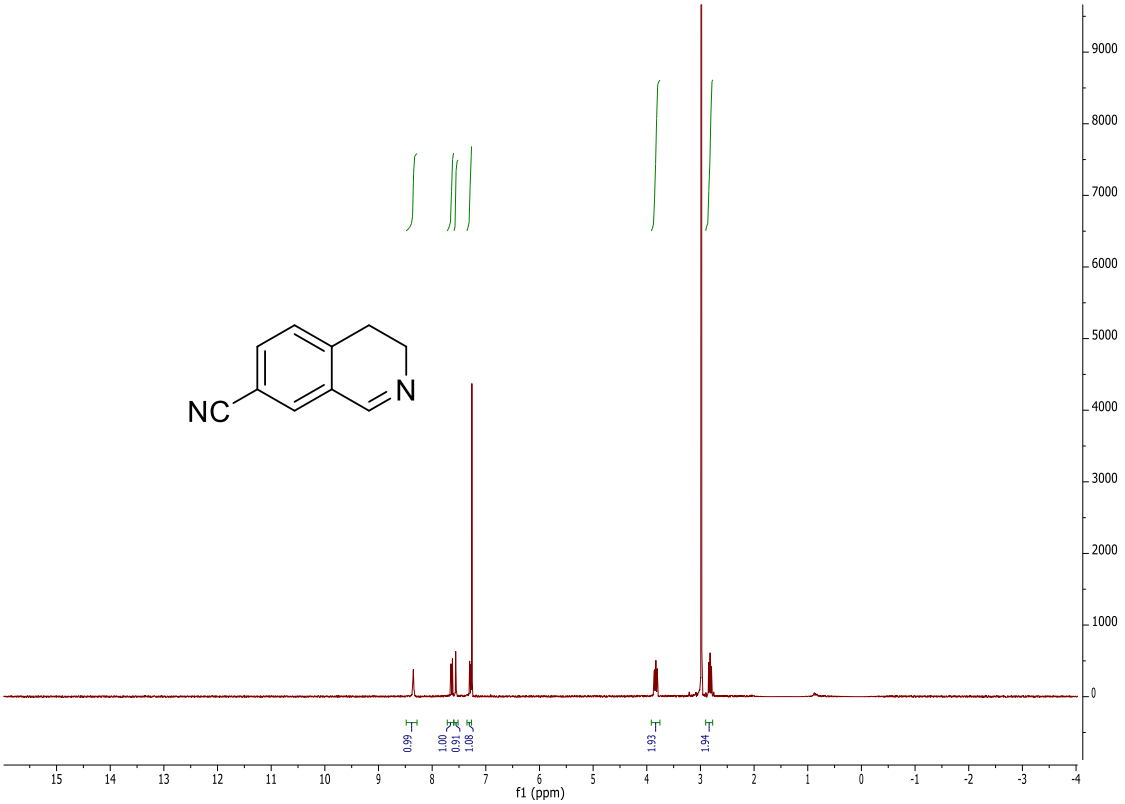

^{1}H NMR spectrum in $CDCl_3$.

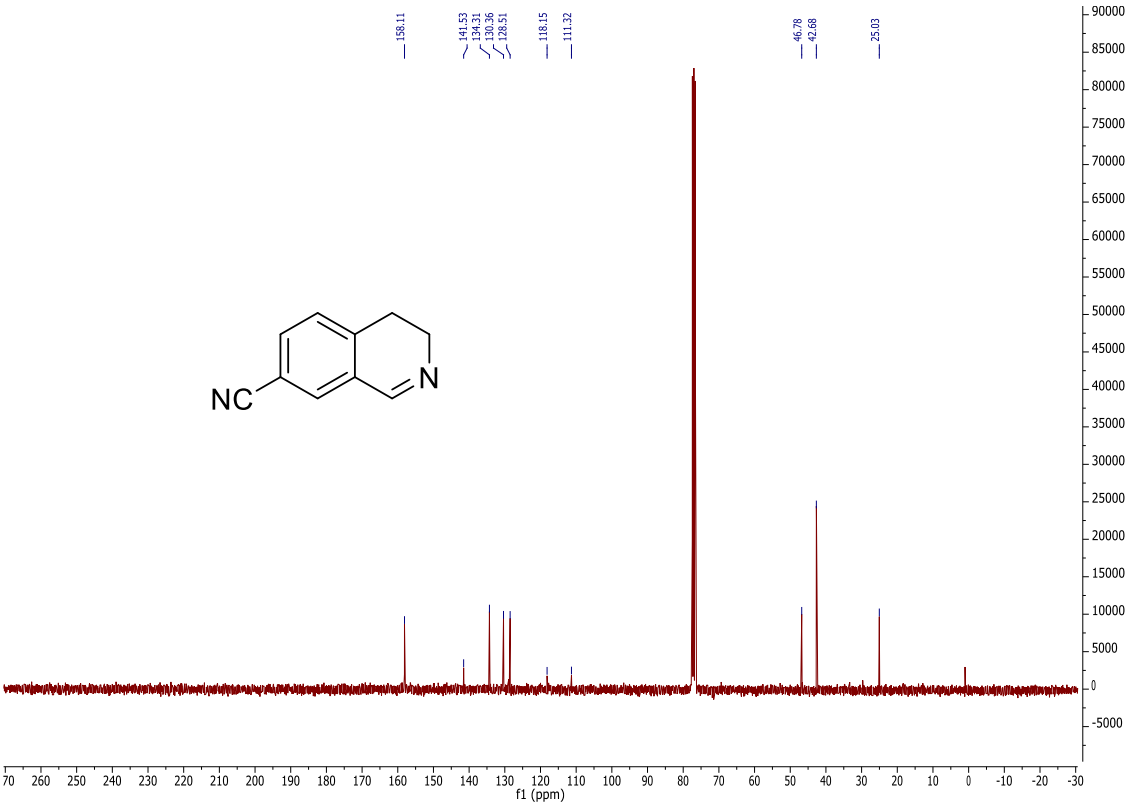

^{13}C NMR spectrum in $CDCl_3$.

17b

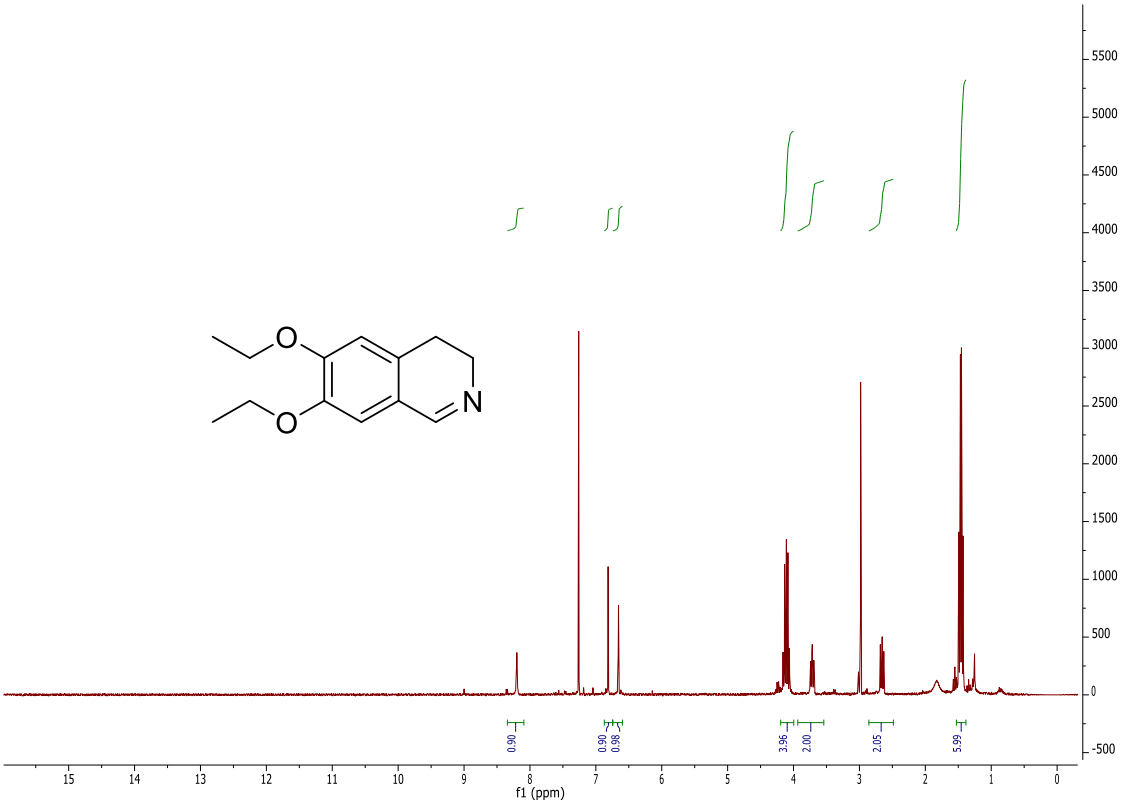

^{1}H NMR spectrum in $CDCl_3$.

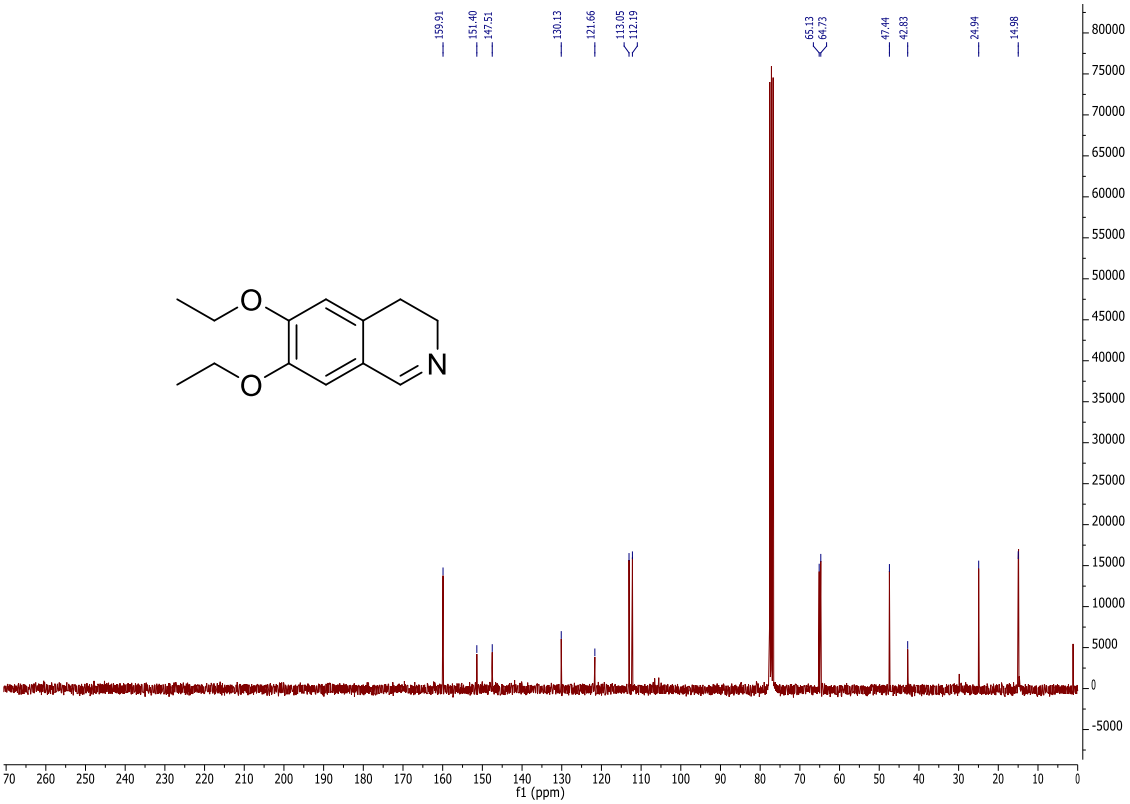

^{13}C NMR spectrum in $CDCl_3$.

18b

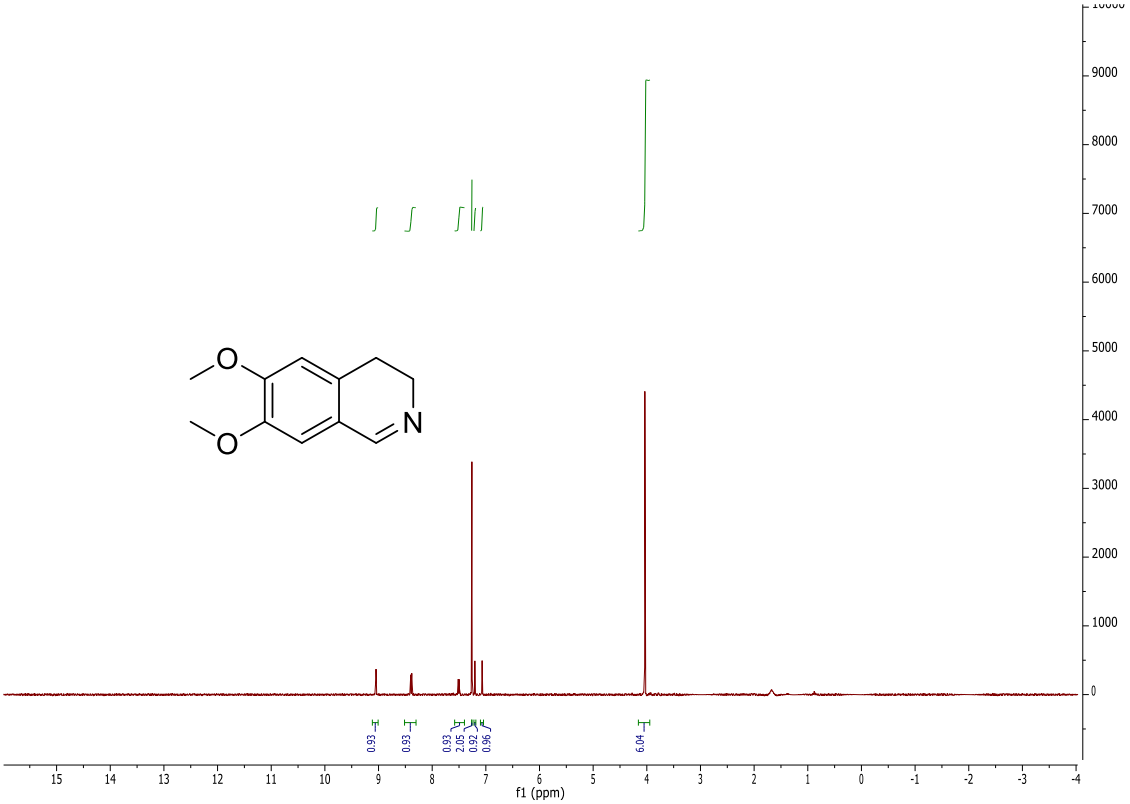

^{1}H NMR spectrum in $CDCl_3$.

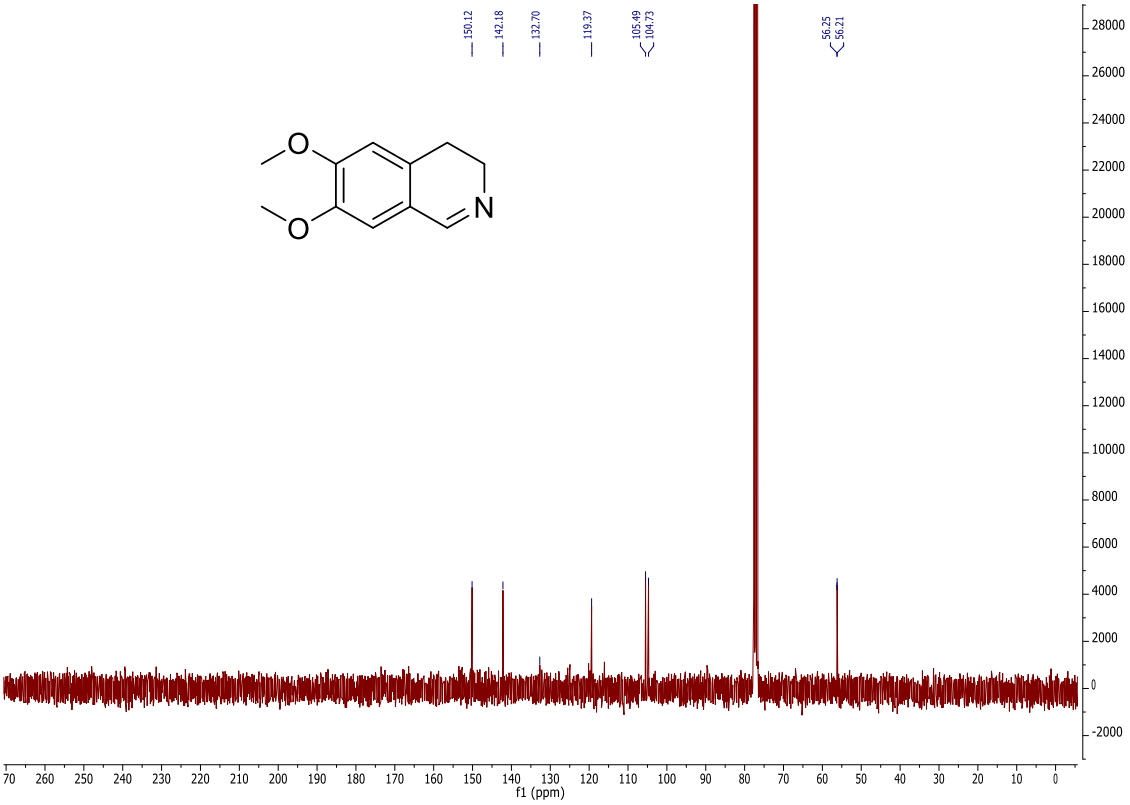

^{13}C NMR spectrum in $CDCl_3$.

19b

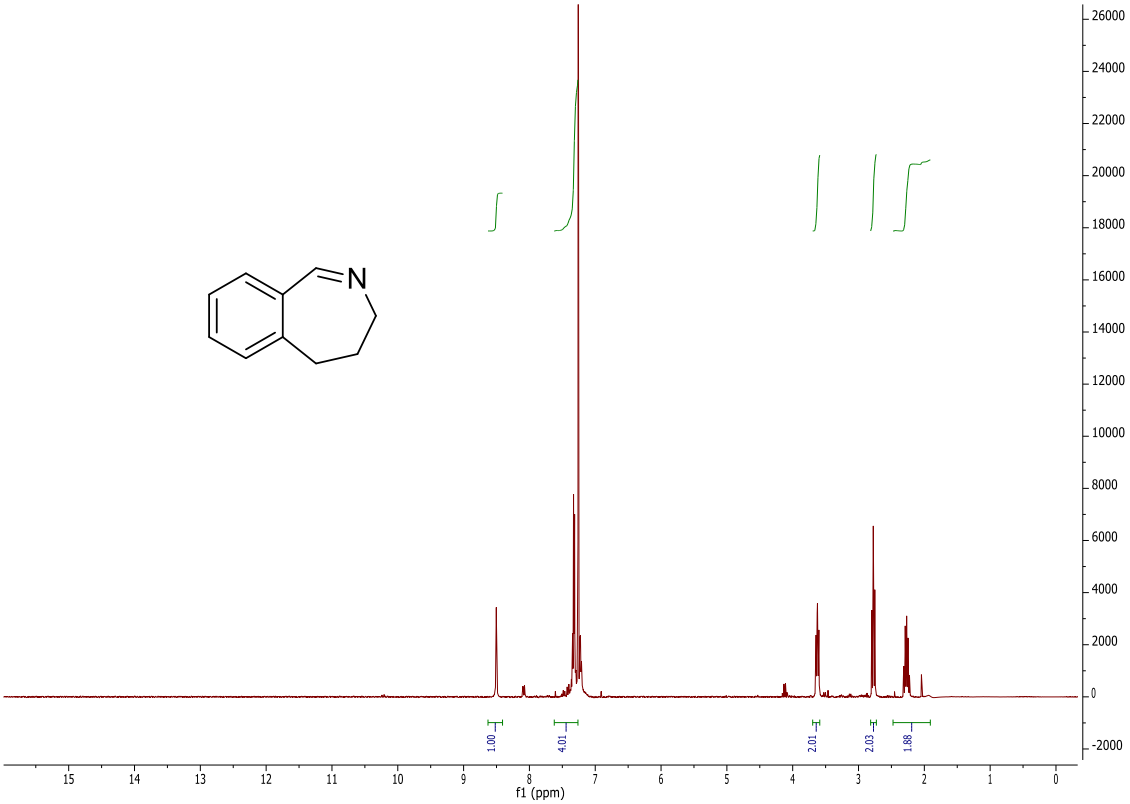

^{1}H NMR spectrum in $CDCl_3$.

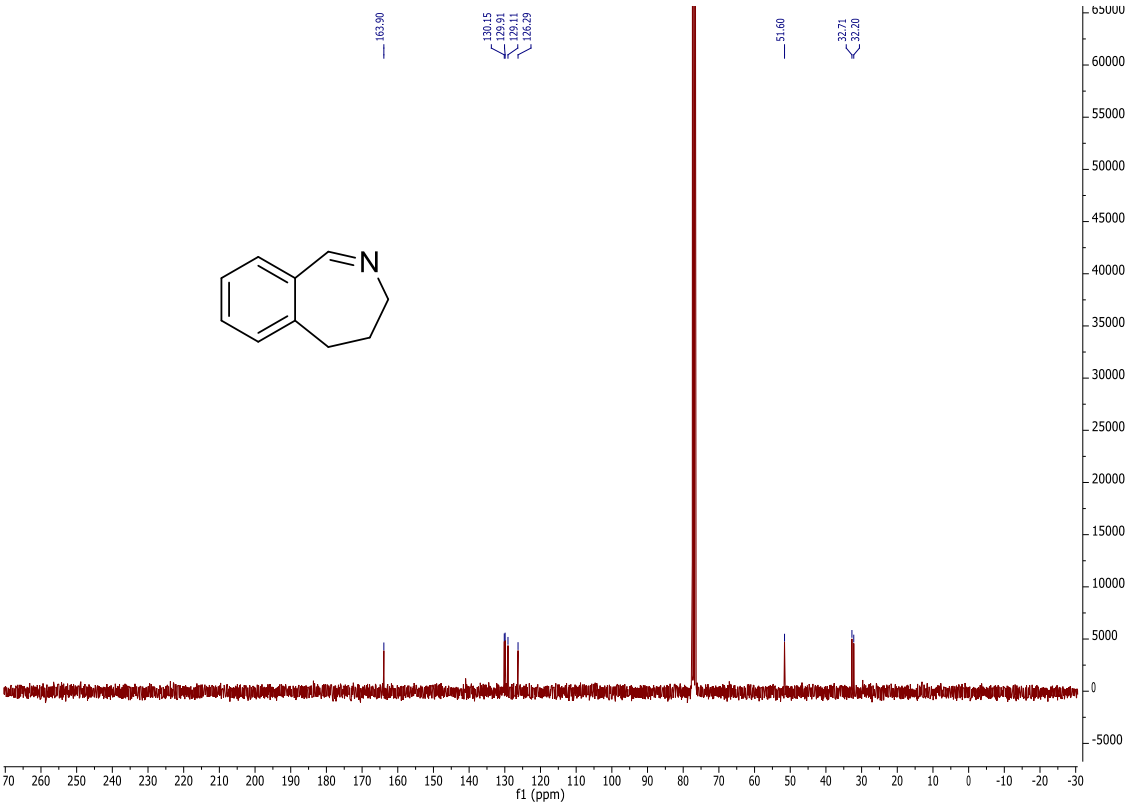

^{13}C NMR spectrum in $CDCl_3$.

20b

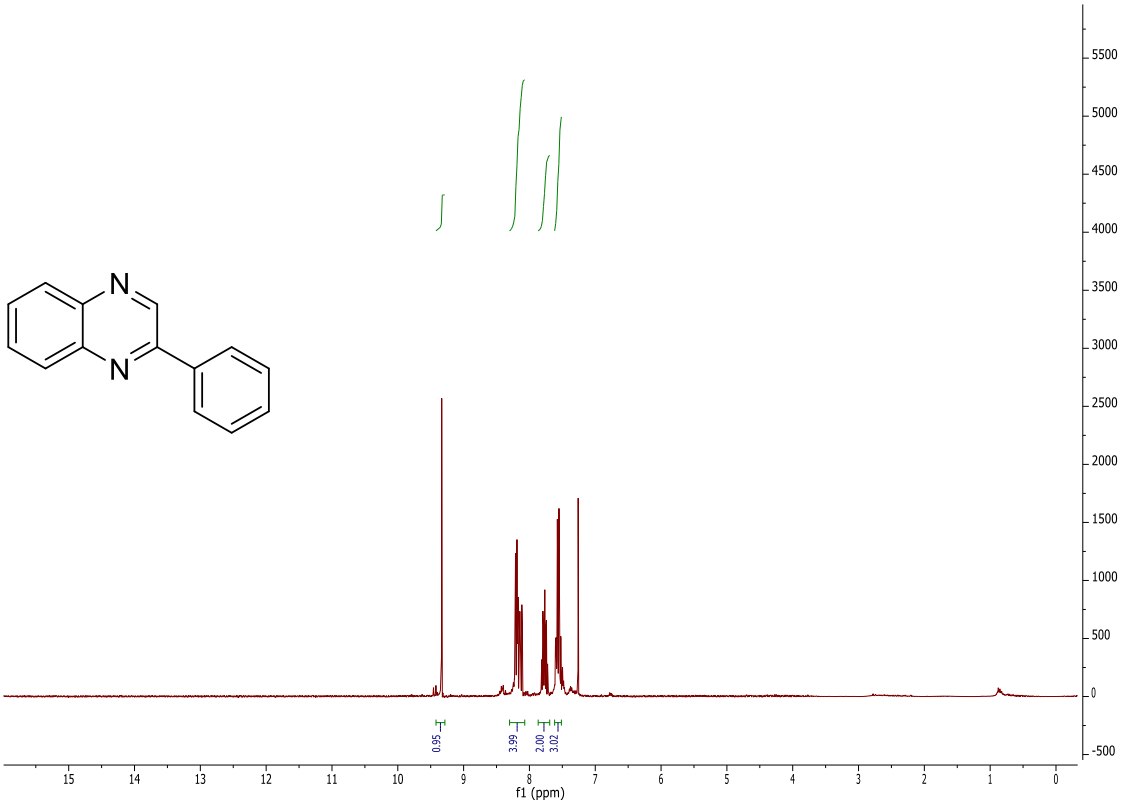

^{1}H NMR spectrum in $CDCl_3$.

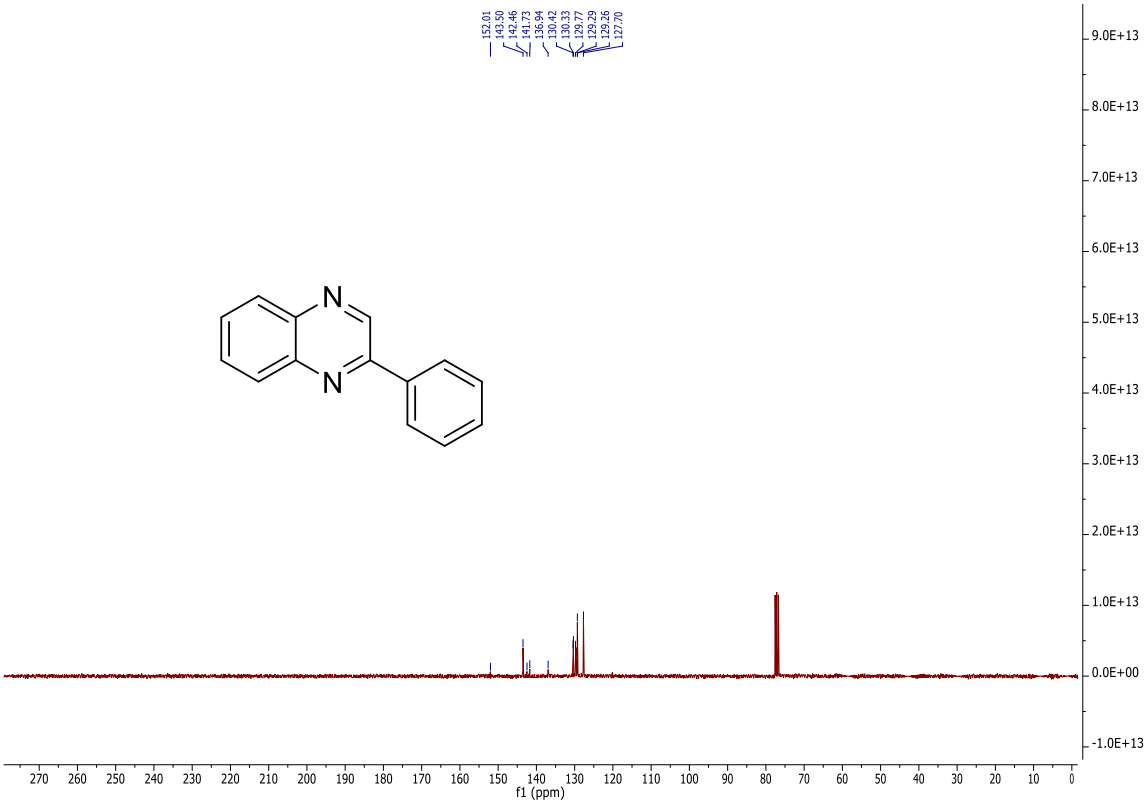

^{13}C NMR spectrum in $CDCl_3$.

21b

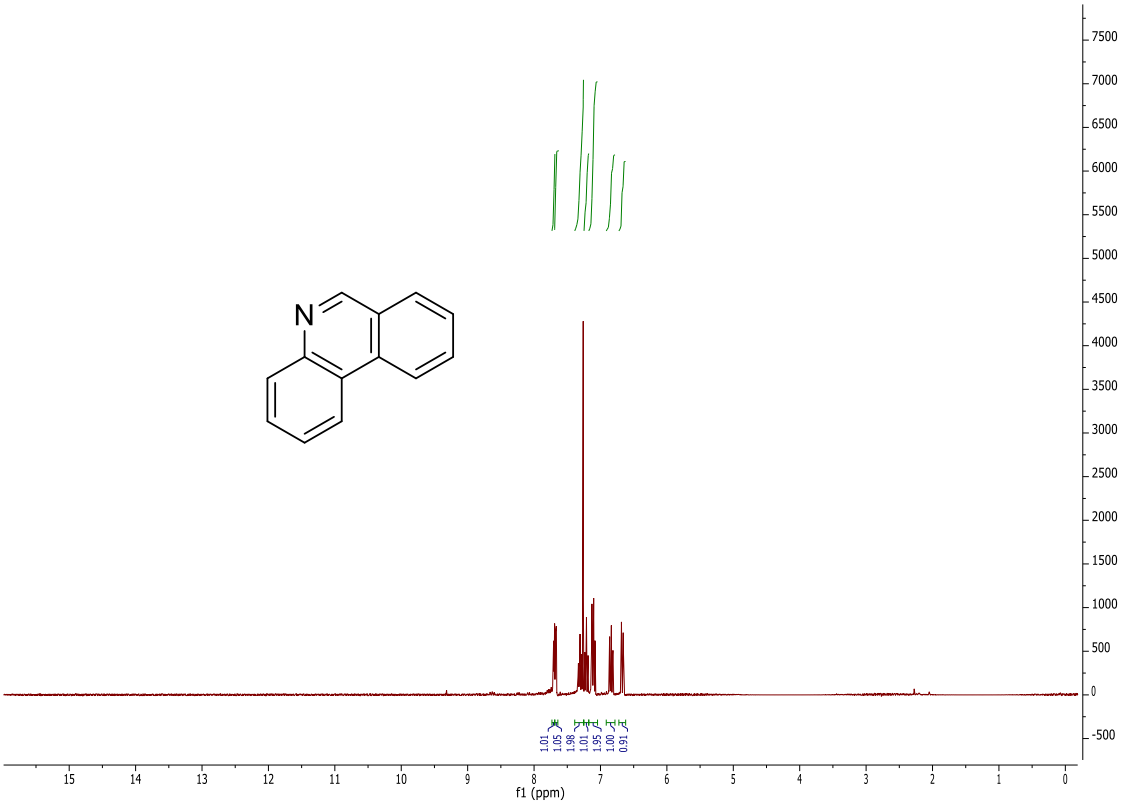

^{1}H NMR spectrum in $CDCl_3$.

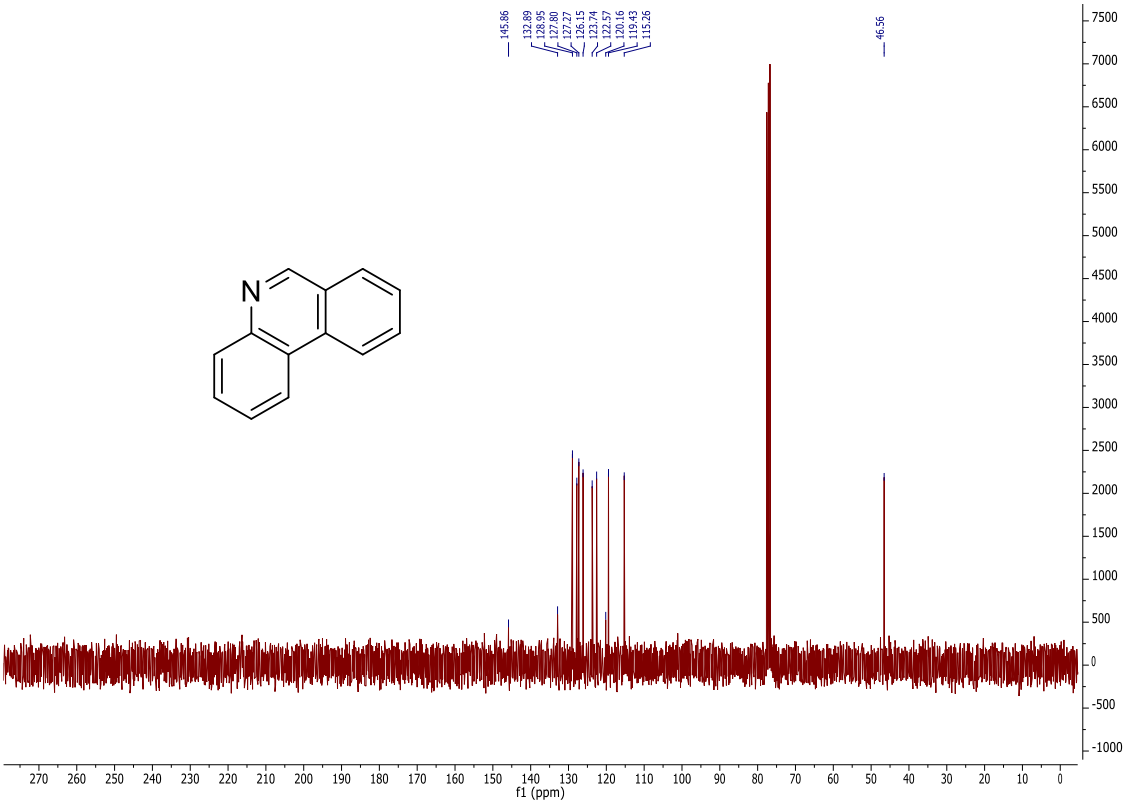

^{13}C NMR spectrum in $CDCl_3$.

22b

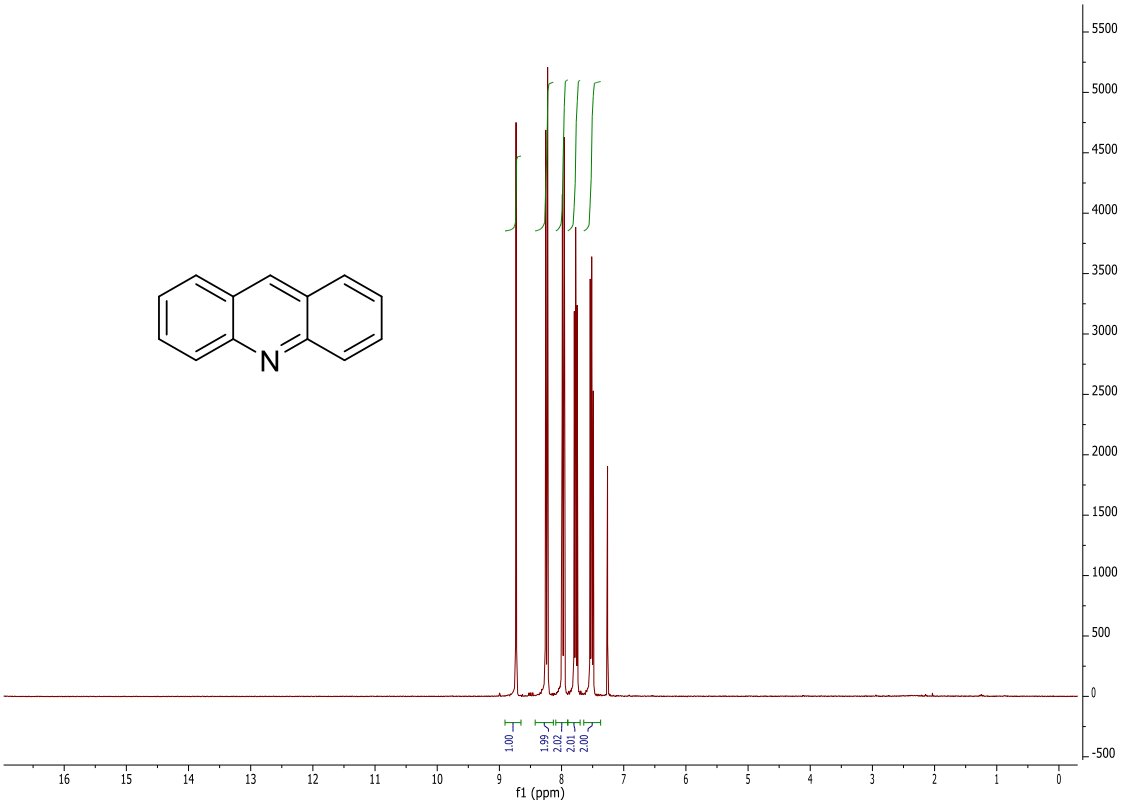

^{1}H NMR spectrum in $CDCl_3$.

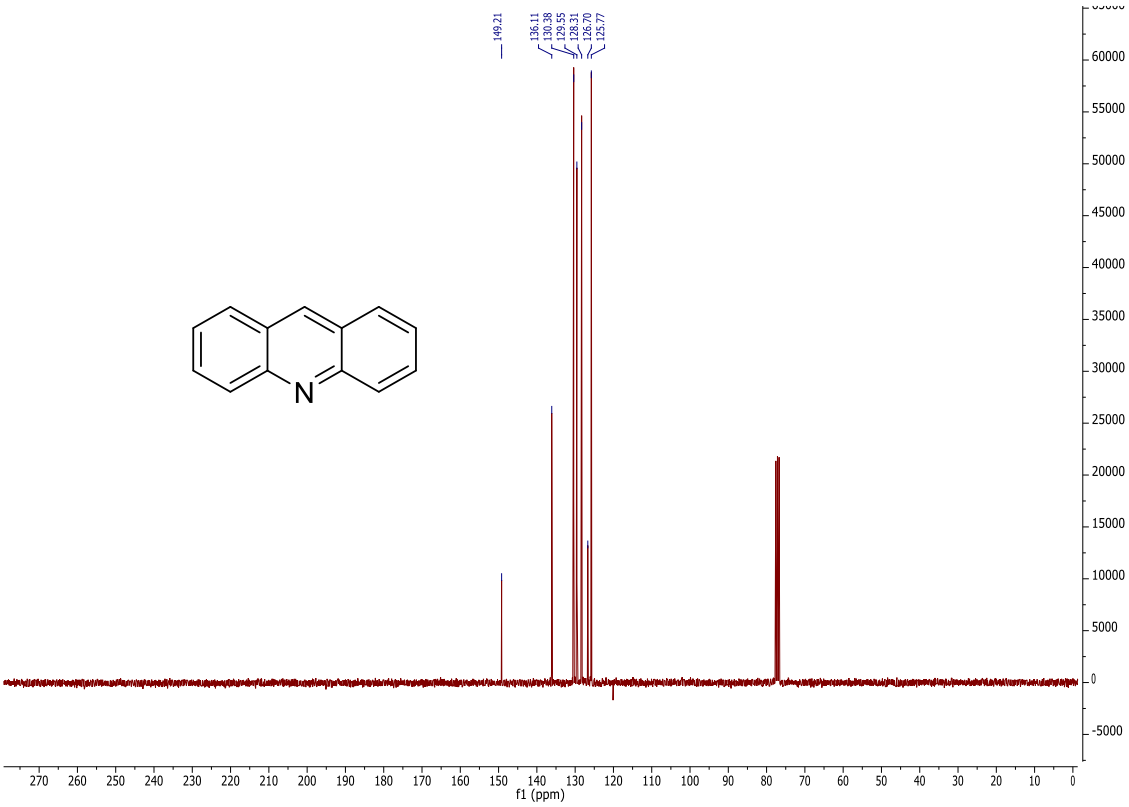

^{13}C NMR spectrum in $CDCl_3$.

23b

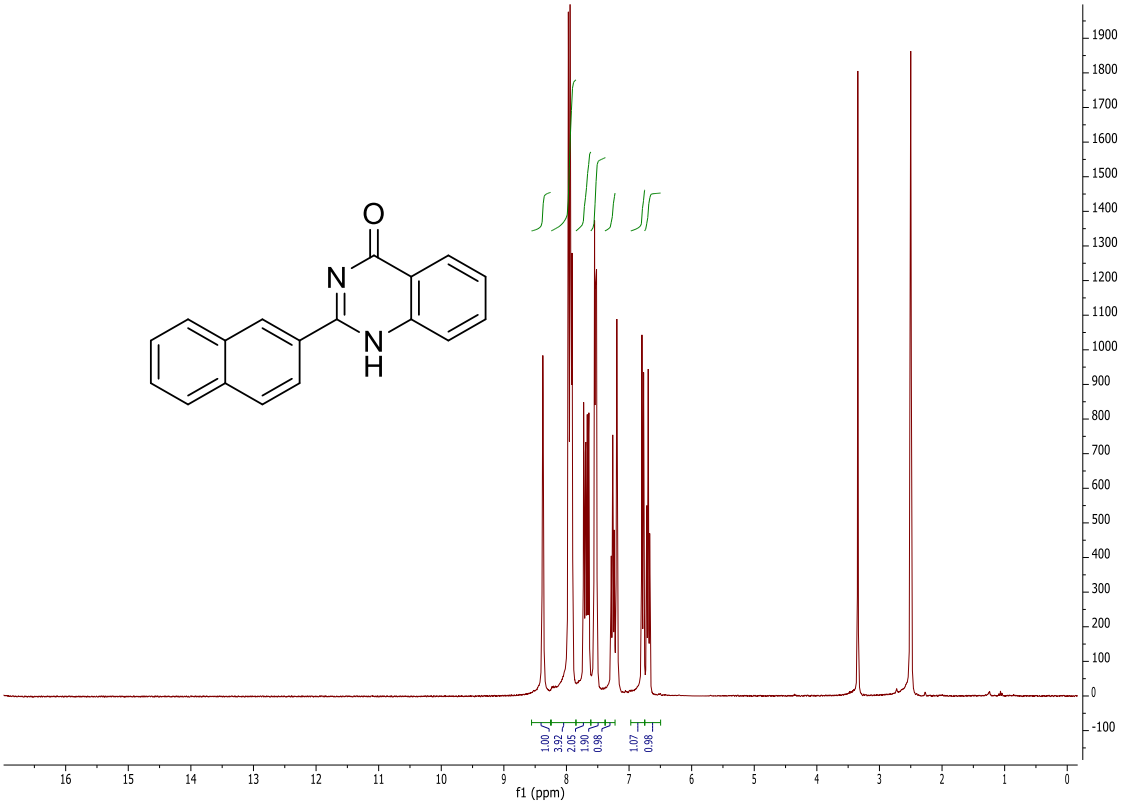

^{1}H NMR spectrum in DMSO-d_6.

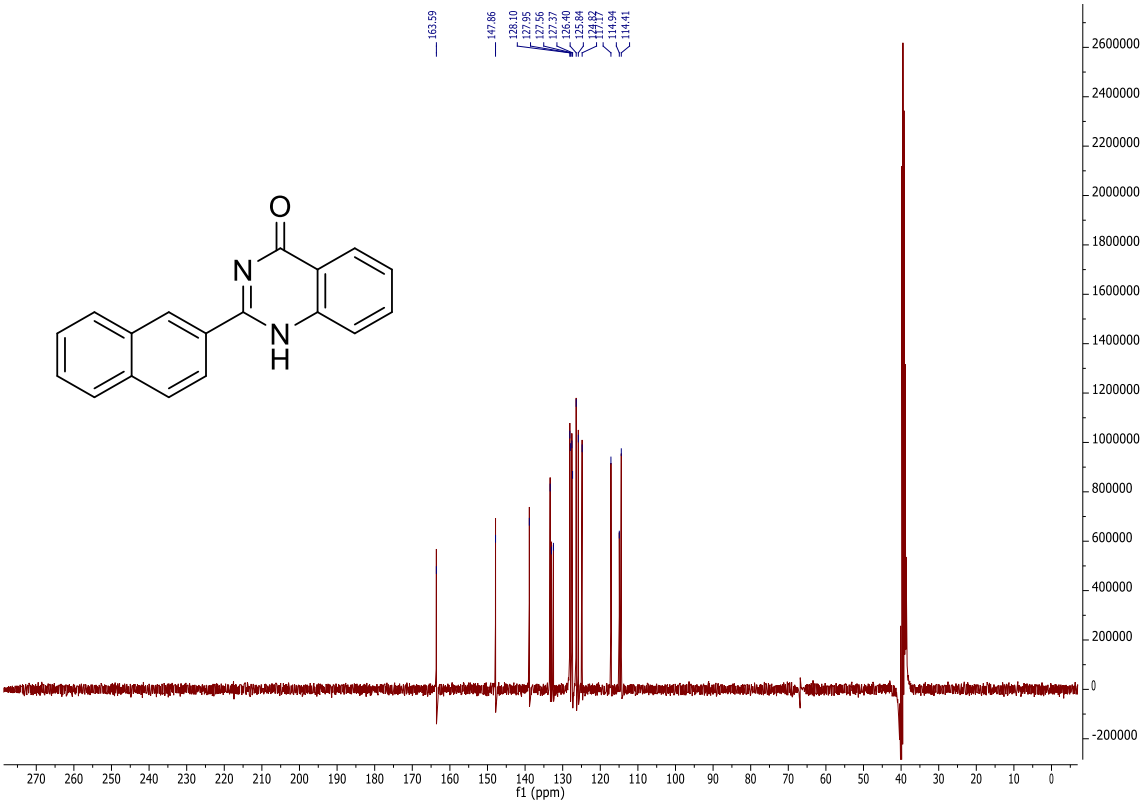

^{13}C NMR spectrum in DMSO-d_6.

24b

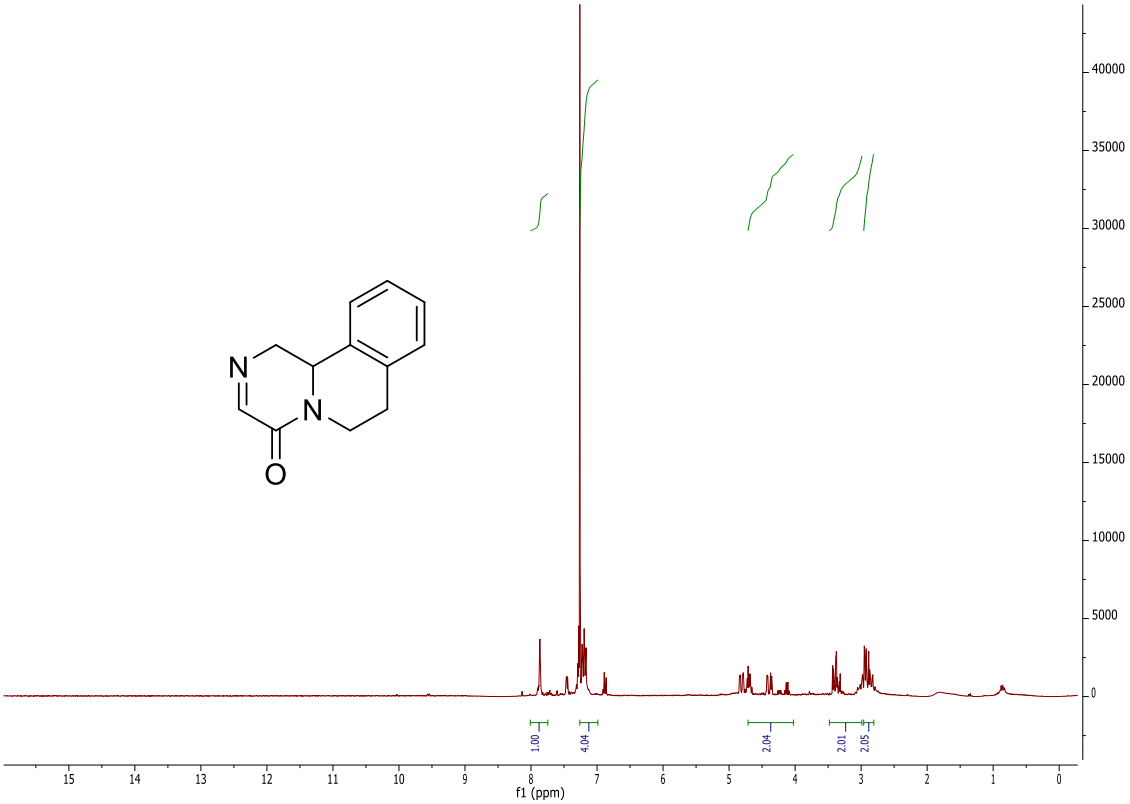

^{1}H NMR spectrum in $CDCl_3$.

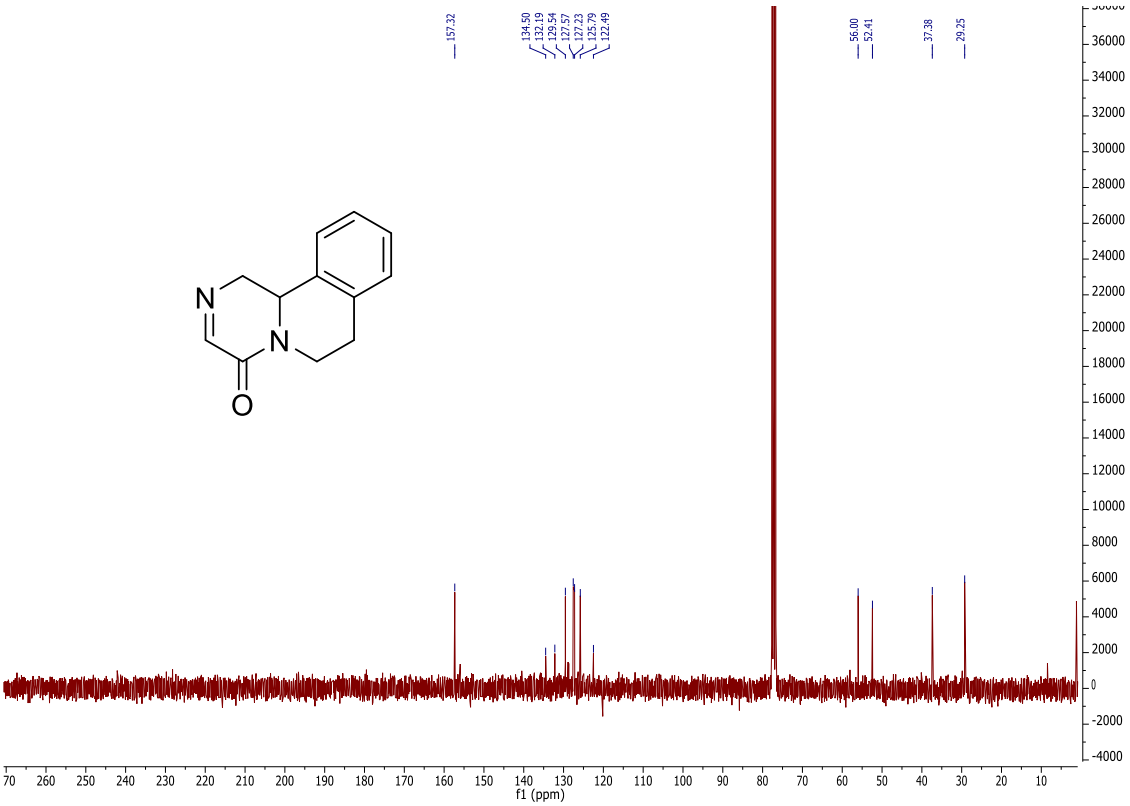

^{13}C NMR spectrum in $CDCl_3$.

25b

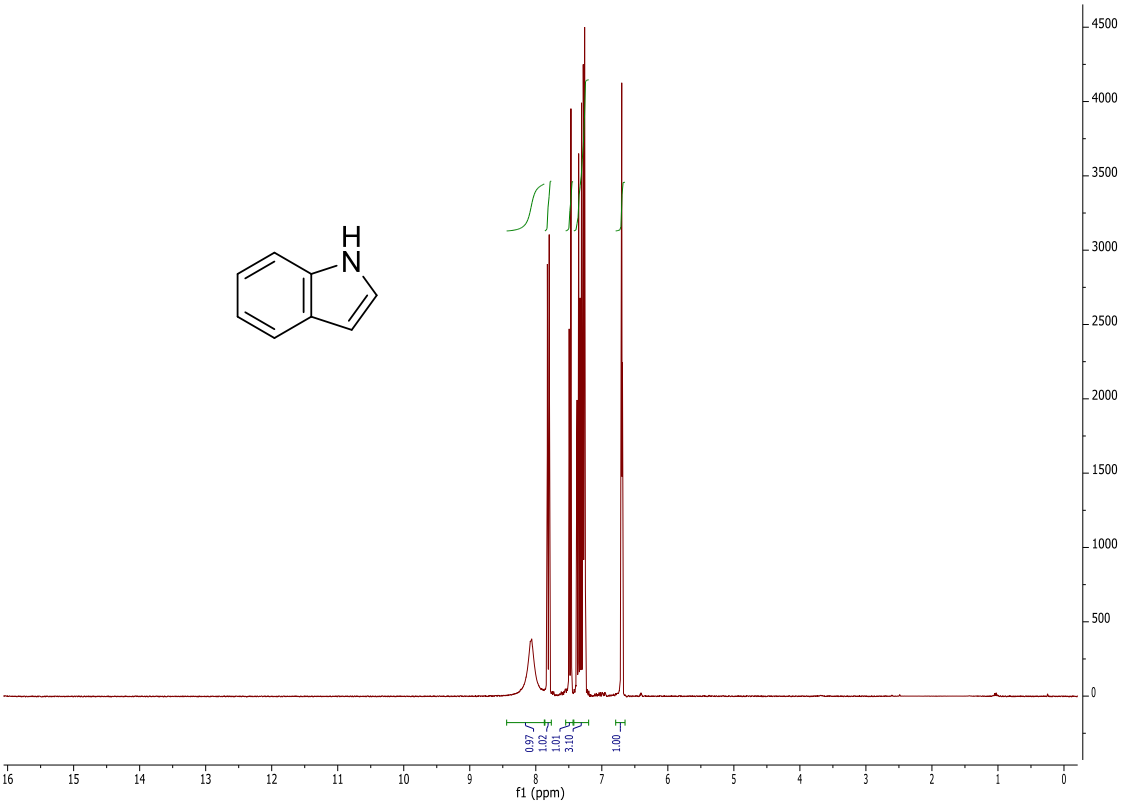

^{1}H NMR spectrum in $CDCl_3$.

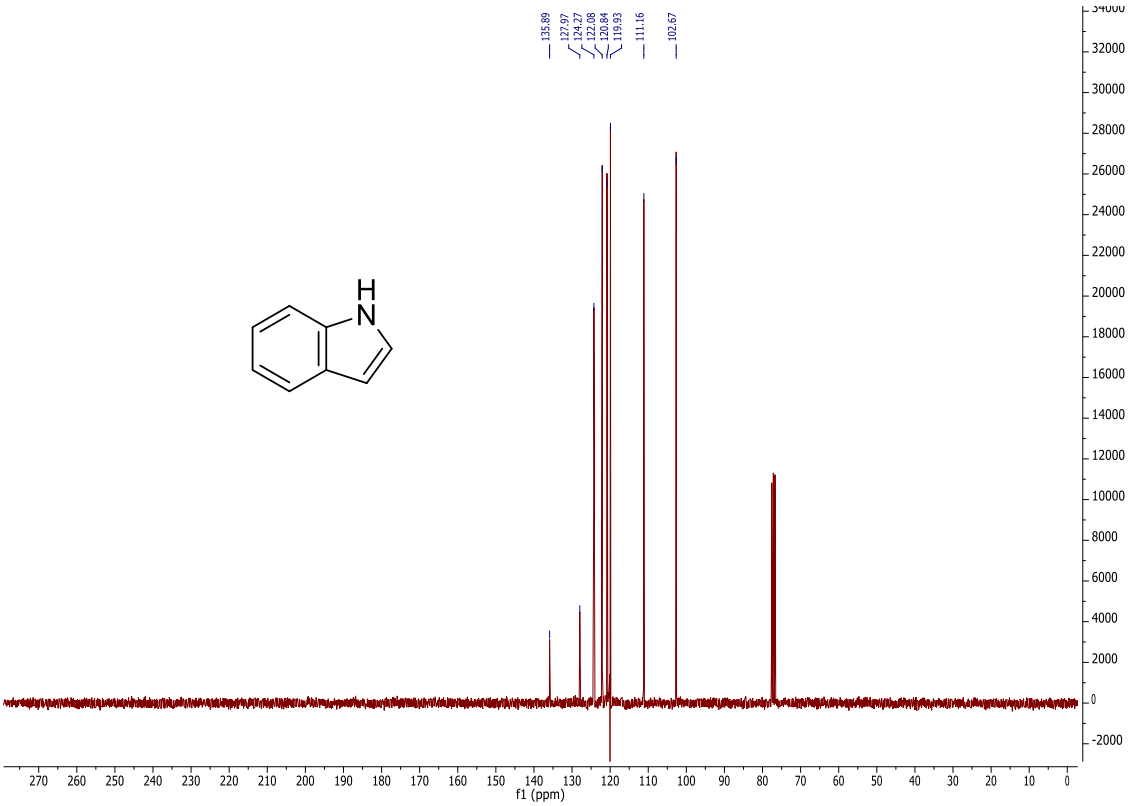

^{13}C NMR spectrum in $CDCl_3$.

26b

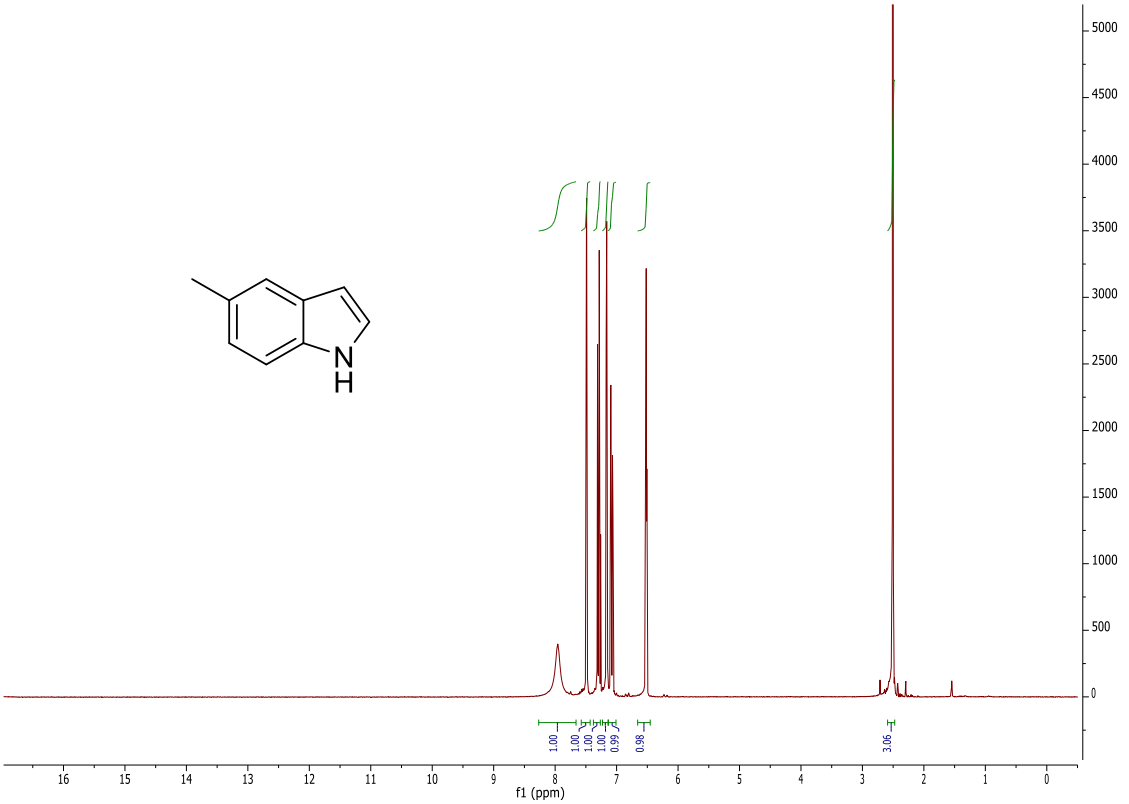

^{1}H NMR spectrum in $CDCl_3$.

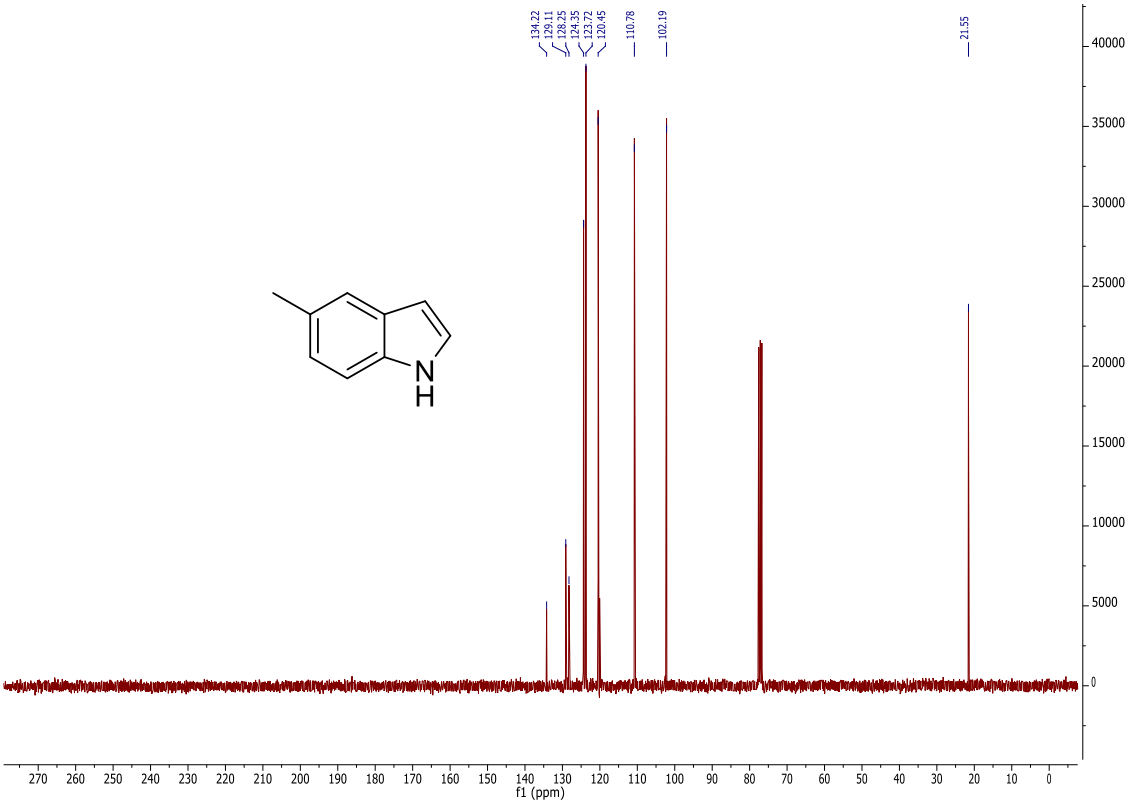

^{13}C NMR spectrum in $CDCl_3$.

27b

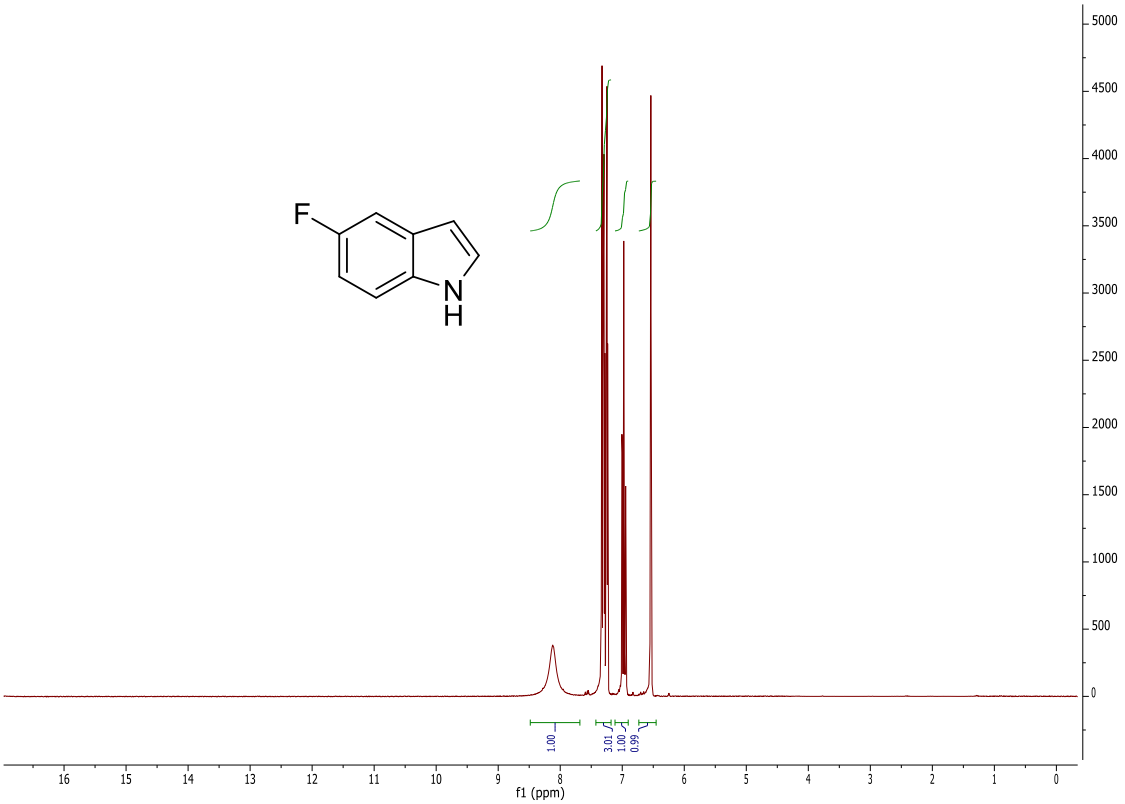

^{1}H NMR spectrum in $CDCl_3$.

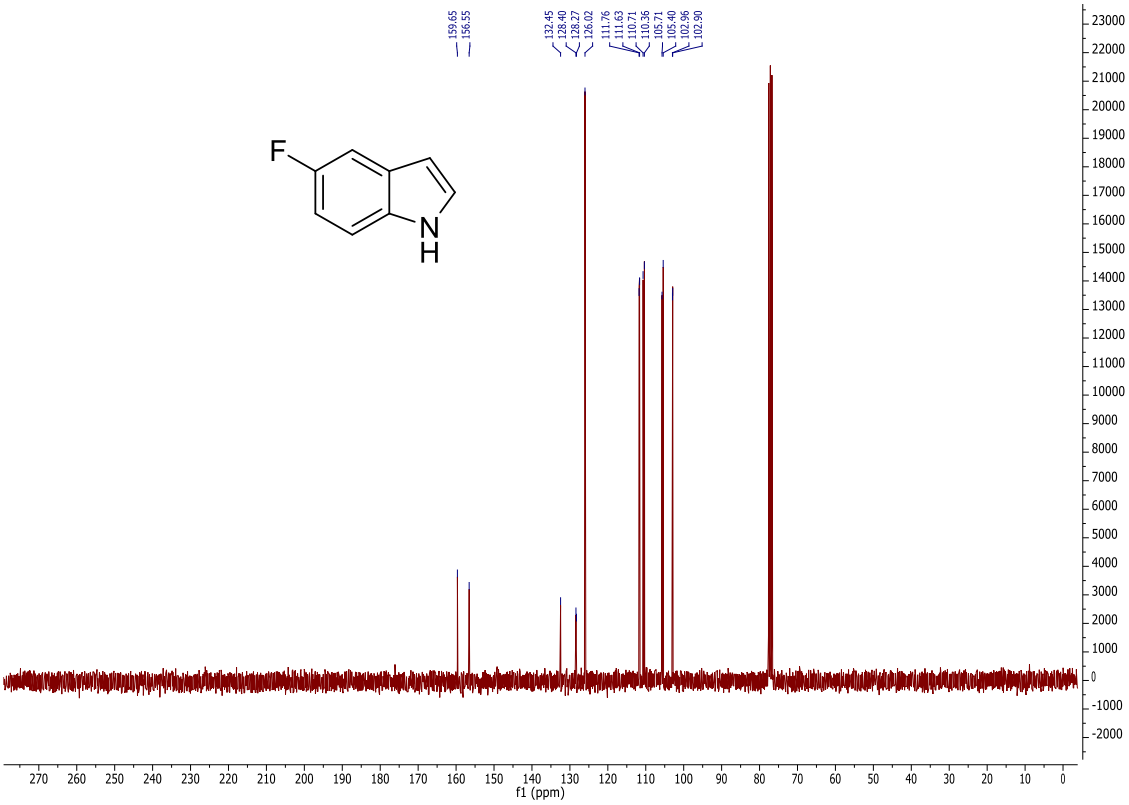

^{13}C NMR spectrum in $CDCl_3$.

28b

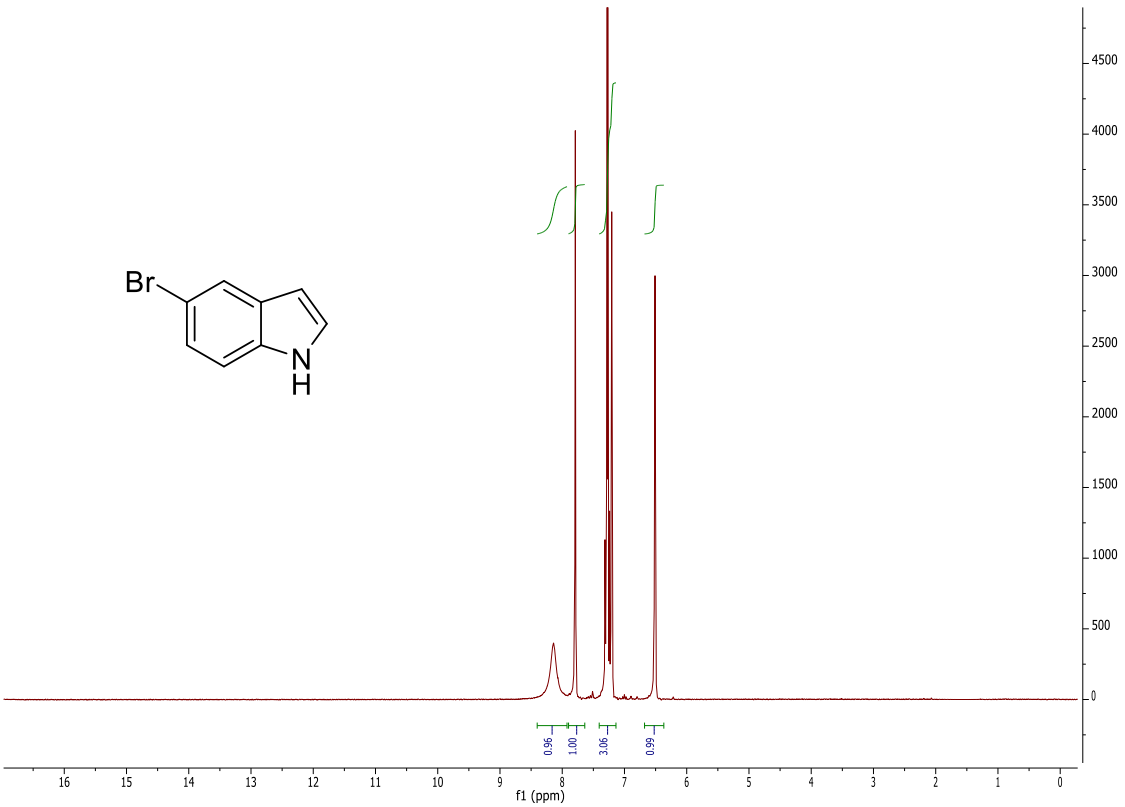

^{1}H NMR spectrum in $CDCl_3$.

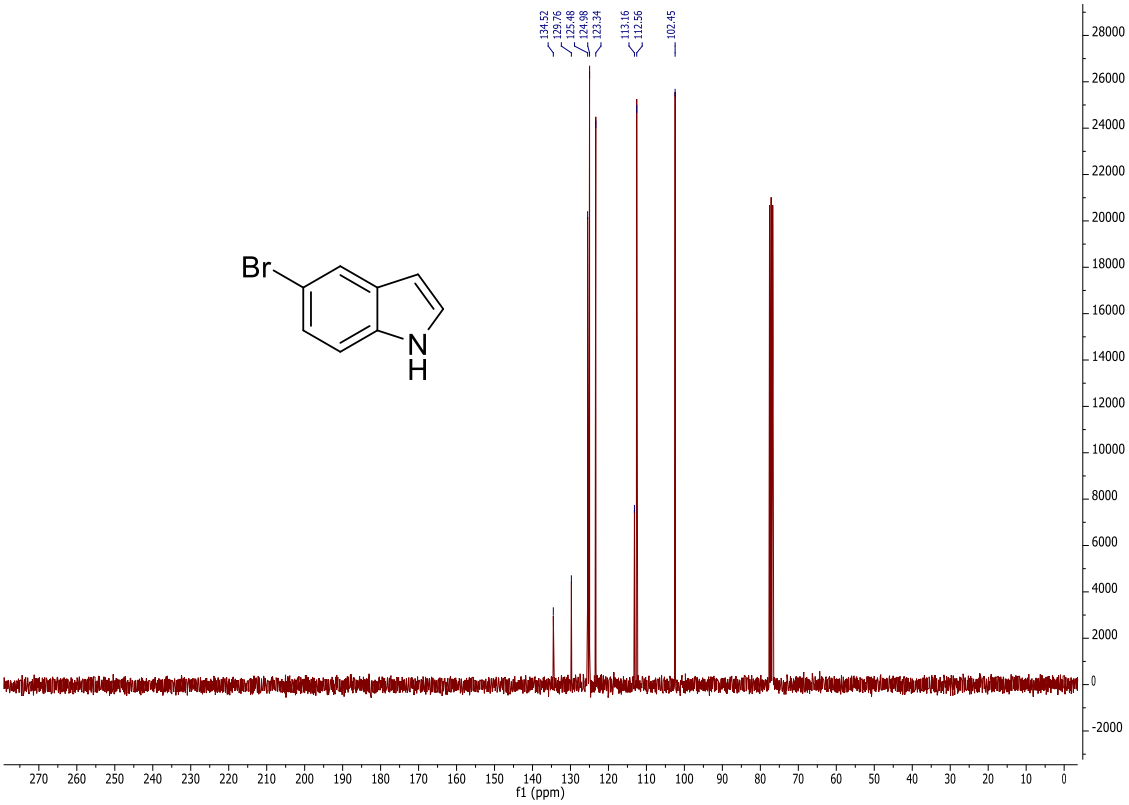

^{13}C NMR spectrum in $CDCl_3$.

29b

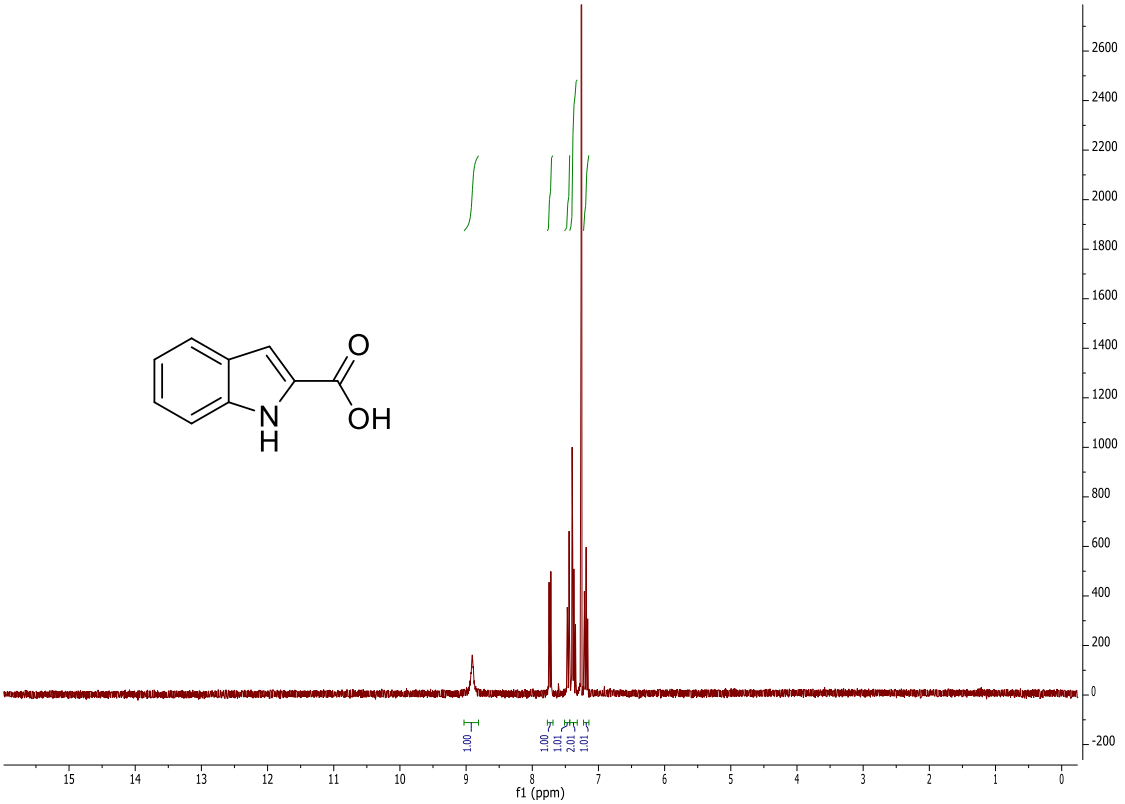

^{1}H NMR spectrum in $CDCl_3$.

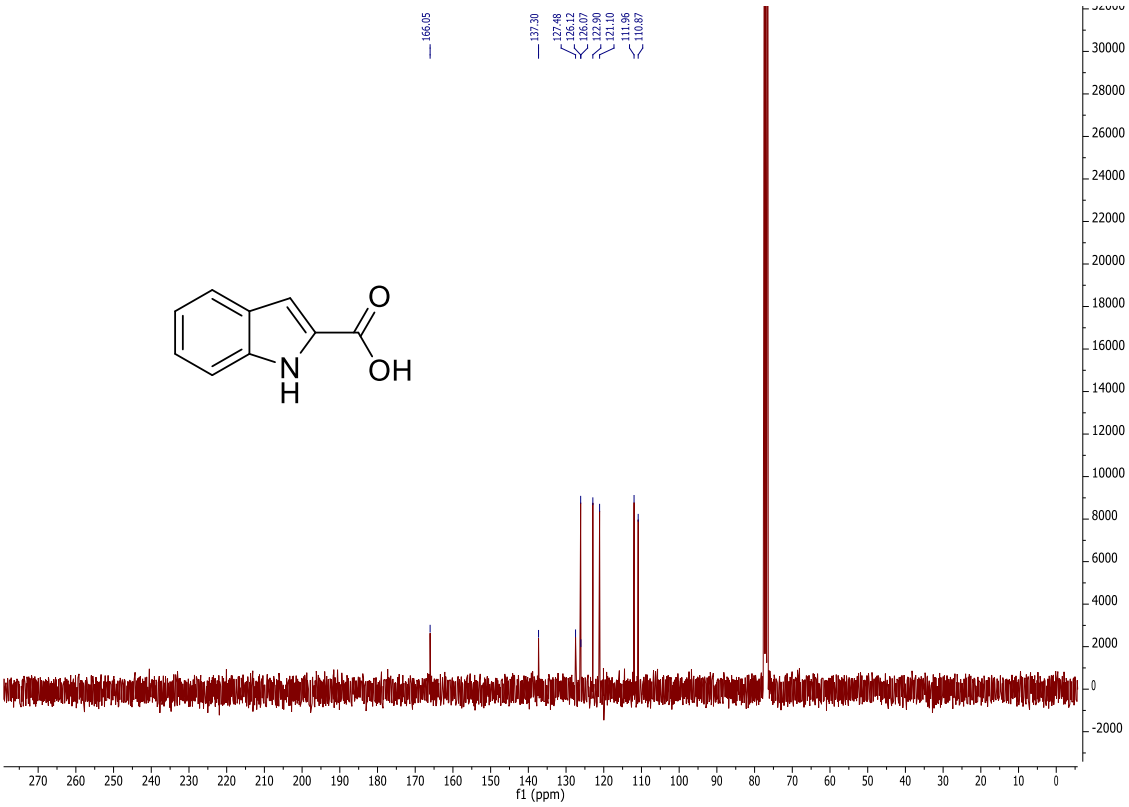

^{13}C NMR spectrum in $CDCl_3$.

30b

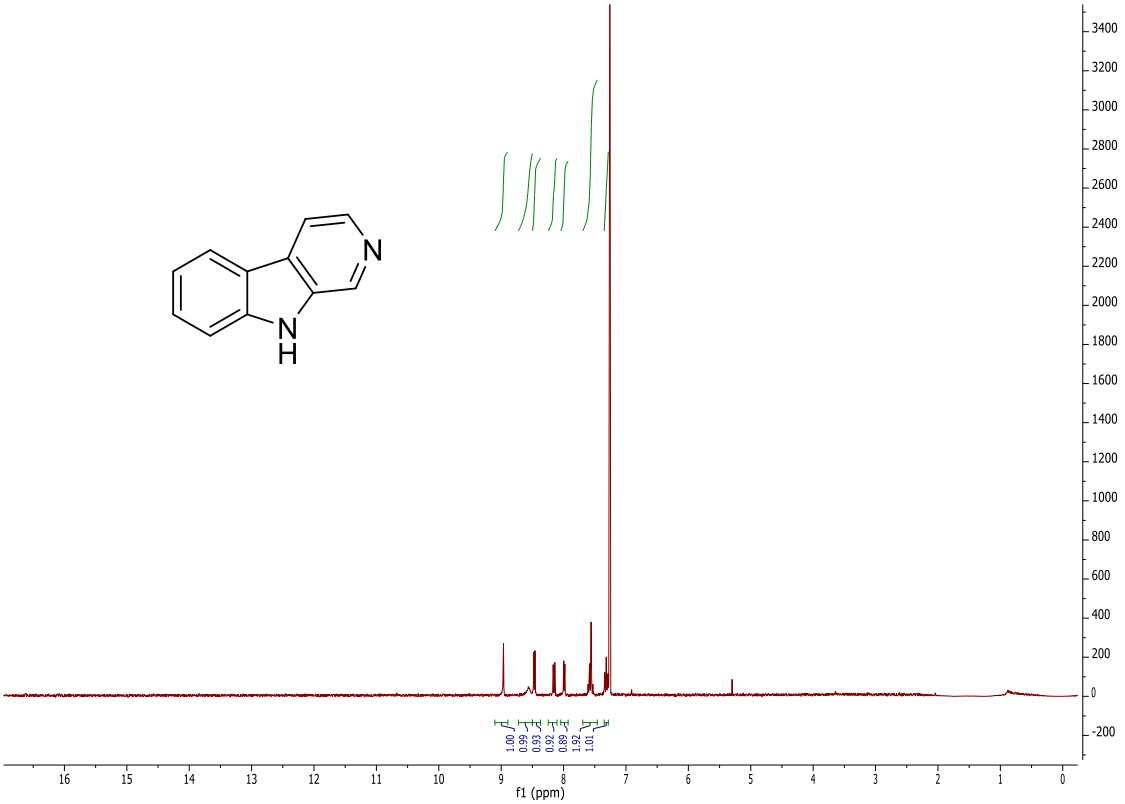

^{1}H NMR spectrum in $CDCl_3$.

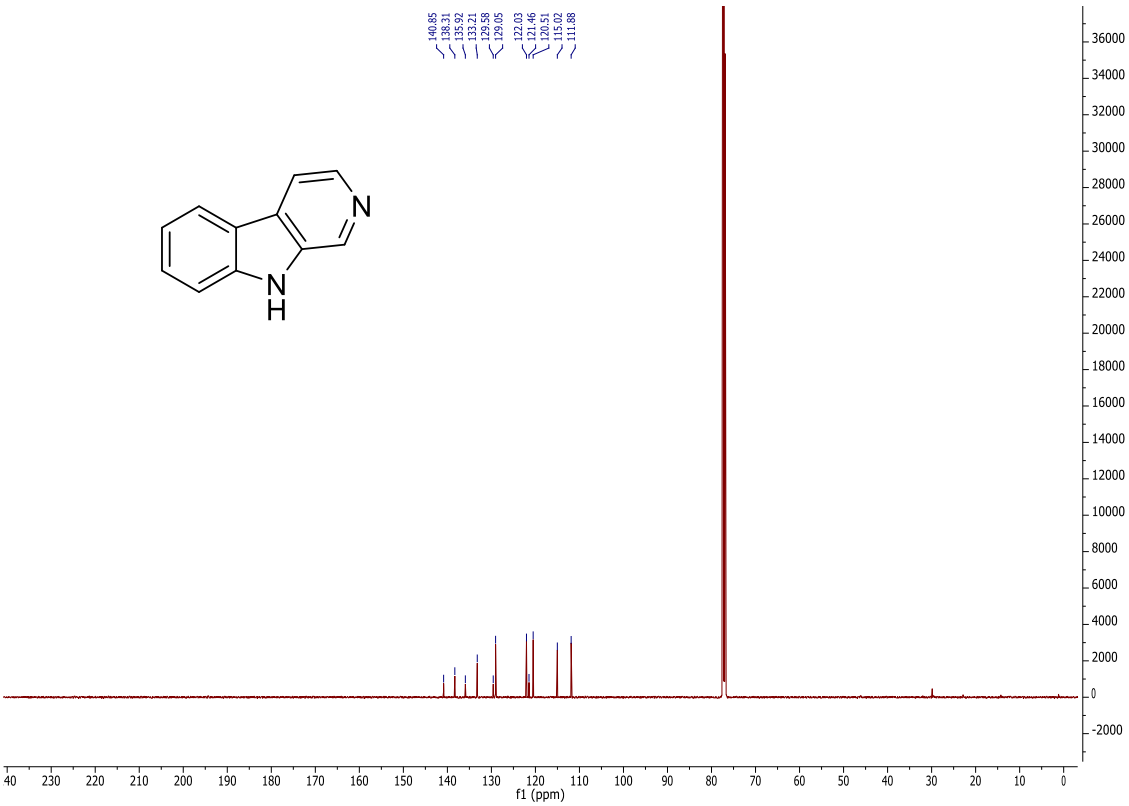

^{13}C NMR spectrum in $CDCl_3$.

31b

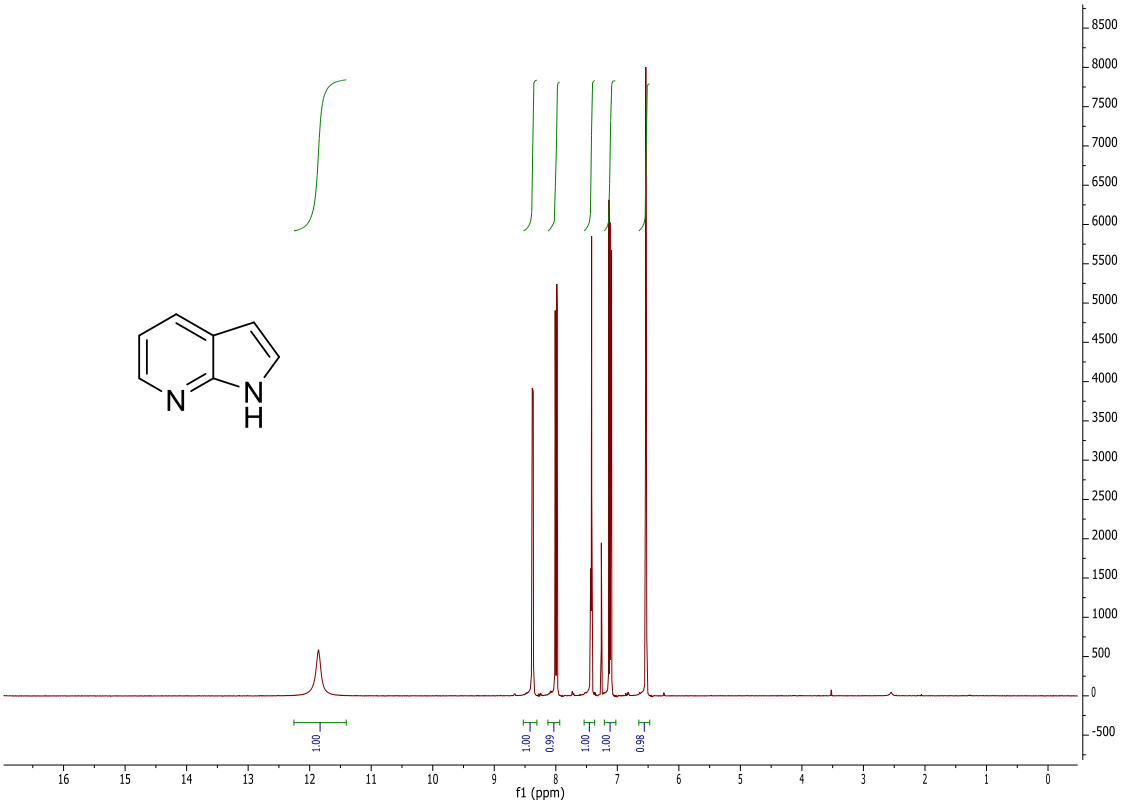

^{1}H NMR spectrum in $CDCl_3$.

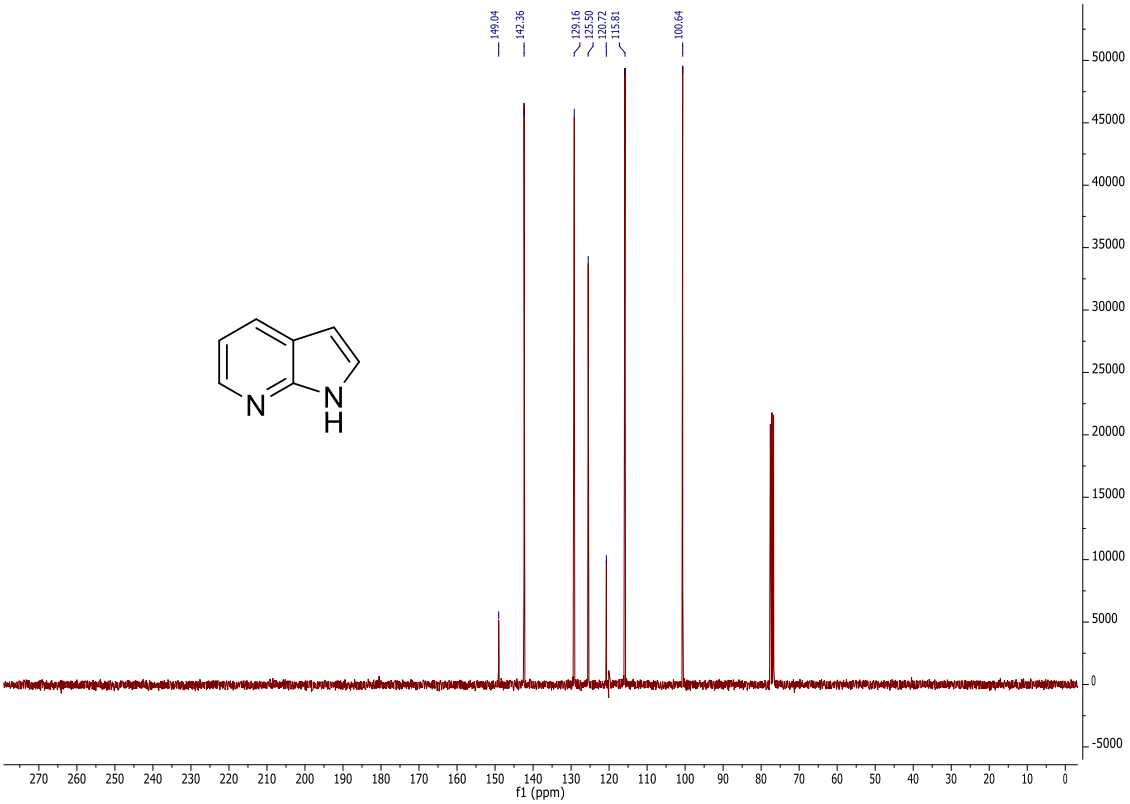

^{13}C NMR spectrum in $CDCl_3$.

32b

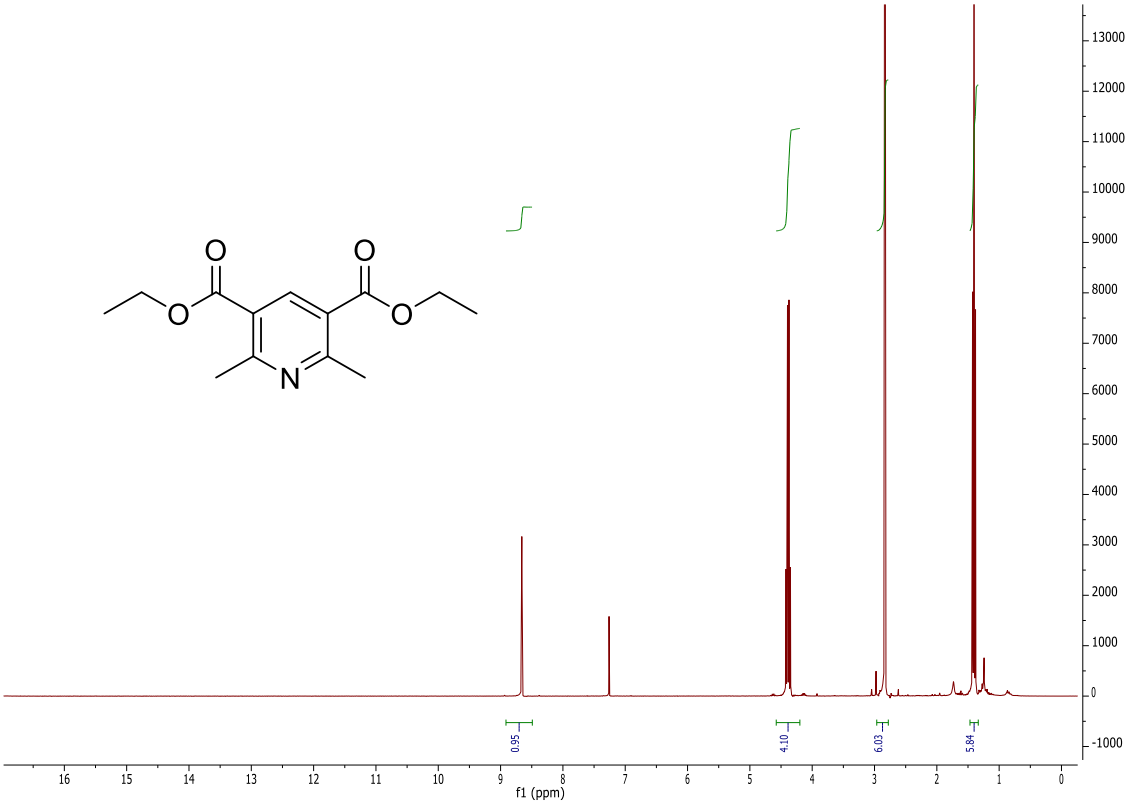

^{1}H NMR spectrum in $CDCl_3$.

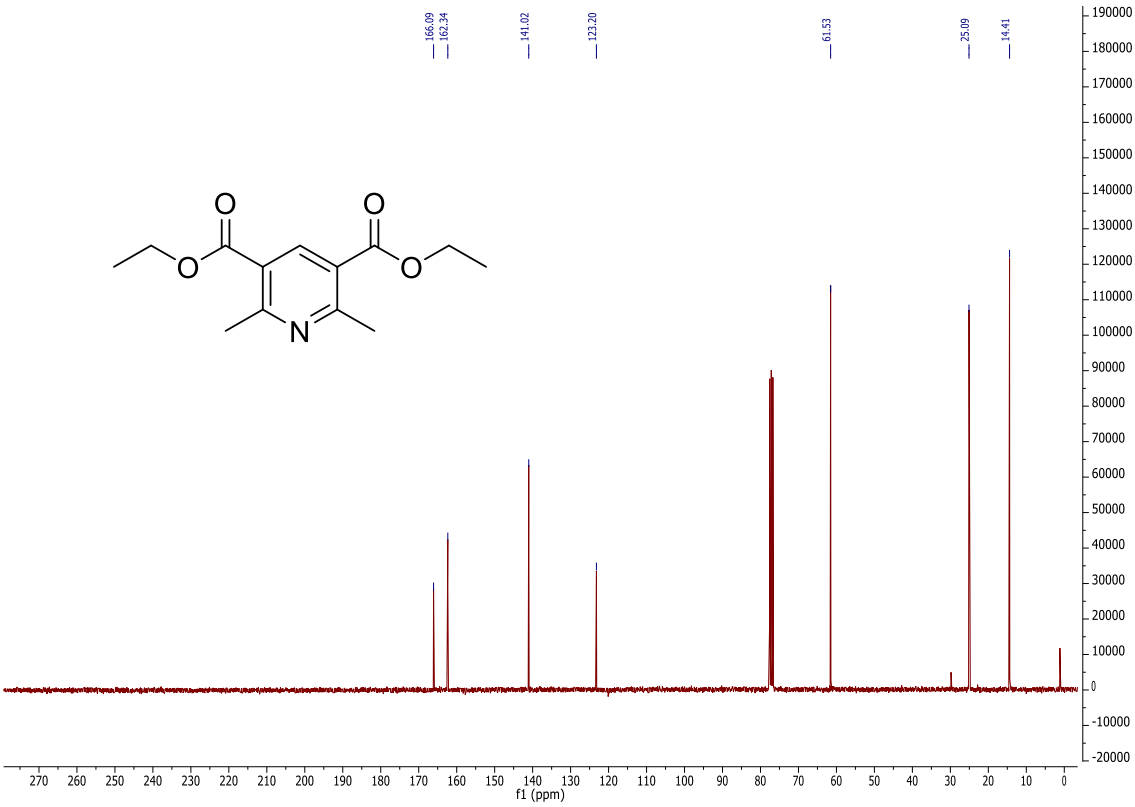

^{13}C NMR spectrum in $CDCl_3$.

33b

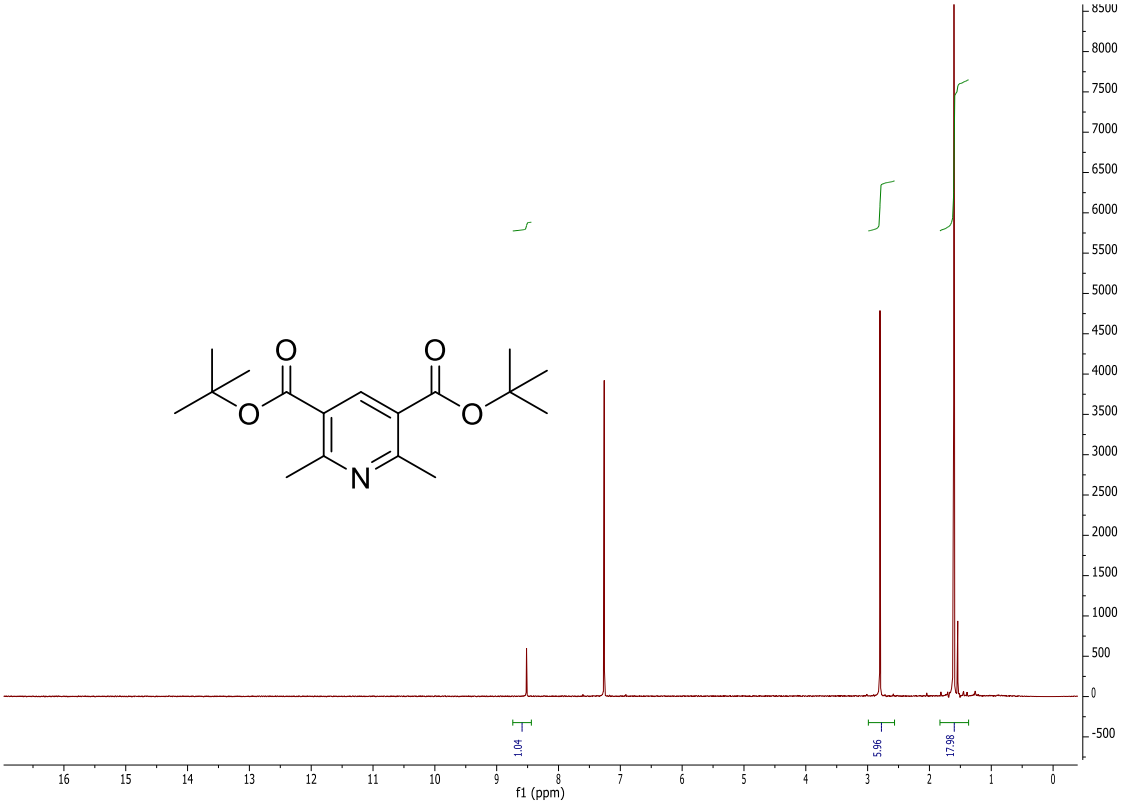

^{1}H NMR spectrum in $CDCl_3$.

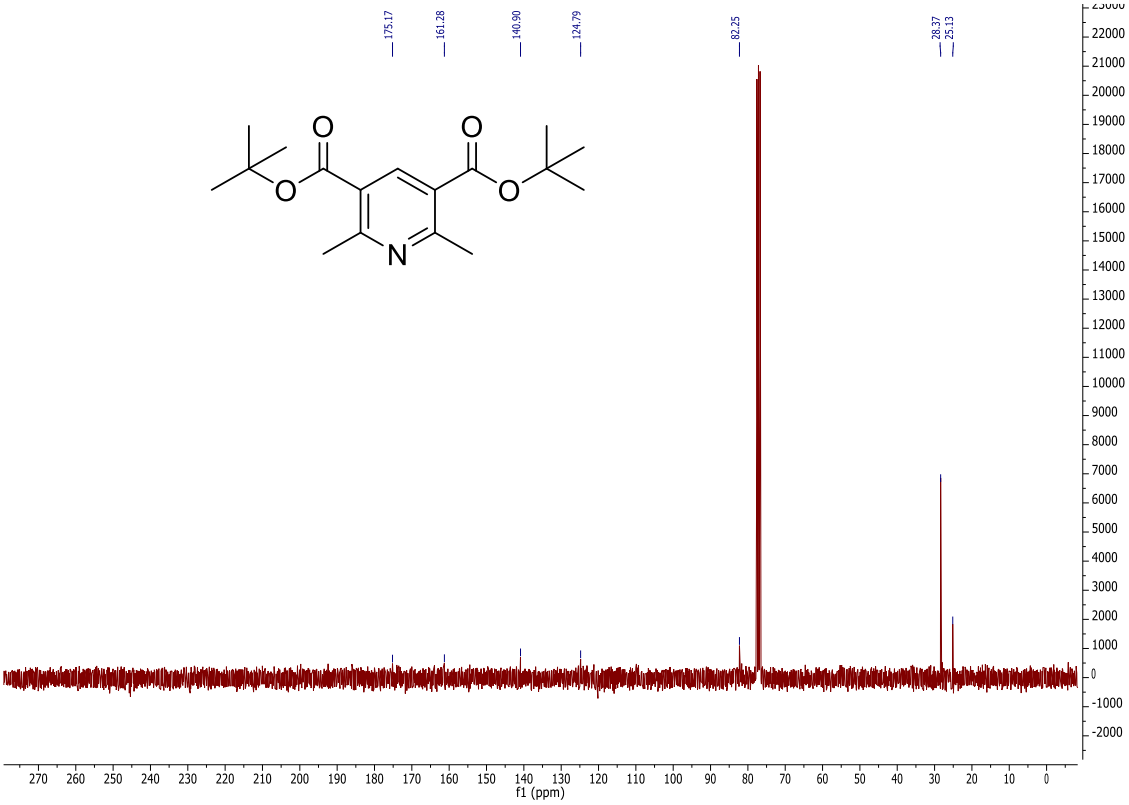

^{13}C NMR spectrum in $CDCl_3$.

34b

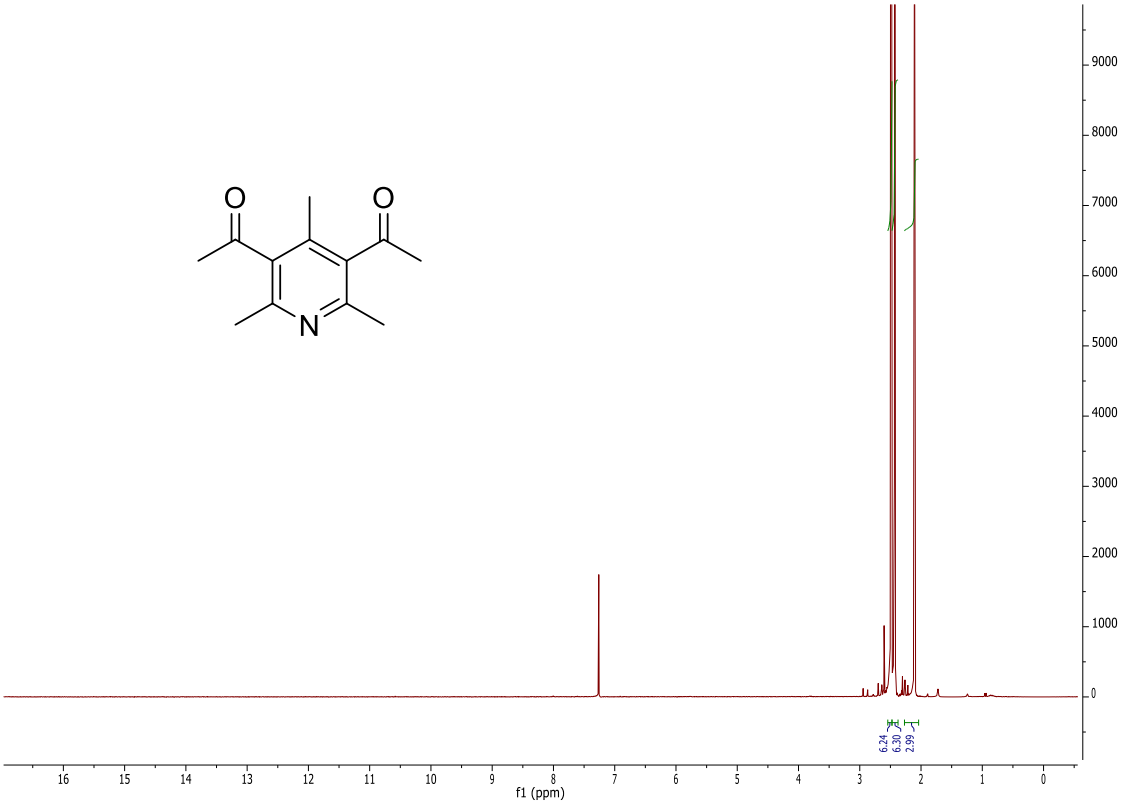

^{1}H NMR spectrum in $CDCl_3$.

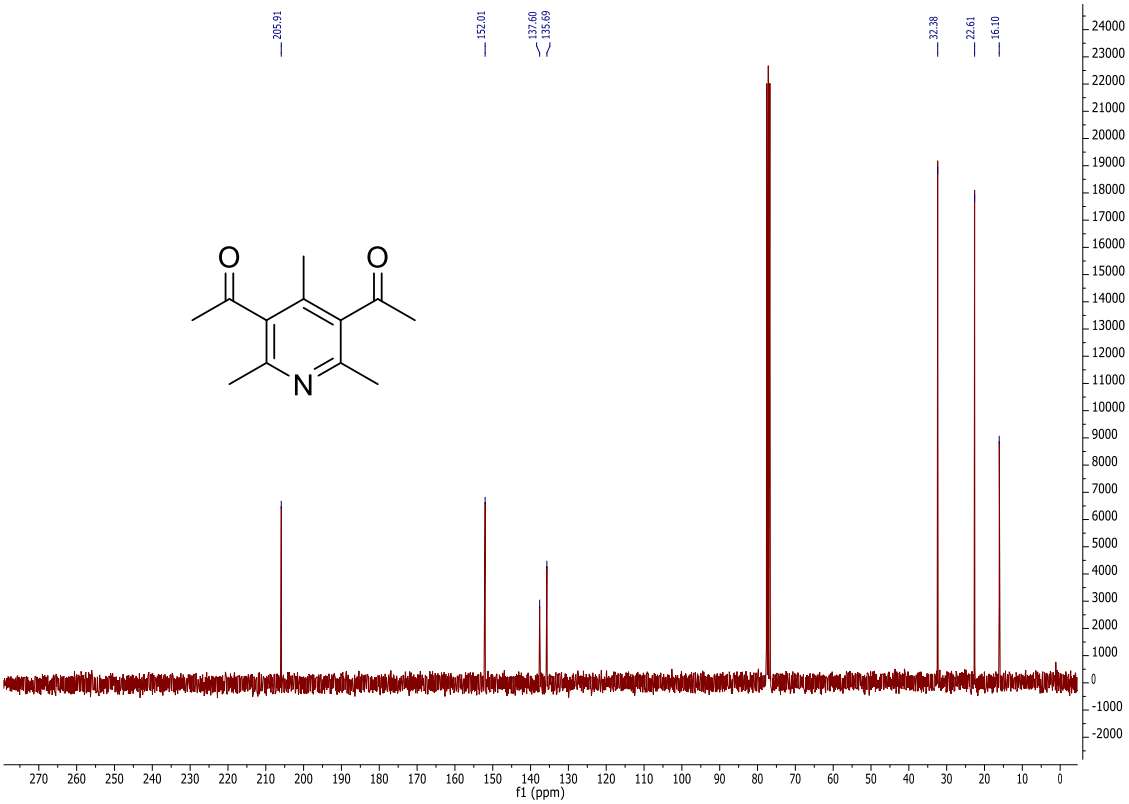

^{13}C NMR spectrum in $CDCl_3$.

35b

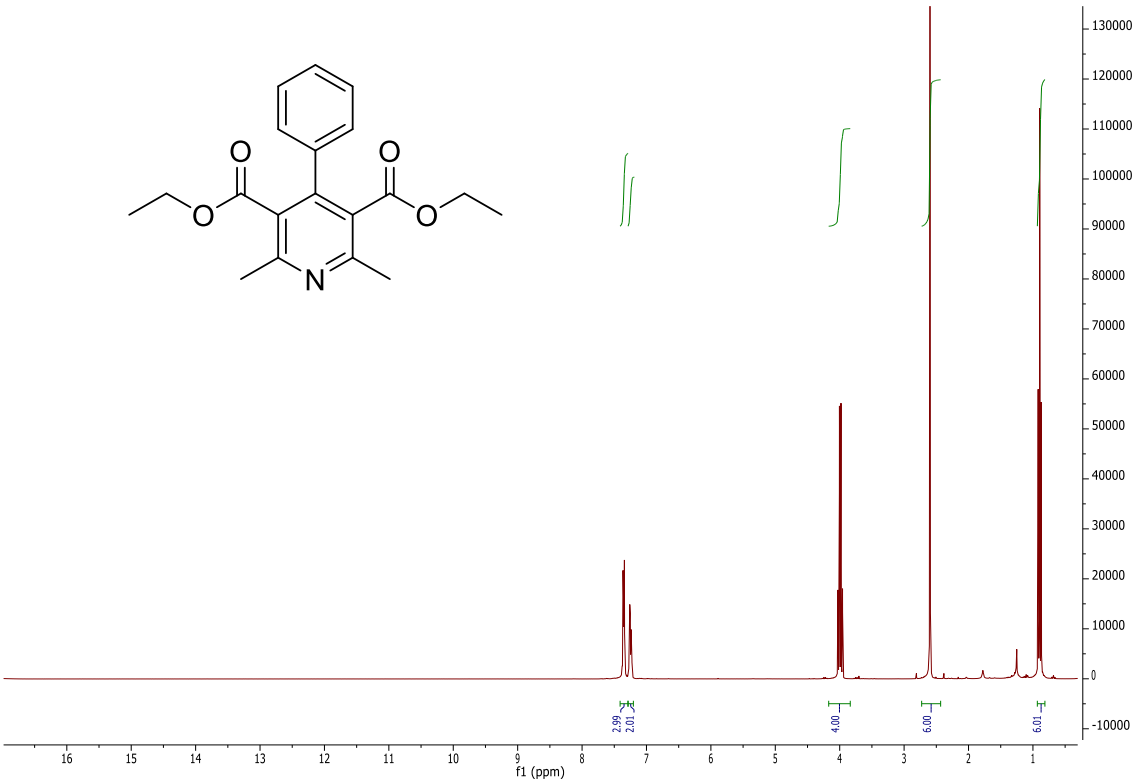

^{1}H NMR spectrum in $CDCl_3$.

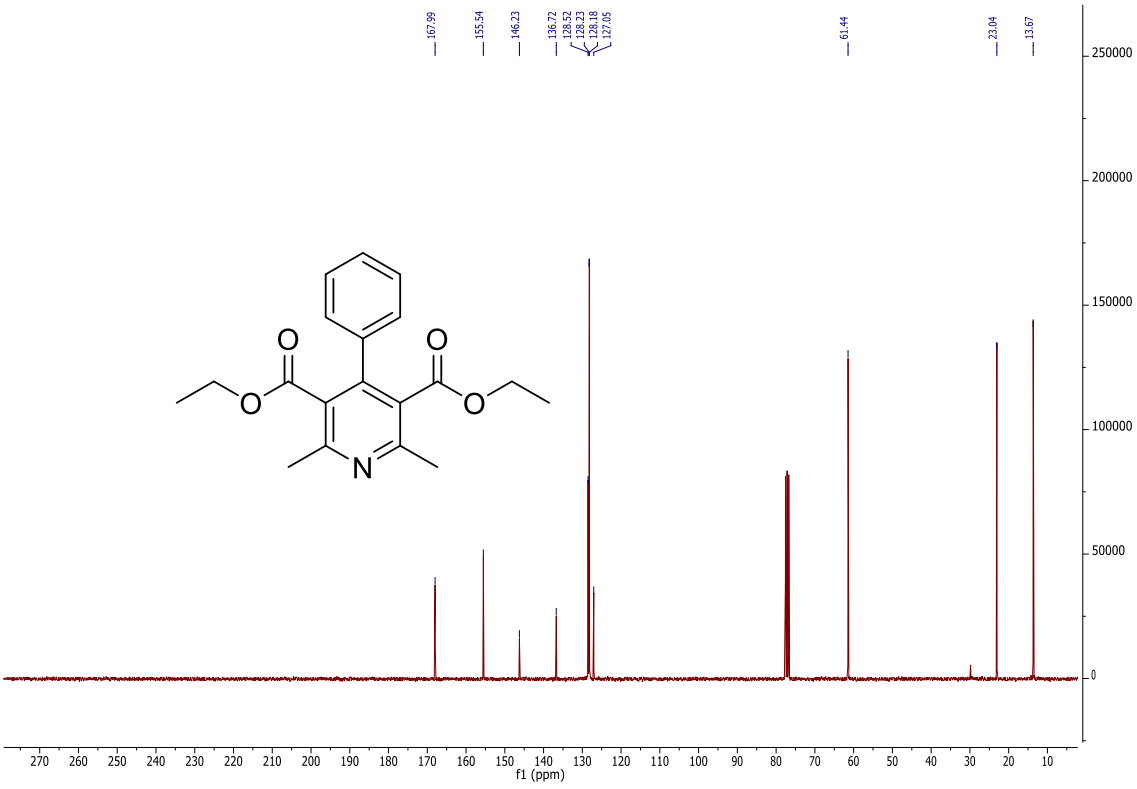

^{13}C NMR spectrum in $CDCl_3$.

36b

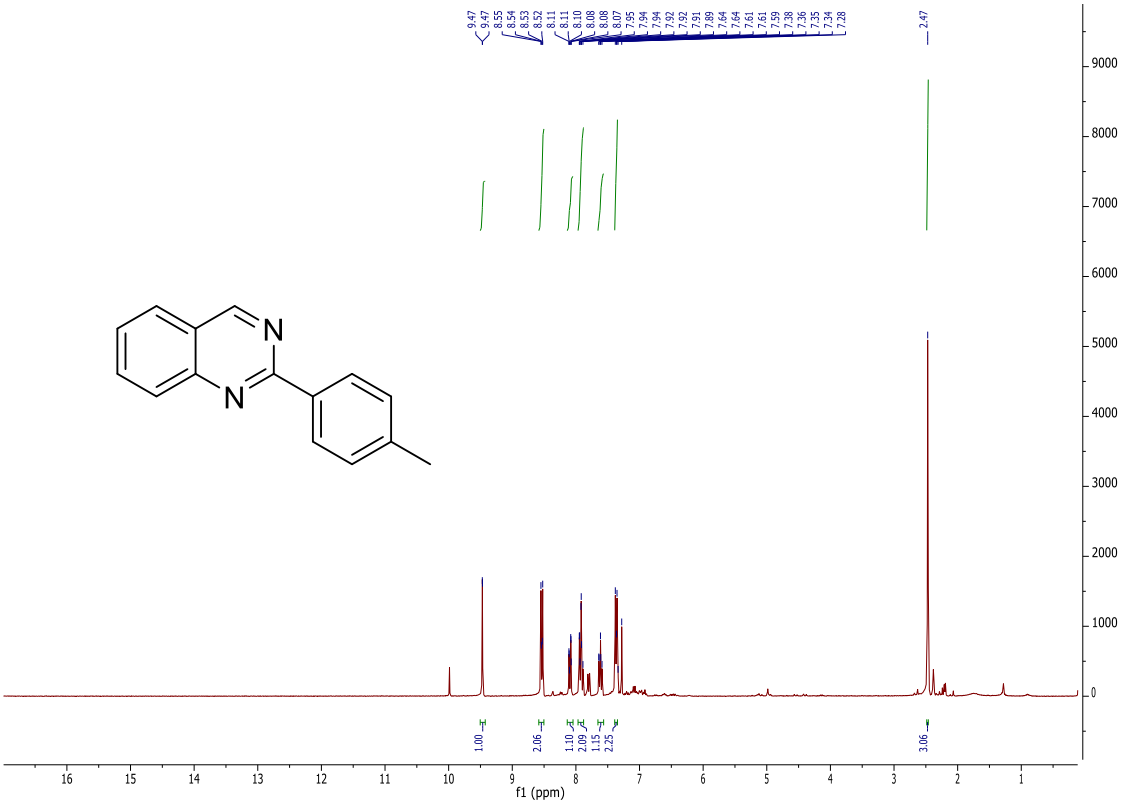

^{1}H NMR spectrum in $CDCl_3$.

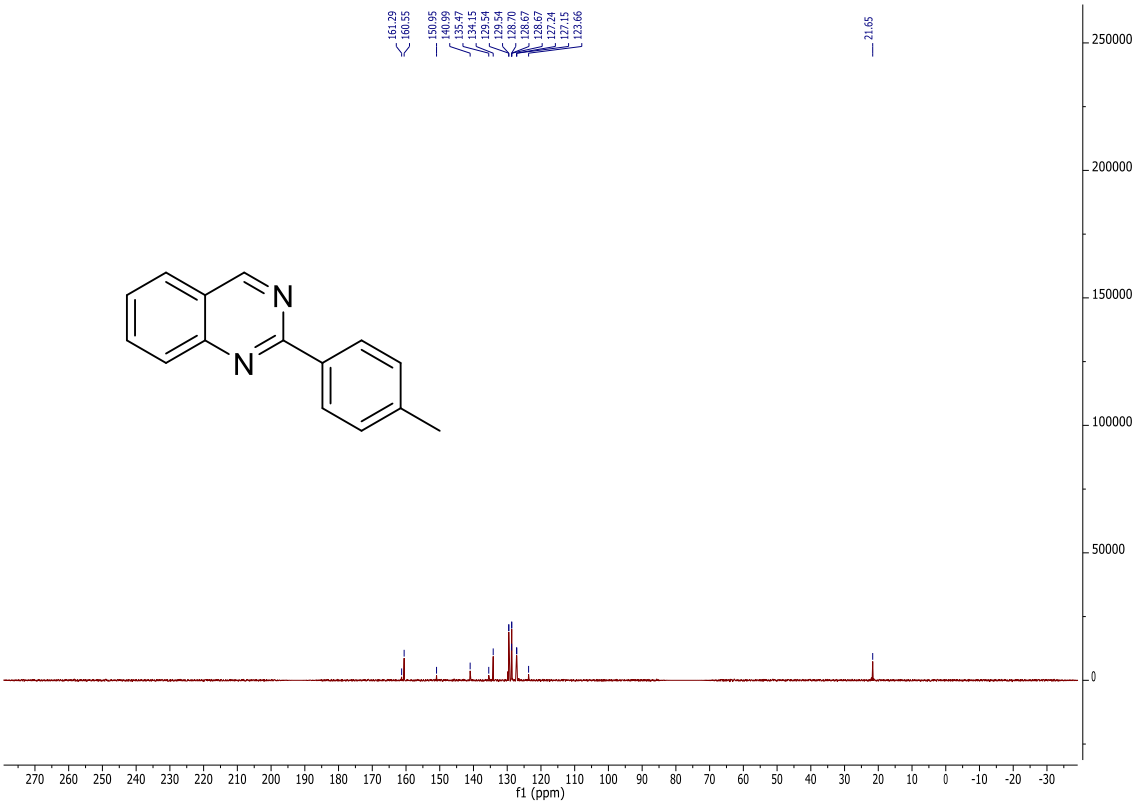

^{13}C NMR spectrum in $CDCl_3$.

37b

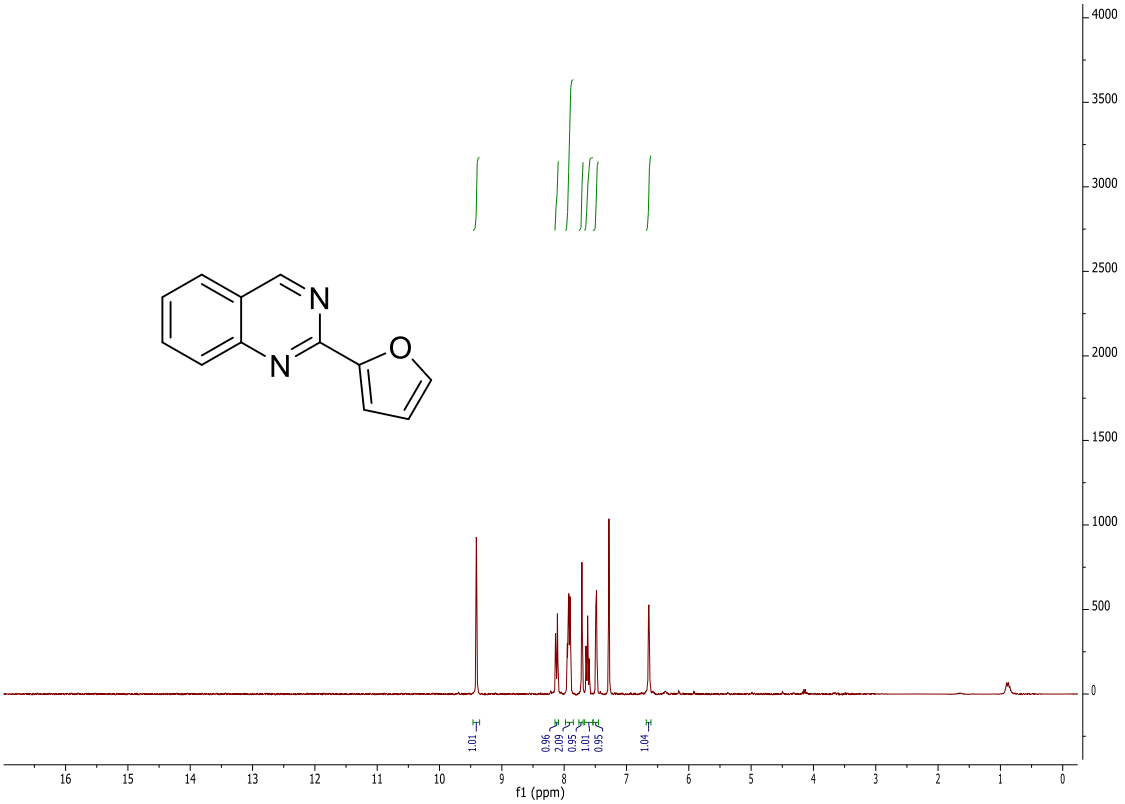

^{1}H NMR spectrum in $CDCl_3$.

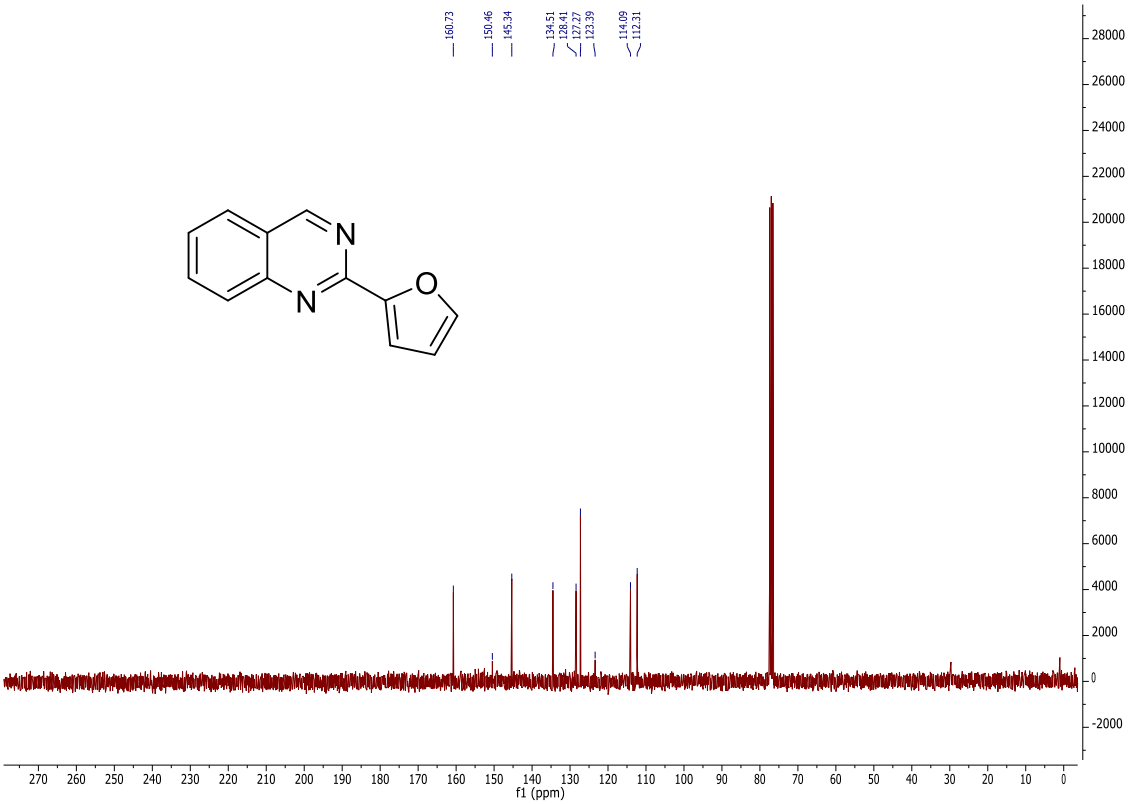

^{13}C NMR spectrum in $CDCl_3$.

38b

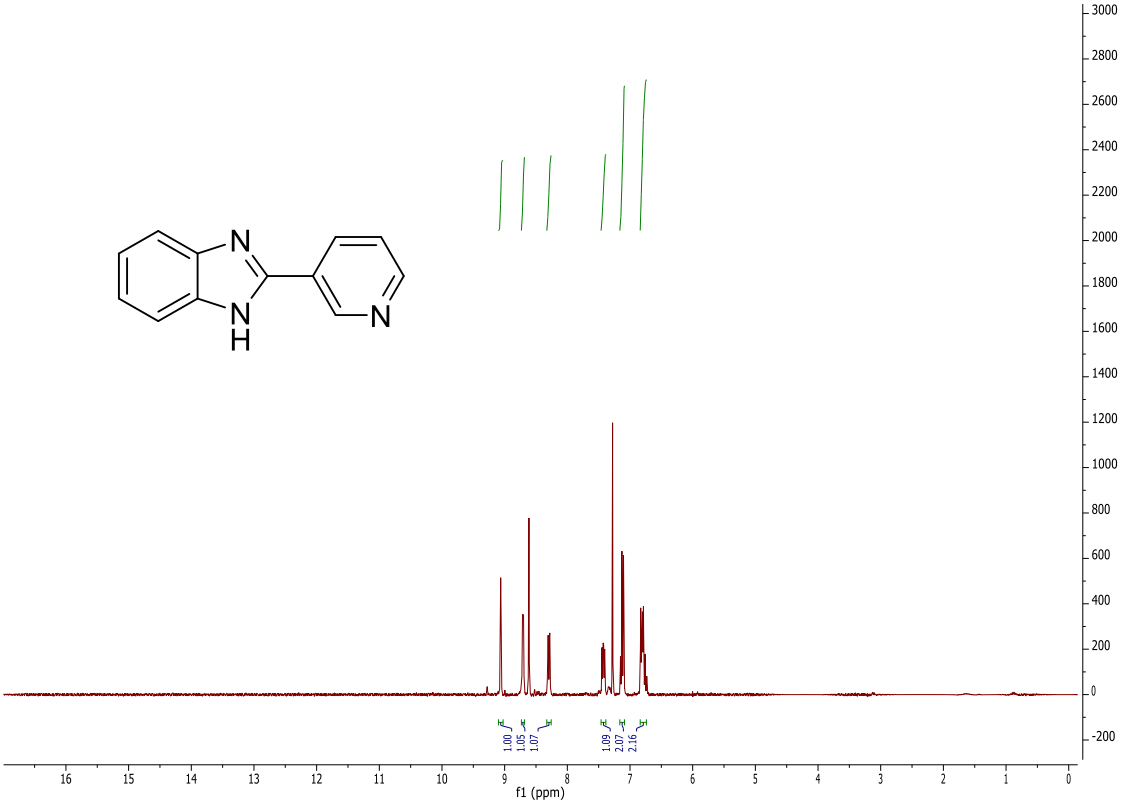

^{1}H NMR spectrum in $CDCl_3$.

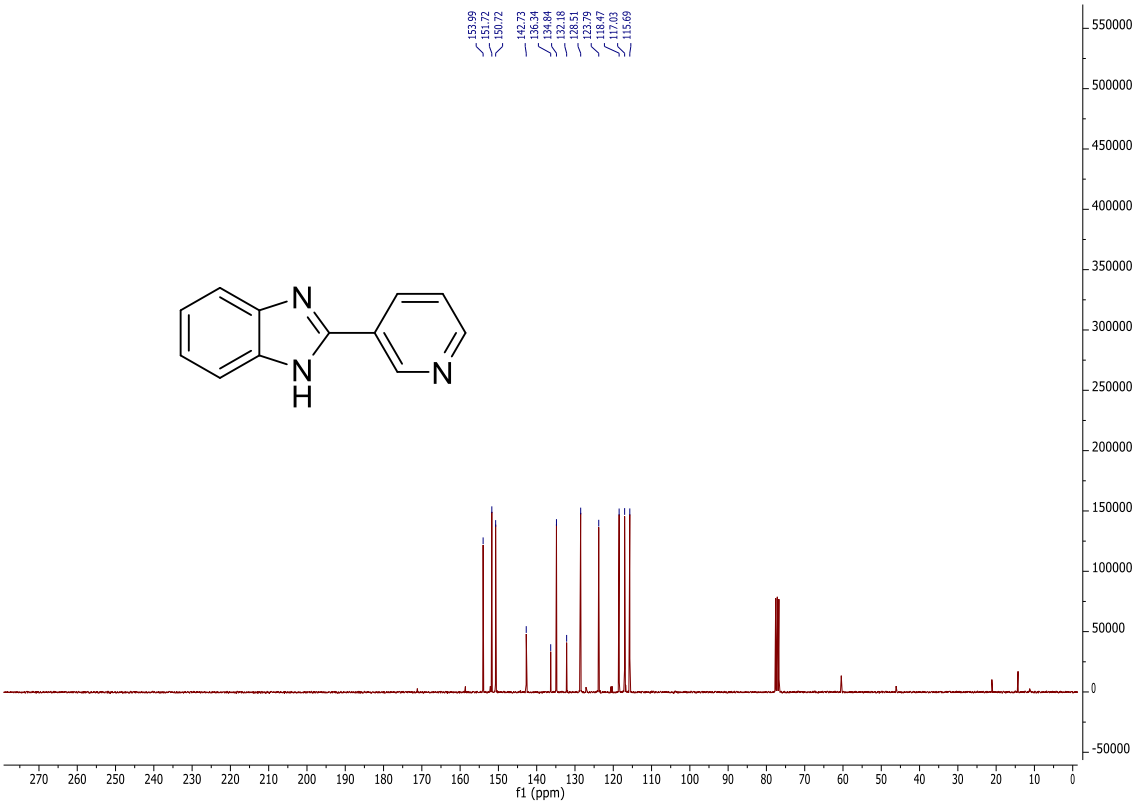

^{13}C NMR spectrum in $CDCl_3$.

39b

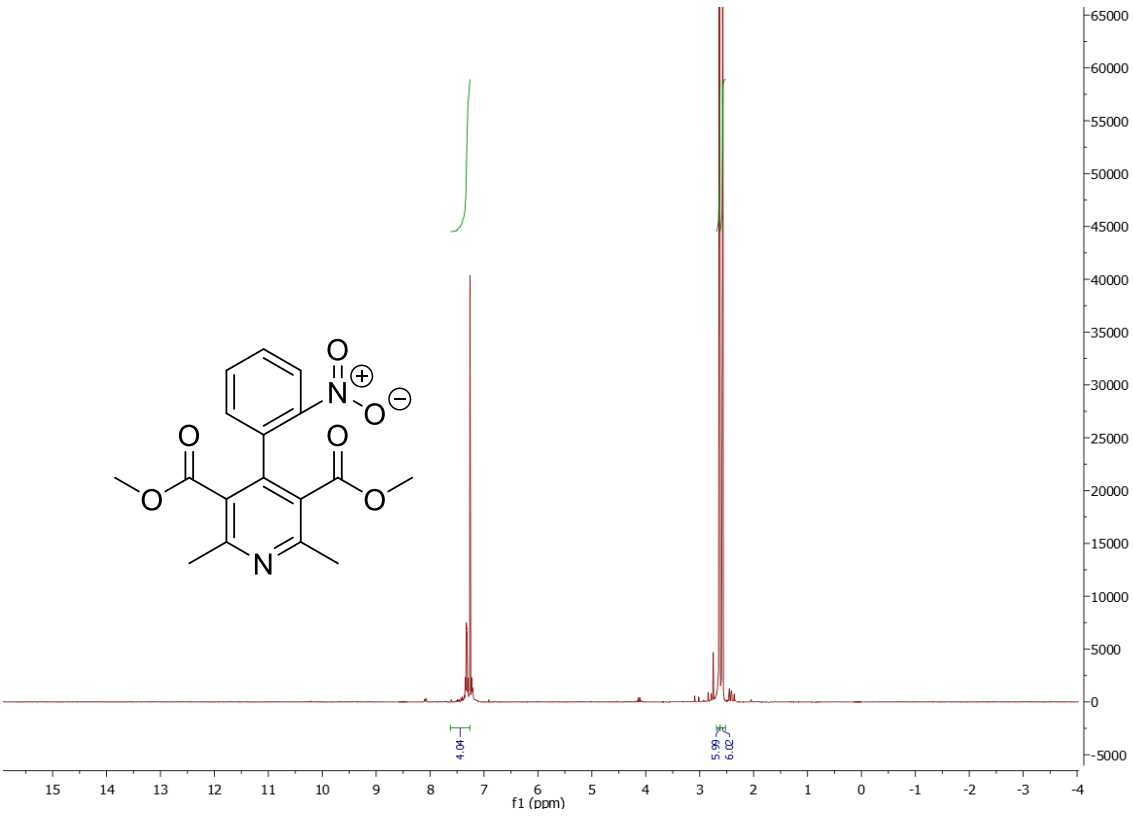

^{1}H NMR spectrum in $CDCl_3$.

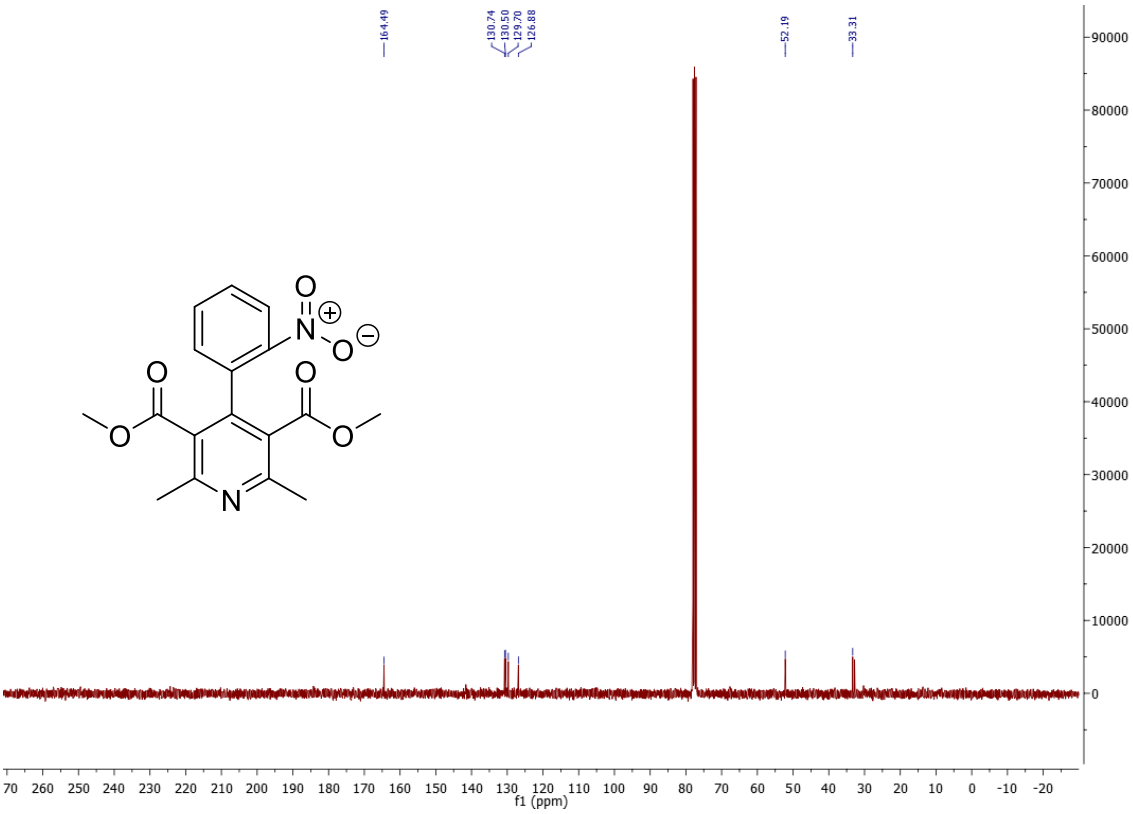

^{13}C NMR spectrum in $CDCl_3$.

40b

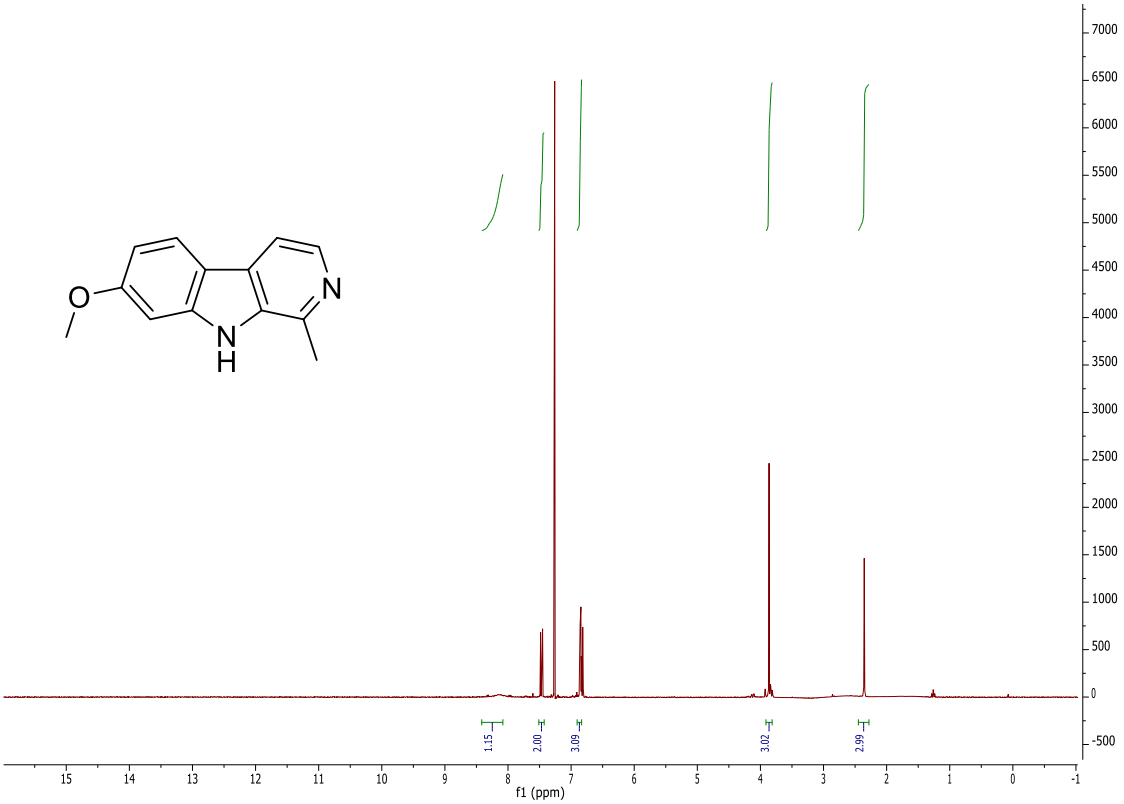

^{1}H NMR spectrum in $CDCl_3$.

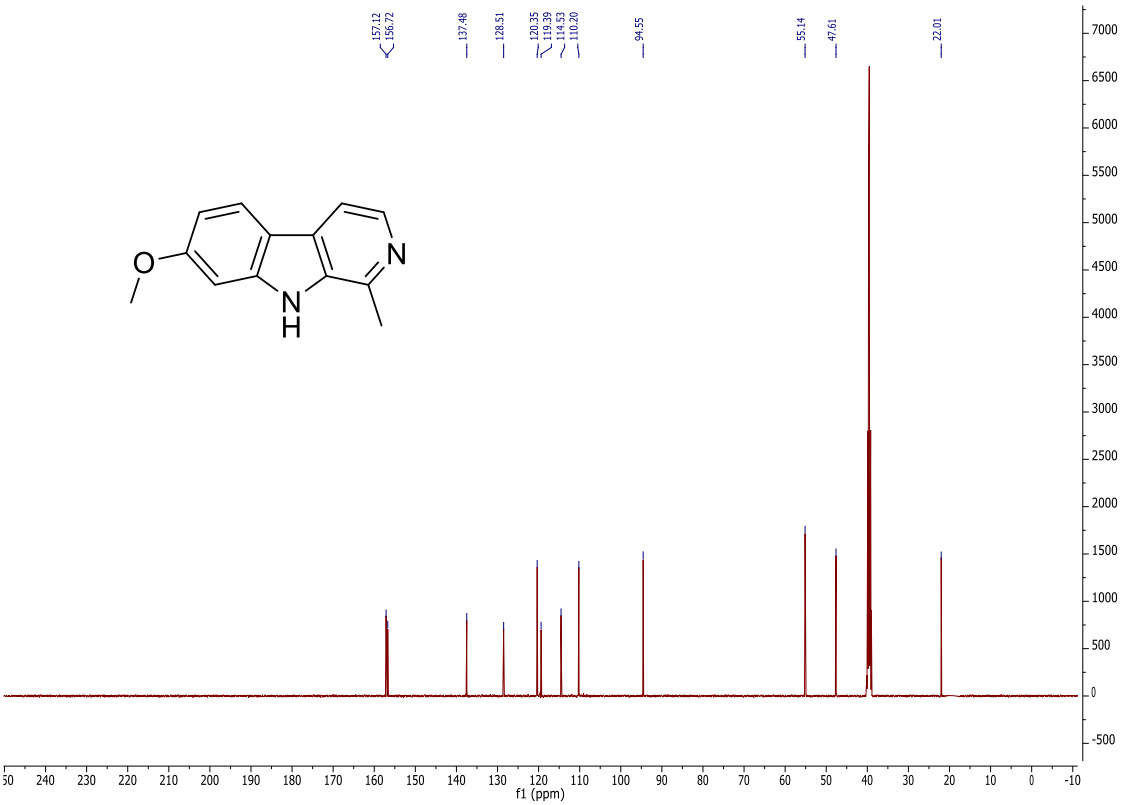

^{13}C NMR spectrum in DMSO-d_6.